The Pennsylvania State University

The Graduate School

Department of Kinesiology

ANATOMICALLY BASED INVESTIGATIONS OF TOTAL ANKLE ARTHROPLASTY

A Thesis in

Kinesiology

by

Andrew R. Fauth

Submitted in Partial Fulfillment
of the Requirements
for the Degree of

Doctor of Philosophy

August 2005

The dissertation of Andrew R. Fauth was reviewed and approved* by the following:

Neil A. Sharkey
Professor of Kinesiology,
Orthopaedics and Rehabilitation
Thesis Advisor
Chair of Committee

Stephen J. Piazza
Associate Professor of Kinesiology,
Mechanical Engineering, and
Orthopaedics and Rehabilitation

John Challis
Associate Professor of Kinesiology

Steve Zarit
Professor of Human Development and Family Studies
Head of the Department of Human Development and Family Studies

James Michelson
Professor, Orthopaedic Surgery
Director of Clinical Informatics
Orthopaedic Surgeon
The George Washington University
Special Member

Philip E. Martin
Professor of Kinesiology
Head of the Department of Kinesiology

**Signatures on file in the Graduate School*

ABSTRACT

The study addressed alignment and orientation issues of the talocrural joint with a specific emphasis on applications for total ankle arthroplasty (TAA). The first phase involved thorough morphological and geometrical characterizations of 8 cadaveric ankle joints, which were completed using a 3D digitization system and numerical optimization methods. The study also explored the design, use, and implantation of prototype surgical instrumentation and joint replacement components as a means of evaluating talocrural joint orientations.

First, the 3D spatial orientations of easily identifiable and palpable anatomical landmarks were calculated along with clouds of points replicating the articular surfaces of the distal tibia, talus, and fibula. The articular surfaces of the tibia and talus were characterized geometrically as cylinders via numerical optimization. Results indicated that the size of the mean radius of curvature of the articular surfaces of the tali and tibiae were within the findings of previous research. Statistical comparisons between the cylinders fit to the tibia and the talus revealed significantly larger radii of curvature for the tibia. In addition, males had significantly larger radii of curvature than females. The articular surfaces were also separated into medial and lateral halves for separate cylinder fits, and comparisons of radius size were made between the medial and lateral fits for the tibia vs. the talus, males vs. females, and the medial and lateral fits vs. the original whole-fits.

Joint surface orientations were identified via the cylinder fits and were compared to the 3D position and orientation of surrounding anatomical landmarks. These

assessments yielded consistent and predictable findings in the coronal plane (neutral varus/valgus), confirming some traditional TAA alignment procedures. The orientations of the joint surfaces in the transverse plane were found to be highly variable, and as a result, no consistent relationship was identified that would predict the transverse orientation of the joint surfaces.

Calculations were also made of the coronal and transverse orientations of vectors connecting anatomical landmarks such as the intermalleolar (IM) axis and edges of the anterior and posterior articular surfaces. Results showed that the orientations of the IM axes were highly variable in both planes, indicating that current TAA alignment procedures that approximate the alignment of the components based on the IM axis may be erroneous.

The results from the initial orientation calculations were applied towards the development of prototype surgical alignment instrumentation and components for TAA. This instrumentation was used to perform TAA surgery and implant experimental TAA components to examine the joint orientations of 5 cadaveric ankles. The simple, congruent, cylindrical component system developed was based on the radius of curvature data from the cylinder optimizations, and allowed unrestricted translation and rotation of the components in the transverse plane that was designed determine the optimum TAA component orientation in this plane.

The cylindrical components were inserted in place of the talocrural joint surfaces, and their orientation was measured at a static, neutral position to evaluate the accuracy of the cuts. Next, the feet were subjected to kinematic experiments involving cycles of plantarflexion and dorsiflexion. Initial and final orientations and translations of the components were calculated, along with intra-experimental rotational oscillations. Final component positions and orientations were compared with the spatial orientation of anatomical landmarks in order to identify repeatable alignment relationships. Analysis of the results showed a great deal of variance in the transverse plane orientation of the components, therefore a mean transverse plane orientation that was representative of all specimens was not identified. In addition, through the plantar/dorsiflexion trials, the components exhibited rotational oscillations in the transverse plane demonstrating that talocrural motion is multi-planar.

The results of the study indicate that a more thorough understanding of the transverse orientations of talocrural joint surfaces is needed before reliable, predictable alignment criteria can be developed for TAA. Nevertheless, the current study identified orientations in the coronal and sagittal planes which confirm certain existing TAA alignment protocols, and also demonstrated that it is possible to develop instrumentation that can improve the accuracy of the TAA bone cuts.

TABLE OF CONTENTS

LIST OF FIGURES

LIST OF TABLES

ACKNOWLEDGEMENTS

I would like to acknowledge all of the people who have helped me with my doctoral work over the last several years. I would especially like to extend my gratitude to my advisor and my committee members, who provided guidance, constructive criticism, and encouragement; all of which helped me to develop as a researcher and get to this point. Also, I would like to thank my friends and colleagues from the Biomechanics Lab, without whom this work would have been impossible to complete. Last, but not least, I thank my family for their love and support over the last five years. I would especially like to thank Beth-- I never would have done it without you.

CHAPTER 1. INTRODUCTION

1.1 The Ankle

The human ankle joint plays an integral role in gait and other movement. Functioning as a link between the leg and the foot, the ankle translates forces between the foot and the lower leg, and its motion allows for smoothness during gait as well as propulsion during complex movement patterns. The normal, healthy ankle joint is a fairly robust hinge-type joint with a balanced complement of bony and soft tissue support (Stauffer et al., 1977). Skeletal support originates from the medial malleolus of the tibia and the lateral malleolus of the fibula, while soft tissues such as strong ligaments and sheath-like retinaculum add substantial stability.

Despite the natural resistance of the ankle to trauma, injuries to the ankle joint are quite common. In addition to bearing the weight of the body, the ankle can experience forces up to 5 times body weight with movement (Stauffer et al., 1977). Ankle injuries often range from strains and sprains to the more serious fractures and dislocations. Injuries like pilon fractures caused by hard impacts such as landing from a height or malleolar fractures that might occur when one "rolls" their ankle can lead to painful and degenerative conditions later in life (Michelson, 1994; Rockett et al., 2001). Often the acute ankle injury (fracture) can be addressed, but long term pathologies such as arthritis still occur due to permanent changes in the surrounding tissue.

1.2 Arthritis and Ankle Pathology

Over 40% of people aged 60 years and older in the U.S. are diagnosed with arthritis (Guralnik, 1989). Osteoarthritis (OA), is a disease that primarily occurs following trauma and that often occurs in the ankle. OA affects over 20 million people in the United States alone and is predicted to be a major health risk factor for over 70 million Americans aged 65 and older by 2030 (NIH, 2002). Rheumatoid arthritis (RA), another variation of the disease, occurs in about 5% (four to six million) of Americans (NIH, 1998). The prevalence of RA has been reported to increase with age, with patients over the age of 65 having the highest prevalence (Jaakkola and Mann, 2004). RA can have a significant affect on the foot and ankle as over 80% of those afflicted with RA develop problems in the lower extremity (AAOS, 2004; Michelson, 1994). In older adults, foot and ankle problems usually manifest after longer periods following the diagnosis of RA, while in juveniles the prevalence of ankle problems occurs almost immediately after diagnosis in 25% of RA patients (Caron et al., 1999). The overall frequency of ankle involvement in RA varies in the literature, but reports estimate a range of 9%-68% of people with RA experience ankle problems (Michelson et al., 1994).

The symptoms of arthritis vary slightly depending on the type, but common symptoms include pain, stiffness, swelling, range of motion (ROM) deficits, tenderness, and crepitus (Rockett et al., 2001). Symptoms such as these result in mobility problems that can affect any or all weight bearing activities and locomotion (Shih et al., 1993), which results in a significant negative impact on people's ability to perform activities of daily living. From an economic standpoint, the medical and surgical treatment for arthritis and the wages lost because of disability caused by the disease add up to billions of dollars annually (NIH, 1989).

The specific etiology of OA is not completely understood however, a basic framework has been proposed to describe the mechanisms leading to joint degeneration and osteoarthritis. First, an initial trauma such as a pilon fracture occurs due to a fall or severe impact. The immediate response to trauma is the secretion of proteolytic and collagenolytic enzymes that soften the joint surface and lead to inflammation. A feedback loop then occurs between trauma and the body's inflammatory response to trauma that causes the secretion of additional inflammatory mediators like prostaglandins. These enzymes eventually can lead to pitting, fissures, osteophytes, or even an altering of the proteoglycans within healthy tissue (Rockett et al., 2001).

The mechanism of disease in RA has been hypothesized to be an inflammatory reaction triggered by a viral infection. RA has been associated with the class II major histocompatibility complex, specifically human lymphocyte antigen DR4 (Jaakkola and Mann, 2004). Synovial proliferation due to protease release from chondrocytes and fibroblasts can lead to ligamentous laxity and direct cartilaginous destruction. The degeneration of the articular surface can lead to joint space narrowing, reduced ROM, and crepitus. Often, an indicator of ankle instability in patients with RA is the presence of an anterior talar tilt in weight bearing radiographs.

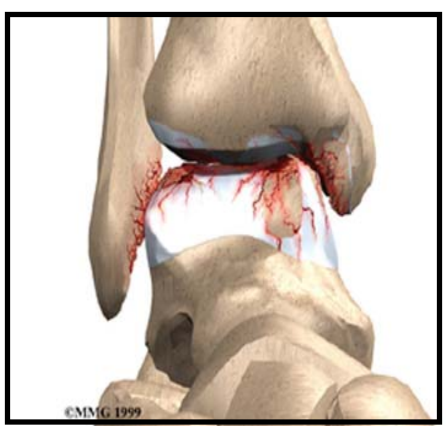

Figure 1.1 Pictoral representation of ankle arthritis including worn cartilage, inflammation, and osteophytes (hhttp://www.agiltyankle.com/xq/ASP/page.content/article_ic61/qx/default.htm).

Besides causing significant pain, ankle arthritis can lead to deficits in ambulation. Most arthritic patients exhibit decreased ranges of motion, especially with plantarflexion and dorsiflexion. This is usually coupled with a reduction in plantar and dorsiflexion ankle torques, making it difficult to walk, especially on uneven surfaces such as stairs. General instability of the ankle due to increased laxity as well as valgus deformities, especially of the hindfoot, is common.

Muscle atrophy usually occurs due to loss of function, and arthritic patients show significant muscle weakness of the affected limb relative to the severity of their arthritis (Stauffer et al., 1977). All of this affects gait parameters as well, leading to a reduction in stance, cadence, velocity, and vertical GRF at push-off for the affected limb (Shih et al., 1993). For treatment of arthritis, non-surgical means are usually employed initially in an effort to reduce pain and restore or maintain function. Oral anti-inflammatories are given, and shoe therapy is also common. Orthotic devices such as rocker-bottom shoes, and/or rearfoot orthoses designed to alleviate hindfoot weakness and valgus deformities may be tried to aid ambulation and reduce pain.

When non-surgical methods of treating arthritis are ineffective, there are several surgical alternatives that are often attempted to try to alleviate the symptoms. For example, arthroscopic or open debridement can be performed to remove impinging bone spurs and alleviate synovitis. If these methods do not help, or if degeneration of the joint continues, then more difficult or invasive procedures such as arthrodesis (joint fusion) or arthroplasty (joint replacement) are pursued. Arthroplasty is the desired procedure, since it aims at maintaining or restoring motion at the joint. Unfortunately, there is a high rate of complications associated with the procedure, leaving many surgeons to choose arthrodesis instead.

Invasive surgical interventions for ankle pain such as arthrodesis and arthroplasty can present a problem for RA patients. Anti-inflammatory drugs used to combat RA should be reduced or stopped prior to surgery, since these medications reduce platelet formation and can lead to wound healing complications, infection, and non-union in both interventions. Also, if RA is concurrently affecting the hand, wrists, or other areas of the upper extremities, the patient may not be able to use assistive devices such as a crutch or walker after surgery (Caron et al., 1999). In addition, arthrodesis of the midfoot and hindfoot in RA patients is not usually an isolated procedure, but is accompanied by fixation of some of the more distal joints in the foot. This is due to the additional stress placed on these joints post-operatively that occurs as a result of altered force transmission through the bones of the foot. Despite these difficulties, RA patients have been included in both arthrodesis and arthroplasty procedures with positive results (Caron et al., 1999). Recent studies have shown that screw fixation and compression arthrodesis can have successful outcomes in RA patients (Caron et al., 1999).

1.3 Surgical Interventions: Arthrodesis & Arthroplasty

1.3.1 Arthrodesis

The first ankle fusion was performed around 100 years ago (Sodha et al., 2000) and has since become the gold standard procedure performed to alleviate pain, restore stability and correct alignment abnormalities of the ankle. Arthrodesis normally involves the fixation of the talocrural joint and often other accompanying joints first by removing the joint surfaces, followed by a bone graft, and finally fixation with pins, screws, or plates until bony fusion is confirmed via radiography. While arthrodesis has been shown to be successful in alleviating pain and restoring some ambulatory function (Rockett et al., 2001), there is still a variety of problems associated with the procedure. Complication rates of up to 34 - 60 % have been reported in the literature for arthrodesis, which can be attributed to the technical difficulty of the procedure as well as the high number of associated risk factors (Sodha et al., 2000; Abidi et al., 2000). Severe complications such as non-union often occur, especially with rigid fixation methods, as well as fracture, supramalleolar pain, nerve damage, infection, limb shortening, and arthritis in the surrounding joints due to abnormally transferred stresses. In fact, reports of arthritis due to micro-trauma in the surrounding joints following arthrodesis of the talocrural joint have been as high as 80% (Neufeld et al., 2000). Additionally, arthrodesis of the ankle leads to a total loss of range of motion, thereby limiting the mobility of the patient.

1.3.2 Arthroplasty

Around 1970 surgeons began experimenting with total ankle arthroplasty (TAA) as an alternative to arthrodesis in an effort to reduce pain, restore function, and simulate normal kinematics. The idea behind TAA was similar to the hip and knee surgical counterparts; replace the articular surfaces and a portion of the biologic bone with artificial materials that provide the mobility afforded by the native joint. Unfortunately, early TAA component designs had several major flaws that limited both their function and lifespan. These early components were either over-constrained or under-constrained, and they tended to oversimplify the ankle joint by treating it like a pure mechanical hinge. These shortfalls lead to pain, infection, loosening, and eventual catastrophic failure. These early attempts at ankle replacement were abandoned in the early 1980's and surgeons returned to arthrodesis.

Due to the continuing dissatisfaction with arthrodesis, a few years later researchers and surgeons began to re-think ankle replacement as a potentially more effective means of improving the lives of those with debilitating ankle pathology. New designs and styles of components were developed, some of which are still in use today, including the standard two-component design as well as the 3-piece design that incorporates a meniscal bearing between the talar and tibial pieces (Figure 1.2). These new designs, referred to as 2nd Generation TAA, incorporate a moderate degree of constraint and attempt to better simulate the true anatomy of the ankle joint. While 2nd generation TAA systems have shown more promise than their 1st generation predecessors, there are still a variety of complications that plague these new TAA systems such as wear, loosening, improper wound healing, and catastrophic failure. Many surgeons still opt in favor of the old standby, arthrodesis.

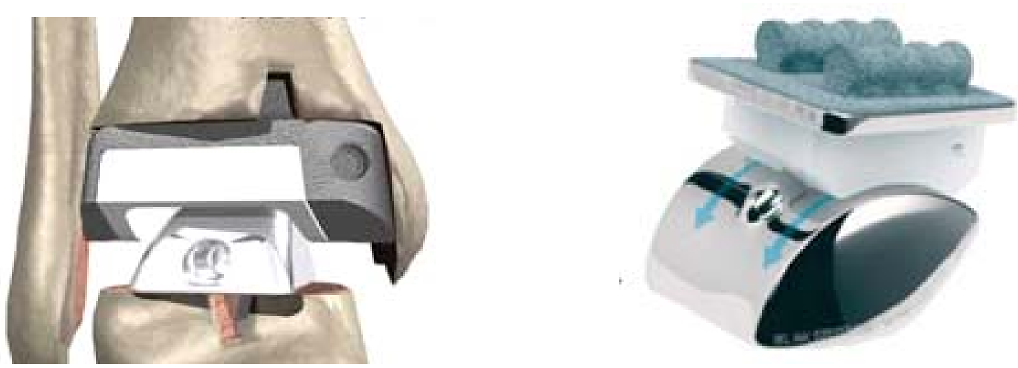

Figure 1.2 Examples of 2-component (left) and three component (right) ankle arthroplasty components designed to replace the talocrural joint surfaces.

1.4 Scope of the Problem

To date, total ankle replacement is only sporadically performed due to lack of positive long-term results. While there are a few TAA systems currently in use, the number of patients who undergo the procedure is quite low. As mentioned earlier, much of the failure that occurs with ankle arthroplasty can be attributed to both the difficulty of the procedure and the lack of alignment knowledge and instrumentation.

There is a strong need for a better understanding of talocrural geometry and alignment if improvements in TAA are to be made. The design philosophies of current components focus too much on mechanical simplicity, and tend to ignore the bony geometry of the joint they are simulating. Furthermore, the surgical procedures rely almost completely on the subjective assessments and assumptions of actual anatomic geometry, rather than specific knowledge.

1.5 Objectives of the Study

This study had four main objectives. Because the ultimate goal of ankle replacement surgery is to replicate the functional anatomy of the ankle joint, the first objective of this study was to expand current understanding of ankle anatomy and function in an effort to improve upon on the surgical procedure, components, and instrumentation involved in TAA. In order to do so, a comprehensive understanding of the geometry and orientation of the articular surfaces of the talocrural joint was necessary. This information was then used to assess the need for either individual or generalized orientation guidelines with respect to alignment instrumentation. The second objective of the current research was to develop prototype surgical instrumentation based on anatomical geometry that would facilitate more accurate alignment of TAA components. The third objective was to use this alignment instrumentation to replace the bony anatomy of the talocrural joint with simple, cylindrical components unconstrained in the transverse plane to assess the natural orientation of talocrural joint, as dictated by its kinematics. The fourth and final objective of the study was to present recommendations for novel, anatomically-based components that would complement the surgical instrumentation.

Specific Objectives of the study were as follows:

1. Characterize the geometry, position, and orientation of the articular surfaces of the ankle joint relative to anatomical landmarks in the foot and leg using a 3D digitizing arm and numerical optimization Routines in Matlab.

2. Develop a prototype alignment jig with cutting guides that can be adjusted to allow precise cut planes based on the specific information from Objective 1.

3. Examine the transverse plane orientations of simple ankle replacement components as determined by the relative anatomy and motion at and around the talocrural joint.

4. Provide recommendations for a novel, anatomically-based total ankle design.

1.6 Hypotheses

The initial portion of this study was concerned with basic data collection in order to characterize the shape and position of the talocrural joint surfaces. Hypotheses were as follows:

1. The 3D orientations of the articular surfaces of the talar dome and distal tibia can be calculated by fitting a simple geometric shape to the surfaces, such as a cylinder.

2. A repeatable relationship can be found across specimens between the orientations of the tibial and talar articular surfaces and the positions and orientations anatomical landmarks on the foot and leg.

The second portion of this study focused on the optimum orientation of simple, cylindrical ankle replacement components as determined by the relative anatomy and motion about the talocrural joint. Hypotheses were as follows:

1. Simple cylindrical components, unconstrained in translation and rotation in the transverse plane, will seat themselves in a repeatable position and orientation after being subjected to a series of cyclical plantar/dorsiflexion movements.

2. The cylindrical components will exhibit coupled motions observed as cyclical internal and external rotations in the transverse plane relative to the plantar/dorsiflexion movements at the talocrural joint.

1.7 Nomenclature

2D	Two-Dimensional
3D	Three-Dimensional
AF	Ankle Fusion (Arthrodesis)
AP	Anterior-Posterior
CS	Coordinate System
CPCS	Cut-Plane Coordinate System
DF	Dorsiflexion
IM	Inter-malleolar Axis
LCS	Local Coordinate System
MA	Motion Analysis
MTP	Metatarsophalangeal
OA	Osteoarthritis
PF	Plantarflexion
PF/DF	Plantarflexion/dorsiflexion
ROM	Range of Motion
RA	Rheumatoid Arthritis
TAA	Total Ankle Arthroplasty
THA	Total Hip Arthroplasty
TKA	Total Knee Arthroplasty
UHMWPE	Ultra-high molecular weight polyethhylene

CHAPTER 2. REVIEW OF LITERATURE

2.1 The Ankle Joint

2.1.1 Functional Anatomy

In order to fully understand the purpose of ankle arthroplasty, as well as the inherent difficulty associated with the procedure, a thorough understanding of ankle joint geometry and function is necessary.

The ankle is officially classified as a hinge joint, and is actually composed of multiple articulations that combined, allow for movements such as dorsiflexion (DF), plantarflexion (PF), slight circumduction, inversion, and eversion. The talocrural joint is the articulation between the tibia, fibula and the talar dome, and is mainly responsible for plantar/dorsiflexion (PF/DF). It is the talocrural joint that is usually considered to be the "primary" ankle joint, and is the joint that is resurfaced or replaced in TAA. Another joint of the ankle is the sub-talar joint, which is the articulation between the talus and the calcaneus that provides the inversion and eversion motions.

In addition to the bony support provided by the malleoli, the talocrural joint also receives substantial support from ligaments and other soft tissue structures. The medial side of the joint is spanned by a large, thick, triangular arrangement of ligamentous strands called the deltoid ligament. The deltoid is composed of the posterior tibiotalar, the tibiocalcaneal, the tibionavicular, and the anterior tibiotalar ligament strands which together provide support against excessive eversion and/or pronation movements. The lateral side of the talocrural joint is spanned by smaller, weaker ligaments, including the posterior talofibular, calcaneofibular, anterior talofibular, and tibiofibular ligaments, all of which help to protect against excessive inversion and/or supination. Due to a combination of less-robust bony anatomy and less support from the weaker ligaments on the lateral side the most common mechanism for ankle sprains is excessive inversion. The ligaments of the talocrural joint also function to maintain congruency between the talus and the tibia during plantar/dorsiflexion. Some researchers have even hypothesized that the ligamentous structures of the ankle act as a four-bar mechanism that dictates proper talocrural motion (Leardini et al., 2000).

Range of motion of the talocrural joint varies across the literature but generally is reported to be around 70 degrees of full motion, although this number is dependent on loading conditions and measurement technique (Boone and Azen, 1979; Weseley et al., 1969; Sammrco et al., 1973; Wright et al., 1964). The typical breakdown of total talocrural motion is usually around 30-40 degrees of plantarflexion, and about 10-20 degrees of dorsiflexion (Boone and Azen, 1979; Roas and Anderson, 1982; Weseley et al., 1969). Michelson and Helgemo (1995) reported slightly different mean PF and DF values for 13 cadaveric lower extremities in an axial loaded testing apparatus of 33.5 degrees (SD = 3.15) and 26.4 degrees (SD = 1.8)respectively. The authors of this study also noted a coupling of PF and DF with internal and external rotations. At maximum range of motion (ROM) values, PF was coupled with about 1 degree of internal rotation, while DF was coupled with around 2.5 degrees of external rotation.

Talocrural ROM during gait has been generally reported to be about 30 degrees during the stance phase (Kadaba et al., 1989; Murray et al., 1964; Stauffer et al., 1977). ROM values have been found to decrease with both age (Allinger and Engsberg, 1993) and disease, such as arthritis (Stauffer et al., 1977). Increasing cadence during gait while keeping step length consistent will decrease the total magnitude of talocrural ROM, while stair walking tends to exhibit increased talocrural ROM (Deland et al., 2000; Andriacchi et al., 1980). DF motion tends to be more important than PF motion with regards to activity. Normal daily activities are thought to require around 10-20 degrees of DF, while more athletic movements and stair climbing is thought to require at least 20-30 degrees DF (Deland et al., 2000).

2.1.2 Morphology

The talocrural joint is composed of the dome-like trochlea of the talus and the distal tibia, as well as the medial malleolus of the tibia and the lateral malleolus of the fibula. The trochlea of the talus is also wedge-shaped; it is larger anteriorly than posteriorly (Figure 2.1 B) (Barenett and Napier, 1952; Hicks, 1953). Inman, in his 1976 book about the ankle joint, reported differences of up to 6mm between anterior and posterior medio-lateral widths in 100 cadavers, with the anterior dimension averaging 2.4 mm more than the posterior (Inman, 1976). The articular facet on the lateral side of the dome is larger than on the medial side, and is orientated at a slightly more acute angle than the medial facet (Deland et al., 2000). The malleolar facets of the tibia and fibula tend to be parallel to their corresponding surfaces of the talus (Inman, 1976).

The literature describing talar dome morphometry generally agree that the dome in a sagittal profile represents the arc of circle or cylinder in 2D (Figure 2.1A) (Barnett and Napier, 1976; Fessy et al., 1997; Leardini et al., 1999; Pappas et al., 1976; Reimann et al., 1986, Waugh et al., 1976). These studies have predominantly relied on radiographs to characterize the talar dome in the sagittal plane by fitting circular arcs to the profile of the dome. There is some disagreement in the literature, however, as to whether a single circular arc can be used to characterize the dome. While some researchers have suggested that a single cylinder is a good representation of the talar dome geometry (Fessy et al., 1997; Pappas et al., 1976) others support the idea that the geometry of the talar dome is both polycentric and polyradial (Barnett and Napier, 1952, Leardini et al., 1999; Waugh 1976). These authors suggest that the lateral profile of the talar dome can be characterized by a single circular arc in 2D, while the medial profile is actually characterized by two separate circular arcs of differing centers and radii. Barnett and Napier (1952) were the first to suggest that the medial profile of the talar dome was characterized by one circular arc that described the anterior third of the talar dome, while the posterior two-thirds of the dome was described by a second arc. Waugh and colleagues (1976) described the articular surface of the talus as a toroidal cylinder with the lateral side having a larger radius of curvature than the medial side.

Despite the fairly small group of studies over the past 30 years that have attempted to describe the talar dome's circular or cylindrical shape in 2D, there are few studies that have examined the geometry of the talar dome in 3D. One study by Medley et al. (1983) examined the surface of the talar dome across its width in an attempt to characterize the talocrural joint as a hydrodynamic concave-convex bearing. These authors examined three cadaver tali and collected data points along anterior-posterior (AP) lines parallel to the AP axis of the foot at several intervals across the articular surface from medial to lateral. These lines were then fit to circular arcs by using a 2D least squares method in order to compare tibial and talar radii of curvature values and the congruency of the interface between the two surfaces. Thus, while the work did examine several areas of the joint, the final analysis was mainly a 2D method. The work by

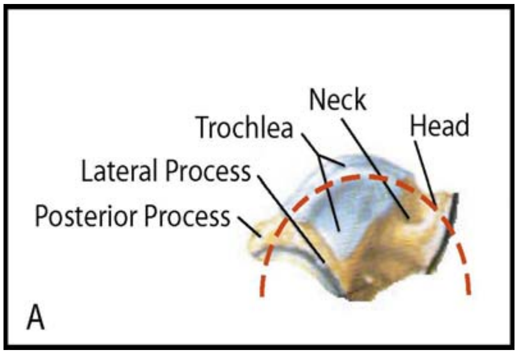

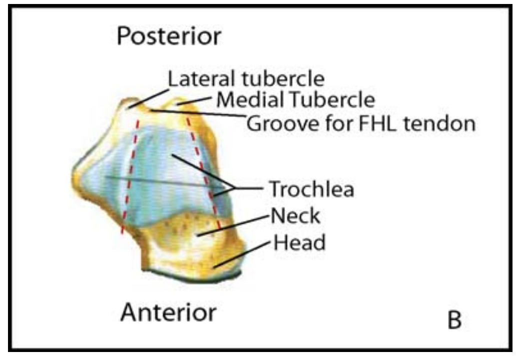

Figure 2.1 A) Lateral view of the talus. Note how curvature of the trochlea approximates a cylinder. B) Superior view of the talus. The dashed red lines demonstrate with how the trochlea is wider anteriorly. Adapted from Netter, F. *Atlas of Human Anatomy*, 1989.

Medley and colleagues did provide data that facilitated comparisons of medial and lateral radius values across the joint. In the study, the AP data points deviated from the circular arcs by about a mean of 0.5mm, and the medial and lateral profiles varied by around 5 percent (Medley et al., 1983).

Regardless of the number of proposed radii that describe the geometry of the talar dome, many of the aforementioned studies report quantitative radius of curvature values for their respective experiments. These values tend to vary across the literature, ranging from less than 18mm to over 28 mm for the talar dome alone. Barnett and Napier (1953) in their early description of the ankle did not provide quantitative values for the talar dome radii of curvature; rather, they described the dome qualitatively. Pappas et al., (1976) referenced values used in an earlier prosthesis, the Newton ankle, as having a radius of curvature of 24 mm, however, there is no specific mention of how this value was obtained. A study by Waugh and colleagues (1976) examined the talar articular surface of 32 cadavers and reported values ranging from 17.8 to 25.4 mm. Fessy et al. (1997) reported a smaller average talar dome radius of 17.7 mm, with a standard deviation of 0.9 mm for 50 subjects using lateral radiographs. Medley et al. (1983), in their quasi-3D study of three cadaver ankles, found the average radius radii of curvature for the tibia and talus to be 20.8 mm and 22.1 respectively. Leardini and colleagues (1999) used a 2D, four-bar linkage numerical model to estimate the radius of curvature for the talus and reported values ranging from 22 to 28 mm. Finally, in a recent study by Stagni and colleagues (2005), a novel, semi-automated radiographic system was used to calculate morphological measurements of the talocrural joints and the associated skeletal anatomy. This study examined 36 subjects and calculated mean radii of curvature values of 23.4 mm (SD =3.1) for the talus, and 27.8 (SD = 4.4) for the tibial mortise.

The axis of movement for the talocrural joint is often assumed to generally lie between the medial and lateral malleoli. While total ankle motion is actually a complex combination of relative talocrural and subtalar motion, individually these joints are often assumed to function as simple hinges. This assumption has been shown to be a reasonable approximation of relative ankle joint motion, but is also recognized as an oversimplification of the talocrural joint (Scott and Winter, 1991).

Barnett and Napier (1952) were the first to report that the axis of the ankle is not a fixed horizontal axis; instead it is an oblique axis that changes orientation according to relative plantar/dorsiflexion. In his detailed book about the ankle, Inman (1976) notes that the plantar/dorsiflexion axis of rotation for the talocrural joint lies just distally to the tips of the malleoli, and is slightly oblique to the articular surface of the talocrural joint. The axis tends to decline laterally in the frontal plane, and postero-laterally in the horizontal plane. Due to this oblique orientation of the movement axis, the foot tends to evert in DF and invert in PF (Deland et al., 2000; Inman, 1976). Sammarco (1977) also analyzed talocrural motion in the sagittal plane in live subjects using radiographs and determined that the instantaneous center of rotation of the ankle joint moves across the dome of the talus during plantar/dorsiflexion. Lundberg et al. (1989) analyzed the axis of the talocrural joint and concluded PF axes are more horizontal or have a more downward and medial inclination than the axes of DF (Figure 2.2 & Figure 2.3).

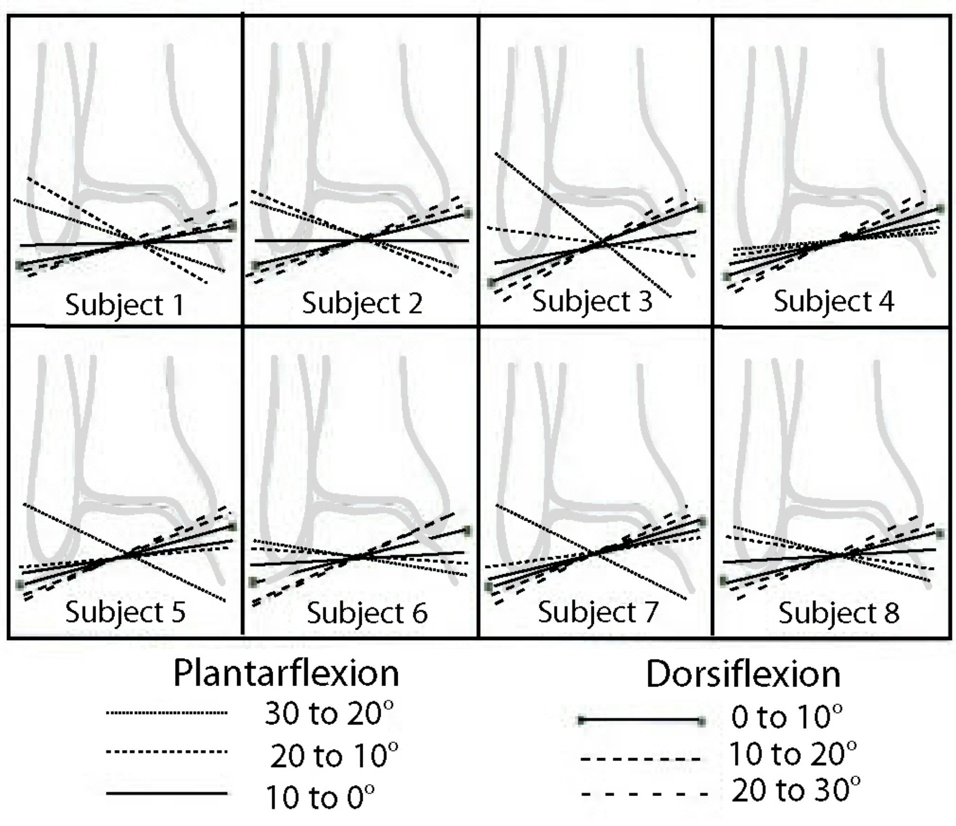

Figure 2.2 Individual discrete helical axes of the ankle joint of eight normal subjects for each 10 deg. interval from 30 deg. of plantarflexion to 30 deg. of dorsiflexion, projected onto a coronal plane. (Lundberg et al., J Bone Joint Surg 1989, 71-B, 96).

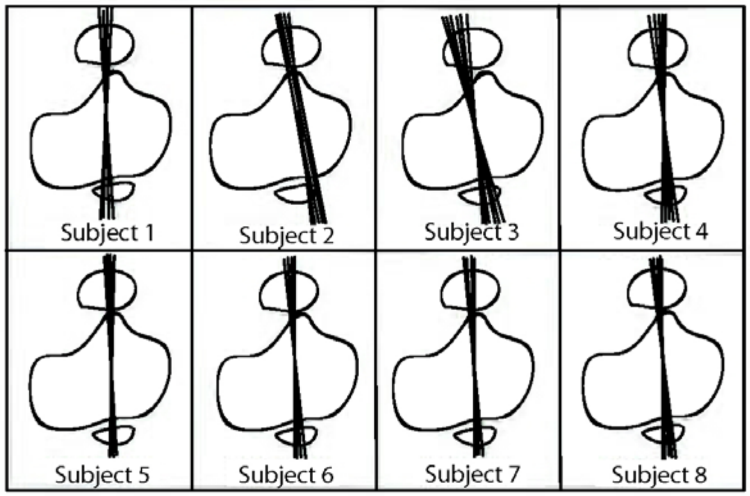

Figure 2.3 Individual discrete helical axes projected onto a horizontal plane in eight normal subjects. Axes tend to fall parallel to a transverse plane through the center of the malleoli (Lundberg et al., J Bone Joint Surg 1989, 71-B, 96).

2.2 Total Ankle Arthroplasty

2.2.1 1st Generation TAA

Accounts of the occurrence of the first ankle replacement surgery differ in the literature, although the date of 1970 is generally agreed upon. One report credits Buchholz with the first TAA (Sodha et al., 2000) while other reports credit Lord and Marrot (Gill et al., 2002; Stamatis and Myerson 2002). Also worth noting are reports of Dr. Morron Murdock attempting TAA in early 1970's using an inverted hip prosthesis (Gould et al., 2000; Henne and Anderson, 2002), although this attempt was quite unsuccessful. Following these initial attempts, a barrage of TAA designs began to emerge, comprising the group that is commonly referred to as 1st generation TAA. Early studies of 1st generation TAA systems showed promise in that initial results were quite good, however, over time failure rates dramatically increased as shortcomings of both the designs and surgical procedure emerged (Neufeld and Lee, 2000; Gill 2002). Problems such as aseptic loosening, infection, wound healing problems, improper alignment and reduced ROM soon lead surgeons to abandon TAA in favor of arthrodesis (Deland et al., 2000; Neufeld et al., 2000).

Many 1st generation TAA designs can be classified as either highly constrained, or almost completely unconstrained, but both tended to use bone cement to secure the prosthesis into the bone. Unconstrained designs included the Waugh/Irvine, the Smith, the Newton, and the St. George. These designs offered increased range of motion over their constrained counterparts, but also provided less stability. While the unconstrained nature did help to minimize the forces at the surface interfaces, the lack of stability often lead to painful malleolar impingement, talar dislocation, and other soft tissue problems. (Sodha et al., 2000; Michelson, 2000).

Constrained designs included the ICLH, the Conaxial, the Mayo, and the Oregon. These designs provided more stability, but lacked range of motion and suffered from increased stresses at the interfaces. Often the constrained designs treated the talocrural joint as a simple hinge, which did not allow for natural coupled motions, torsional stress transmission, or natural rotations (Henne and Anderson, 2002; Michelson, 2000). This type of simplified, constrained motion lead to rapid loosening at the implant-bone interface and eventually to failure of the implants.

Another major problem with early TAA was the use of bone cement. The amount of bone resection required for the use of bone cement is too great, therefore exposing the more vulnerable soft, cancellous bone and leaving too little bone stock for fixation

(Nuefeld and Lee, 2000). Calderdale et al. (1983) noted that the removal of the cortical shell of the talus placed abnormal stresses on the remaining talar cancellous bone, and also noted that bone strength was non-uniform across the distal tibia. These findings indicate that there is minimal bone stock available for arthroplasty of the ankle joint, making resection to be a problem. Due to the inherent drawbacks of bone cement, most TAA procedures began using cementless fixation in the early 80's as an effort to reduce gross fixation problems at the bone-implant interfaces.

Besides the different types of constraints, different design philosophies were also used in early TAA. Early ankle replacements tended to focus more on representing a basic mechanical action with disregard to anatomy (hence, the early simple hinge designs) (Neufeld and Lee, 2000). Since there was no "gold standard" to go by, early designs showed great variety in their use of pegs, stems, bars, etc. Early designs also had polyethylene tibial components that would experience high stresses causing wear that would lead to osteophytes, aseptic loosening and other complications.

First generation TAA systems also experienced problems attributable to operative procedure and surgeon error. There was little or no instrumentation available to insert the prostheses in the early days of TAA, leaving issues such as distraction and alignment purely up to the subjective eye of the surgeon (Henne and Anderson, 2002). Lack of experience with the procedures, as well as a basic ignorance for the proper kinematics of the ankle at the time, led to a high rate of failures caused by complications like infection, mal-alignment, loosening, and wear.

Several of the issues of early TAA components were addressed in the late 1970's to mid-1980's by the key researchers of the period. For one, early polyethylene tibial components were replaced with metal components. In addition, in 1976, the New Jersey TAA was developed by Buechel, and it was one of the first systems to recommend ligament tensioning using different size polyethylene thickness on a free- floating polyethylene bearing. Freeman was the first to develop instrumentation for TAA, and Schultz is credited as the first to install a porous coated, non-cemented implant in 1984 (Gould et al., 2000).

Despite these improvements in the early 1980's failure rates ranging up to 60% were noted in most follow-ups greater than a few years, causing surgeons to revert back to arthrodesis and other methods (Sodha et al., 2000). While TAA fell out of favor, it was not abandoned altogether. The success of hip and knee replacement in recent years has rekindled interest in TAA. This change in thought is fueled by improved technology, a better understanding of ankle kinematics and kinetics, and a desire to improve upon the often problematic ankle fusion. The revival in TAA from the late 80's to the present is generally referred to as 2nd generation TAA.

2.2.2 Second Generation TAA

The 2nd generation implants can be classified as either 2-component or 3-component, semi-constrained designs. Whereas 1st generation TAA systems were designed as simple, mechanical reproductions of general motion, 2nd generation TAA systems better replicate the native anatomy, and incorporate a medium of constraint that has led to improvements in the performance of these more modern implants. In addition, most 2nd generation TAA systems do not use bone cement to secure the implants to bone, but rely on skeletal in-growth. Basic 2-component designs feature resurfacing components for the talus and the tibia, while 3-component designs feature these with the addition of an articulating meniscal bearing, usually constructed of ultra high molecular weight polyethylene (UHMWPE). The inclusion of the bearing is an attempt at stress shielding by increasing the contact area and congruency between components, as well as an attempt to improve the kinematics by allowing rotation and gliding. An example of a 2-component design is the Agility, while 3-component designs include the Buechel-Pappas, LCS and STAR. A variety of design types are also seen, ranging from congruent designs (spherical, cylindrical, etc.) to incongruent (trochlear, convex, concave, etc.) (Neufeld and Lee, 2000).

Second generation ankle replacements have indeed shown great improvements over their early predecessors, although there are still a variety of problems associated with them, and long-term results are still discouraging (Neufeld and Lee, 2000). Recent studies have shown failure rates after long term follow-up for second generation implants to range between 20-60% leaving doubt as to the merit of the procedure (Gould et al., 2000; Henne and Anderson, 2002; Sodha et al., 2000). Those studies that do report high success rates are often reported by the designers of individual implants, and studies have shown a lack of repeatability in their findings (Koefed et al., 1998).

Second generation implants also continue to exhibit a variety of the problems that existed in first generation implant systems such as infection and wound healing problems, implant wear and aseptic loosening, nerve damage, fractures, and impingement which can be attributed to the surgical procedure (Conti and Wong, 2001; Rockett et al., 2001). Second generation TAA systems rely more on alignment instrumentation during implantation than 1st generation systems, but much of the alignment procedure is still based on subjective assessment. The complication rate of the surgery has been correlated with the difficulty and attention to detail associated with the TAA procedure, as well as a surgeons ability to overcome the steep learning curve associated with the procedure (Stamatis and Myerson, 2002).

Malalignment and high contact stresses are two major problems associated with 2nd generation TAA. A normal foot goes through 0.9 million gait cycles per year leading to a potential of 500,000 wear particles per step, which suggests the potential buildup of billions of particles that can lead to osteolysis and aseptic loosening (Deland et al., 2000). Studies have shown that the ankle joint can experience between 3.5-5.5 times body weight in force per step, which can generate huge contact stresses between implants (Sharkey and Hamel, 1998; Stauffer, 1977). Research suggests that the use of a mobile bearing may reduce shear stresses, as well as maintain congruency between interfaces (McIff, 2002). Nevertheless, finite element analyses (FEA) of the mobile bearings have shown extremely high non-uniform stresses in the bearings due to small variations in design. Attaining proper alignment, or even knowing what constitutes proper alignment, remain unresolved issues. Even a small degree of off-axis loading can result in abnormal shear stresses and moments that are transferred either to the polyethylene bearing, or to the bone-implant interface leading to loosening. Alternating tension/compression forces on different sides of a tibial base plate can cause micro-motion that will inhibit bony in-growth and prevent proper fixation (Gill et al., 2002). Research has also shown that errors in alignment of only 4 degrees valgus or more can lead to significant pain and implant morbitity (Pyevich et al., 1998, Saltzman et al., 2004).

2.2.3 Soft-tissues and TAA

Ligament balance is a major concern in maintaining the stability of the ankle joint as well as proper congruency. Even the slightest deviations in ligament tensioning (1-2mm) can lead to significant problems such as impingement, pain, implant dislocation, and implant loosening (Newton, 1982; Stamatis and Myerson, 2002). Recent studies by Leardini and colleagues (1999, 2000) have suggested that ligament balance at the ankle joint is critical in the success of TAA, based on sagittal plane anatomical and computational studies. This research assumes that the tibiocalcaneal and the calcaneofibular ligaments maintain isometric tension throughout the motion of the ankle in order to maintain congruency of the surfaces, and allow for variation in the center of rotation as the anatomy dictates the normal kinematics of the ankle. It should be noted that these studies are done in an unloaded state and that the ankle complex is assumed to function as a four-bar mechanism, while the joint itself is modeled as a simple “unrestrained” single degree of freedom joint. Saltzman et al. (2004) examined perturbations to TAA alignment during walking in cadaver specimens using the Agility TAA system. The effects of mal-alignment on the peri-articular ligaments such as the anterior and posterior talofibular ligaments, the calcaneofibular ligament, and the tibiacalcaneal ligament were studied using differential variable reluctance transducers. The results of this study showed that for tibial displacements from neutral, all the examined ligaments exhibited atypical changes in length. The anterior talofibular ligament was sensitive to transverse plane displacements, while the tibiocalcaneal ligament was sensitive to coronal plane displacements (Saltzman et al., 2004). Conti and Wong (2001) also stressed the importance of ligament balance and alignment when they reported that even the smallest varus/valgus deviations in component placement can lead to medial gutter impingement, sub-fibular impingement, lateral foot pain, and abnormally high stresses on any polyethylene components.

2.3 Current TAA Systems

2.3.1 The Agility System

The Agility ankle prosthesis was developed by Dr. Frank Alvine and DePuy orthopaedics, and is currently the only FDA approved TAA system used in the United States. The original design of this second-generation, semi-constrained implant was first used in patients between 1983 and 1987 (Saltzman and Alvine, 2002). The components are porous and press-fit, so no cement is used. The Agility consists of two components; a cobalt chromium talus, and a one-piece titanium-backed tibia with a polyethylene insert secured to it. The design of the Agility allows for internal and external rotation as well as medial/lateral translation because the tibial piece is wider than the talar piece. The implant is inserted so that 20 degrees of external rotation is incorporated to approximate the orientation of the intermalleolar axis. The interface between the components allows 60 degrees of flexion/extension. The components are available in 6 different sizes to accommodate size variance in the patient population.

Surgical Techniques

The Agility TAA system has its own specially designated instrumentation for aligning and inserting the prosthesis. The patient is supine, and an external fixator is applied medially to distract the ankle. The talocrural joint is typically distracted around

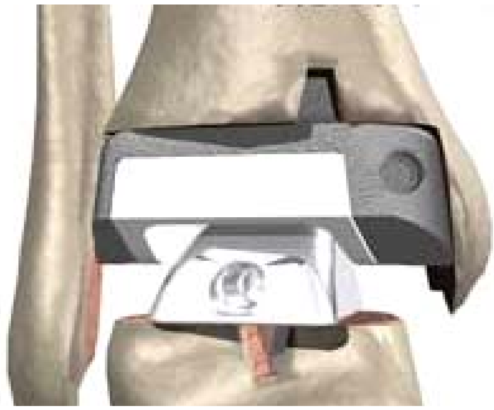

Figure 2.4 The Agility ankle composed of a titanium tibial piece with a UHMWPE bearing, and a cobalt chromium talar component (DePuy Orthopaedics, Inc., www.agilityankle.com).

5-10 mm, and varus/valgus alignment is controlled with the external fixator. An anterior approach is used to open the joint capsule between the tibialis anterior and the extensor hallucis longus tendons, and an antero-lateral approach is performed at the tibiofibular syndesmosis (Pyevich et al., 1998).

An alignment jig is then fixed to the tibia using the tibial tubercle and tibial crest for positioning. The long rod of the jig is placed over the tibial crest to obtain coronal plane alignment, and parallel to the crest for sagittal plane alignment. This procedure is done using palpation and subjective observation by the surgeon. The tibial cutting jig is moved from medial to lateral and from proximal to distal using micro-dials until its position allows for the removal of all cartilaginous surfaces, including the medial and lateral malleoli. The Agility is obliquely rectangular, so it articulates with both the tibia and the fibula. Therefore, the removal of some bone tissue from the medial and lateral walls is necessary, but caution is exercised to remove as little bone as possible. The components are then inserted according to the cut locations, and their positions are confirmed by fluoroscope. A graft is then placed in the syndesmosis, and screws are used to help fuse it to provide better fixation and force transmission. Finally, the fixator is removed, and the skin is closed (Pyevich, et al., 1998; Agility video, DePuy).

Agility Literature

The Agility has been used in over 2000 patients in the US. Pyevich and colleagues were the first to report on intermediate-term outcomes for the Agility system. In their study, 83 patients were examined at an average follow-up of 4.8 years. Fifty-five percent reported that their ankles were not painful, 28% reported that their ankles were mildly painful, and 79% of patients rated the operation as very satisfactory (13% satisfied). Six percent of patients had undergone revisions, and 28% showed loosening or migration of components. Postoperatively the mean range of plantarflexion-dorsiflexion at follow-up for these patients was 36 degrees.

Several papers by Drs. Saltzman and Alvine, the creators of the implant, have reported follow-ups on the Agility implant, however, the same sample of patients are used in each study (Pyvich et al., 1998; Saltzman, 1999; Saltzman and Alvine, 2002). These papers summarize the results of the first 100 patients to undergo TAA with the Agility by stating that the implant yields reliable function and good radiographic stability at an intermediate follow-up (Saltzman and Alvine, 2002). Patient satisfaction was also evaluated in this study, with 79% of patients rating their satisfaction level as extremely satisfied, 12% satisfied, and 8 % as indifferent, disappointed, or unhappy. Soft-tissue balance is stressed, as well as proper alignment, and caution is advised as frequent intra and post-operative problems are still associated with the procedure or implant. The reports by Saltzman and Alvine (2002) also highlighted the potential for a high complication rate with the use of the Agility based on patient selection criteria, the necessary precision of the procedure, and the soft tissue balancing. Projected Kaplan-Meier survivorship curves were presented for 207 phase 2 Agility systems implanted from 1990-1996. Projected revision rates were 7% (15/207) with a 76% survival rate at 9 years, and the 95% confidence interval was 56.6%-95.5% (Saltzman and Alvine, 2002).

Rippstein (2002) reported on the success of three types of implants, the Agility, the STAR, and the Buecchel-Pappas (BP). For the Agility, 27 ankles operated on by the same surgeon were examined, 19 of which because of trauma, and 8 because of the presence of RA. Eight of the 27 patients had to undergo revision and several others had complications. Post-operative ROM in the patients averaged 20.6 degrees (range 9-38 degrees). The authors felt that use of the Agility necessitated the removal of large amounts of bone stock which left little room for future revision. Additionally, the lack of improvements in post-operative ROM, coupled with the difficult learning curve of the procedure eventually led to the abandonment of its use in favor of fusion (Rippstein, 2002).

A 2003 study by Myerson and Mroczek reported on a retrospective study of the first 50 patients who had undergone TAA with the Agility in order to examine the complications associated with the implant, as well as difficulty of the surgery. Patients were grouped by the first 25, and the second 25 to undergo TAA with the Agility. The authors found that the incidence of minor wound complication decreased from the first to the second group, as well as the number of intra-operative fractures. They also noted that the variance in component alignment decreased by 9% from the first to the second group. The conclusions of the study were that the implant was extremely difficult to insert correctly, and that a very difficult learning curve was associated with the procedure. The authors did note, however, that experience did correlate with a lower rate of complications.

Due to the infancy of the Agility system, there has been a lack of intermediate to long-term results reported in the literature. In a recent paper, however, Knecht et al. (2004) reported on seven to sixteen year follow-ups with 132 patients who had undergone TAA with the Agility system from 1984-1994. The mean follow-up period was nine years, and patients were surveyed by questionnaire. If available, patients' post-operative radiographs were re-examined to judge component subsidence or lucency. Thirty-six patients had died, and fourteen (11%) had undergone either revision of the implant or fusion. In all, sixty-seven implants were clinically followed and 90% reported satisfaction with the surgery and decreased pain. Radiographs showed that 19% had subtalar arthritis, 15% had talonavicular arthritis, 8% had syndesmosis nonunion, and 76% showed peri-implant lucency. Survivorship curves based on the results of this study indicated a 65% survival rate at 132 months for the implant.

2.3.2 The STAR

The STAR implant was developed in Denmark by Koefed. The STAR has been primarily used in Europe, where over 1000 implants have been inserted. The STAR does not currently have FDA approval in the US, but is undergoing clinical trials. It was initially concieved as a cemented implant, but eventually switched to a cementless design because the cemented version showed survivorship rates of less than 70% after 10 years (Sodha et al., 2000). The current STAR is a 3-component system with a highly polished tibial plate that has a flat surface and 2 pegs. The talar component has an AP rib for a stabilization, and spacer that is a polyethylene bearing with a flat dorsal surface and a concave plantar surface. The motion of the STAR is restricted by soft tissue such as the ligaments and tendons, as well as the malleoli (Gittens, 2002). The implant is available in 5 sizes, with a thickness range for the poly spacer of 6-10 mm (Gould et al., 2000). Functional ROM is 10 degrees dorsiflexion to 20 degrees plantar flexion.

Studies of STAR have shown varying complication rates. Gittens (2002) reported a 62% satisfactory rating of the STAR with complications including aseptic loosening, chronic pain with talar necrosis, technical difficulties, late infections, synovial fibrosis, and pre-existing failed arthrodesis. In a small study comparing the STAR with another cemented ankle replacement, at a mean follow-up for the STAR of 5.4 years, all 7 of the studied implants were performing well clinically at the time of the study, without signs of radiographic lucency (Wood et al, 2000). One STAR patient suffered an intra-operative malleolar fracture that was successfully repaired. The authors felt that the inclusion of

Figure 2.5 The STAR total ankle implant, composed of a metal tibia and talus with a free-floating polyethylene bearing (http://www.mayoclinic.org/checkup-2003/july-ankle.html).

the mobile bearing reduced contact stresses that resulted in less wear as observed through lucency examinations. In contrast though, Rippstein (2002) abandoned STAR because of unnecessary mallealor removal and talar side resurfacing.

2.3.3 THE BP New Jersey Low Contact Stress Ankle (NJLCS)

There are a few other implants that have been reported in the literature that are currently undergoing FDA trials in the United States. The Beuchel-Pappas NJ TAA uses a mobile bearing and has shown promising results, especially in more mild cases of arthritic intervention. Nevertheless, the same high complication rates plague this implant. According to Rippstein (2002) the BP TAA is easier to insert than either the STAR or Agility, so surgeon error is less likely to occur. The BP works similar to the STAR, but maintains the malleolar joints and talar sides. The BP, with a deep-sulcus, mobile bearing design was reported to have a survivorship of 93.5 % at 10 years as reported by its designers, but these data included prospective reports (Beuchel and Pappas, 2002).

2.3.4 Other TAA Systems

Koefed (1998) reported on his own, non-commercial prosthesis that used congruent cylindrical movement with a polyethylene meniscus, and a stainless steel talar cap and tibial plate. Results for this implant were around 75% survivorship at 10 years, although this information has yet to be duplicated and may not be attainable by others. The HINTEGRA Ankle, recently developed by Hintermann in Switzerland, attempts to specifically address issues such as minimal bone resection, ligament balancing, and contact stress. The components consist of a flat tibial piece, a conical talar component, and a UHMWPE congruent bearing. In a 2004 assessment of the results of 122 cases of

TAA using the HINTEGRA ankle, Hintermann and colleagues reported an 82 percent success rate at a mean follow-up of 18.9 months. The HINTEGRA Ankle provided an average ROM of 39 degrees, and showed good radiographic results post-operatively (no signs of lucency). In addition, other researchers have reported moderate success with the use of components composed of alternative materials such as ceramic implants (Takakura et al., 1990)

2.4 TAA Summary

While the long-term success of today's modern TAA systems is still unknown, the question still remains as to whether or not TAA is a valid procedure for orthopaedic surgeons to recommend to their patients who suffer from severe ankle pathology. A recent study by SooHoo and Kominski (2004) examined TAA using a decision model analysis method for end-stage ankle arthritis. Using utility factors taken from outcomes in the literature, the effectiveness of the procedure was assessed in quality-adjusted life years. These figures, combined with gross-cost estimates from Medicare and reimbursement data led to the conclusion that because TAA has not yet demonstrated predictable results with respect to durability and function, the procedure was not yet cost-effective. Despite this conclusion, the authors also noted that with future long-term, positive clinical outcomes, TAA does have the potential to be a cost-effective procedure as an alternative to arthrodesis (SooHoo & Kominski, 2004). In order for TAA to become a mainstream, successful procedure, significant improvements need to be made in all aspects of the procedure ranging from component design to surgical equipment and technique. To realize these improvements, a better understanding of the functional anatomy of the talocrural joint is needed.

CHAPTER 3. METHODOLOGY: TALOCRURAL ARTICULAR SURFACE EXAMINATIONS

3.1 Introduction

The following chapter details the methodology used to characterize the morphology and spatial orientations of the talocrural articular surfaces. The tibial and talar articular surfaces were mapped using 3D digitization, and cylinders were fit to the surfaces using least-squares optimization routines. The cylinder fits facilitated examinations of the general shapes of the articular surfaces, as well as a means to describe the static orientation of the surfaces with respect to the positions and orientations of surrounding anatomical landmarks.

3.2 Specimen Preparation

3.2.1 Specimens

Eight (8) fresh-frozen, non-embalmed, non-paired cadaver specimens were used for the microscribe experiments. Specimens were composed of the foot, tibia, and fibula and were purchased through medical suppliers and stored at -10° C until the time of testing. Each specimen was thawed just prior to experimentation in order to preserve the integrity of the tissues. Equal numbers of left and right, as well as male and female feet were tested with a specimen age range of 25-80 and a mean age of 60.25 years.

3.2.2 Radiographs

Prior to any data collection, reference radiographs were taken. The radiographs were taken in house using a KCD-12MC mobile x-ray unit (Toshiba America Inc., New

York, NY) with a technique of 2 mAs and 42 kV at 50 cm. The films were developed by radiology technicians at Penn State University Health Services. Both lateral (Figure 3.1) and anterior-oblique (Figure 3.2) views were taken to enable a multi-dimensional assessment of the joint surface positions as well as the placement of the steel markers. The anterior-oblique view was chosen over the straight anterior view because the 10-15 degrees of medial rotation in the oblique view provides a more definitive outline of the talar dome.

Figure 3.1 Lateral radiograph of the talocrural joint.

Figure 3.2 AP-oblique radiograph of the talocrural joint.

3.2.3 Test Preparation

Prior to testing, each specimen was subjected to the following anthropometric measurements: medial foot length (heel to big toe), lateral foot length (heel to 5th toe), forefoot width, heel width, medial and lateral malleolar height, malleolar width, and arch height. The measurements were taken in order to evaluate any possible relationships between joint surface orientations and foot anthropometry. Individual and mean values for these measurements are shown in Appendix A. After collecting the anthropometric data, a series of 19 landmarks on the foot, ankle, and tibia were implanted with 1mm steel beads. The landmarks represent points of reference that can be easily identified by a surgeon either visually or by palpation. A list of the landmarks is shown in Table 3-1. The beads were implanted by first using a spring loaded punch to create an indentation in the bone. Next, jeweler's forceps were used to insert the beads, and finally they were secured with cyanoacrylate adhesive. An example of the selected the landmarks are illustrated in Figure 3.3.

Table 3-1 List of anatomical landmarks and their abbreviated data labels.

LANDMARK NAME	FIG. LABEL
Tibial Crest (1-3)	TC (1-3)
Medial Malleolus	MM
Lateral Malleolus	LM
1st Metatarsal Head Plantar	MTH1T
5th Metatarsal Head Plantar	MTH5T
1st Metatarsal Head Dorsal	MTH1B
5th Metatarsal Head Dorsal	MTH5B
First TMT Joint	TMT 1
Base of Calcaneus	CB
Talus Medial Anterior Corner	TALMA
Talus Lateral Anterior Corner	TALLA
Talus Medial Posterior Corner	TALMP
Talus Lateral Posterior Corner	TALLP
Tibia Medial Anterior Corner	TALMA
Tibia Lateral Anterior Corner	TALLA
Tibia Medial Posterior Corner	TALMP
Tibia Lateral Posterior Corner	TALLP

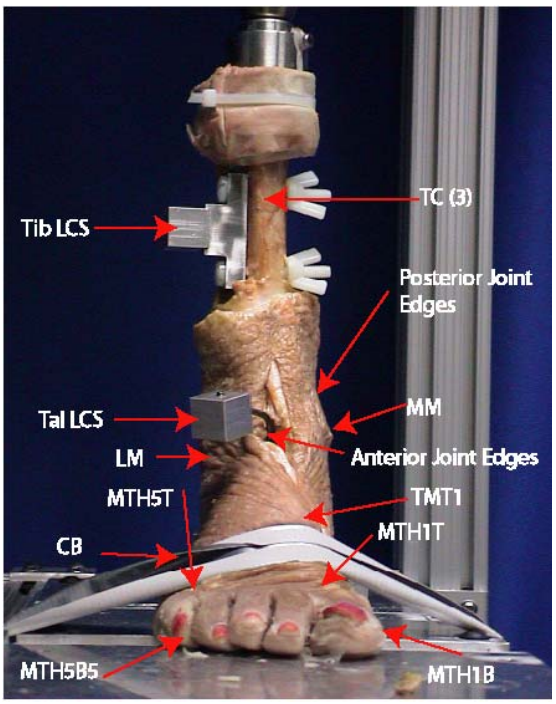

Figure 3.3 Anatomical landmarks and reference points of interest.

In addition to the steel beads, coordinate systems consisting of steel arms (for bony attachment) and 25 mm^2 aluminum registration cubes were secured to the tibial shaft and the talar neck. These registration cubes were used to establish local Cartesian coordinate systems fixed to the tibia and talus. These local coordinate systems facilitated positional transformations of the landmarks and joint surfaces. Finally, the proximal tibia was fitted with stainless-steel mounting hardware composed of an intermedullary shaft, fibular pin, and a pot filled with bone cement. The mounting hardware served to secure the proximal fibula to the tibia, as well as to provide a rigid connection between the tibia and the digitization frame. Once the intermedullary rod was implanted in the tibial shaft and the fibular pin was secured, the pot was filled with polymethylmethacrylate (COE Tray Plastic, GC America Inc.).

3.3 Intact Testing

3.3.1 Setup

Following preparation and radiography, each specimen was mounted in a custom-built digitization frame made from 80/20 aluminum (80/20 Inc., IN USA). The frame consisted of a set of adjustable base plates for the plantar surface of the foot, along with heel blocks and a calcaneal pin, a rigid bar fitted with a drill chuck to constrain the tibia, and platforms (upper and lower) for the digitizing arm (Microscribe model 3DX, Immersion Corporation, USA) (Figure 3.4). The foot was placed on the frame, and the base plates were adjusted so that the first and fifth metatarsal heads and the calcaneal markers could be seen from below the plates. The calcaneal blocks were adjusted to rest securely against the medial and lateral sides of the calcaneus, and the calcaneal pin was inserted through both blocks and the calcaneus. Next, the drill chuck was secured to the tibial hardware and tightened down to prevent any tibial movement. Finally, the forefoot was secured to the platform using duct tape.

Once each specimen was secured in the digitization frame, digitization of the intact foot was carried out with the digitizing arm was positioned on the upper platform. First, fiducial markers on the frame were digitized to establish a global XYZ coordinate system. Next, the talar registration cube was digitized to establish a talus-based local coordinate system (xyz). To do this, ten points on three mutually perpendicular cube faces were collected using standardized ordering of xz, yz, and xy planes. After the talus cube data was collected, the tibial registration cube was digitized using the same protocol. The bony landmarks listed in Table 3.1 were then digitized. All landmarks except for those on plantar surface of the foot were digitized with the digitizing arm on

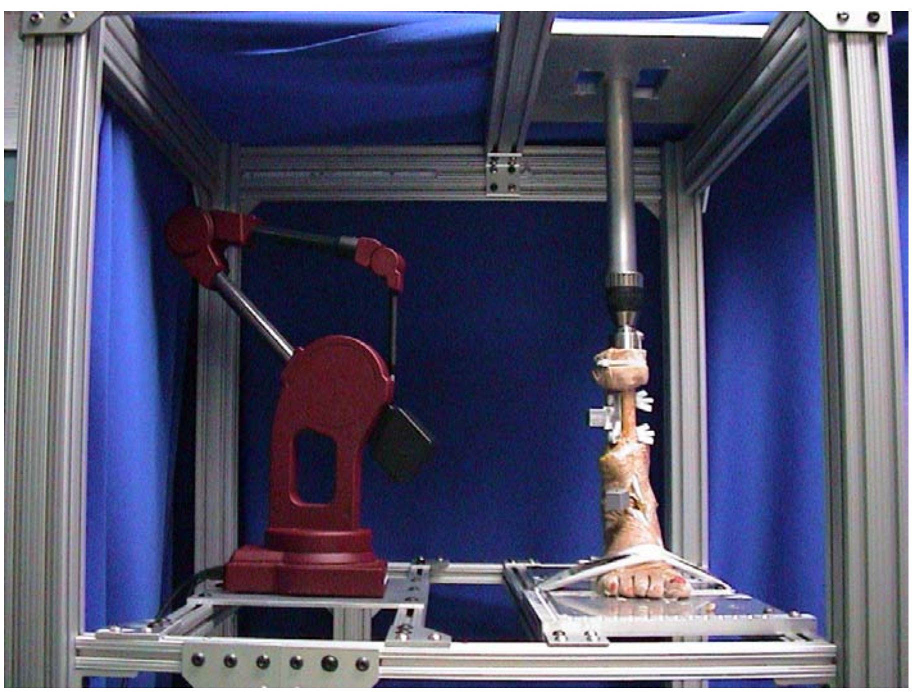

Figure 3.4 A foot mounted in the digitization frame along with the 3D digitizing arm.

the upper platform. The three plantar surface landmarks (first and fifth metatarsal heads and calcaneus) were digitized with the microscribe on the lower platform. The global coordinate system was preserved by re-digitization of the fiducial markers on the digitization frame.

The entire data collection protocol was performed 5 times. This redundancy ensured that usable data were collected in the event of procedural errors. This was a necessary precaution because once the foot was dissected, no further data could be collected.

3.3.2 Pilot & Reliability Testing

Prior to the onset of cadaver testing, a wooden foot model was used to troubleshoot the testing protocol and assess the repeatability of the microscribe test method. The wooden foot consisted of two pieces of wood that could be secured together to represent the intact foot, or separated to represent the dissected ankle joint (separate shank and foot). Steel markers were placed on the wooden foot in locations that approximated the anatomical landmark locations, and local registration cubes were attached to the upper and lower portions of the wooden model that represented the tibia and talus. The wooden foot was placed in the digitizing frame and secured in the same fashion as the cadaver specimens. In order to assess the reliability of the microscribe procedure in locating the 3D positions of the landmarks, the digitization testing procedure outlined previously was performed on the intact wooden foot model 10 consecutive times. Data were imported into Excel software for statistical analysis.

Following the 10 intact reliability trials, the wooden foot model was separated to represent the dissected ankle joint comprising a tibial half, and a talar half. Each of the separate halves was then used to develop the protocol for the joint surface data collection outlined in the following sections, as well as the Matlab analysis code.

In addition to the wooden foot reliability testing, a palpation study was also performed to evaluate the repeatability of locating the bony landmarks via palpations, as would be done in a surgical setting. One cadaver specimen was placed into the digitizing frame without the embedded steel beads to mark the landmarks. The intact digitizing procedure was then carried out ten consecutive times, using only palpation to identify the locations of the landmarks. For this test, only the locations of the external landmarks were digitized, including the medial and lateral malleoli, the 1st tarsometatarsal (TMT) joint, the plantar calcaneus, the plantar first and fifth metatarsal heads, and the dorsal first and fifth metatarsal heads. Data were exported into Excel for statistical analysis.

3.4 Articular Surface Data Collection

3.4.1 Talar Testing

Once the intact testing was completed for each specimen, the ankle was resected to isolate the talus from the rest of the foot and ankle. Care was taken to not disturb the registration cubes needed to define the local coordinate system. The talus was completely removed from the foot and cleaned of soft tissues, and several screws were partially driven into the underside of the bone to serve as anchors for bone cement. A round aluminum fixture fitted with adjustable set-screws was used to pot the talus in bone cement to a level just below the articular surfaces. After fixation, morphological measurements were collected from the articular surfaces of each talus (Figure 3.5). The measurements for each specimen can be found in Appendix B.

Coordinate data were collected following the same protocol used in the intact data collection procedure. First, points on the local coordinate system cube were collected, followed by the anatomical landmarks. The anatomical landmarks collected included the four corners of the articular surface and a fiducial point on the marker mount. Next, points were collected on the articular surface. A grid was first mapped onto the bone by drawing ink lines onto the cartilage using a flexible guide to keep the lines straight. The grid consisted of perpendicularly crossing lines at approximately 1 mm spacing (Figure 3.6). After the grid was mapped onto the surface, data was collected using the microscribe. The microscribe tip was placed on a line and points were collected while the tip was moved along as well as in between lines. Each set of coordinate data for the talar articular surface was comprised of between 900 and 2000 data points, depending on the size of the specimen being examined.

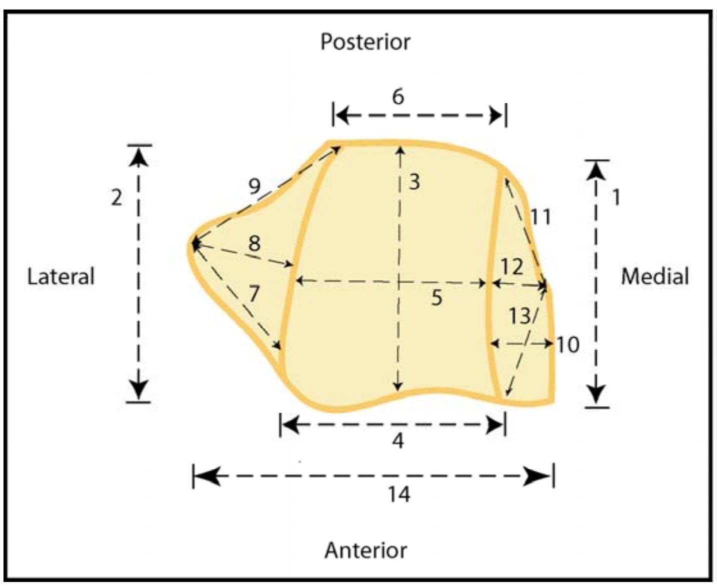

Label	Measurement
1	Medial Side Length (Ant./Post.)
2	Lateral Side Length (Ant./Post.)
3	Center Length (Ant./Post.)
4	Anterior Width (Medial-Lateral)
5	Center Width (Medial-Lateral)
6	Posterior Width (Medial-Lateral)
7	Lateral Side, Anterior Radius
8	Lateral Side, Center Radius
9	Lateral Side, Posterior Radius
10	Medial Side, Anterior Height
11	Medial Side, Posterior Radius
12	Medial Side, Center Radius
13	Medial Side, Anterior Radius
14	Overall Width (Medial-Lateral)

Figure 3.5 Morphological measurements of the talus.

Figure 3.6 A potted talus with the digitizing grid drawn on the articular surface of the talar dome.

3.4.2 Tibia/Fibula Testing

The tibia/fibula complex with the proximal cap was separated from the foot and all extraneous soft tissues were removed, with caution exercised so as not to damage the articular surface. Each tibia was secured in the digitization frame by inserting the stainless-steel rod on the tibial hardware into a rigid mount fixed to one of the base plates, inverting the articular surface. The proximal fibula was secured to the side of the mount with a bone pin, and the distal tibiofibular syndesmoses was left intact. Morphological measurements were collected from the articular surfaces of each tibia/fibula (Figure 3.7) and are presented in Appendix B.

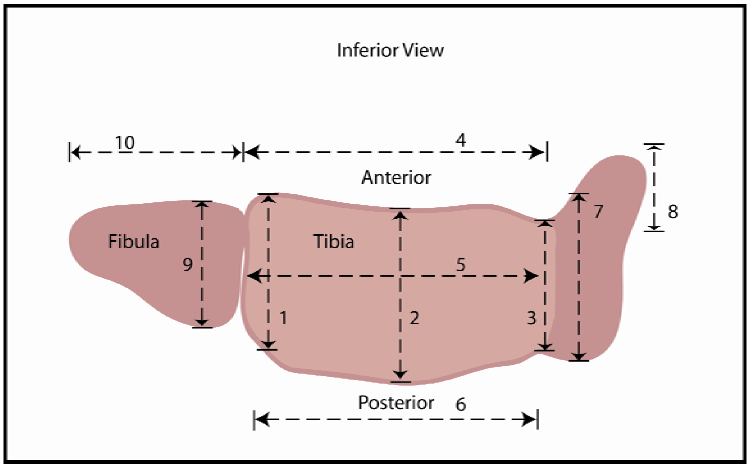

Label	Measurement
1	Medial Side Depth (Anterior-Posterior)
2	Center Depth (Anterior-Posterior)
3	Lateral Side Depth (Anterior-Posterior)
4	Anterior Width (Medial-Lateral)
5	Center Width (Medial-Lateral)
6	Posterior Width (Medial-Lateral)
7	Medial Malleolus- Wide Width
8	Medial Malleolus- Narrow Width
9	Fibula (Lateral Malleolus) Width
10	Fibula (Lateral Malleolus) Length

Figure 3.7 Morphological measurements of the articular surface of the distal tibia and fibula.

The articular surface digitization of the tibia/fibula complex followed the same procedure that was used for the talus. The anatomical landmarks digitized on the tibia/fibula included the medial and lateral malleoli and the four corners of the articular surface. After constructing the grid on both the tibia and fibula (Figure 3.8), points were digitized on the articular surfaces of each bone independently. Each set of coordinate data for the tibial articular surface was between 900 and 2000 data points, depending on the size of the specimen being examined. Data files representing the articular surface of the fibula ranged from 250-400 points.

Figure 3.8 A tibia with the 1mm x 1mm grid drawn on the articular surface with an ink pen.

3.5 Surface Positioning

3.5.1 Transformations

All data collected by the microscribe were saved as text files in Microsoft Excel. Once a data file was collected and saved, it was then imported into Matlab (Mathworks, V.7) for analysis. Custom Matlab code was written to read in the Excel data files, identify the landmark positions, and construct the coordinate system. An optimization routine was used to find the three planes of the local registration cubes in order to create a Cartesian coordinate system located at one corner of each cube (Figure 3.9). The optimization routine employed was the "lsqnonlin" (least-squares non-linear) function which utilizes the Levenberg-Marquardt optimization routine. The Levenberg-Marquardt algorithm is an iterative procedure that interpolates between the Gauss-Newton and gradient-descent search methods, and is commonly used for least squares curve fitting minimization problems. The method is considered more robust than the Gauss-Newton method in that it tends to find solutions even if the initial guess is far from the minimum. In addition, because the algorithm switches between Gauss-Newton and gradient-descent methods, it often reaches convergence faster than either method alone (Belegundu and Chandrupatla, 1999).

To establish the local coordinate systems, initial plane equations were formulated using the first three points from each of the cube faces. Then, the orientations of the initial planes were determined by a least-squares optimization that fit the planes to each of the ten collected points from each face. The intersecting corner of the three planes was designated as the origin, and a set of unit vectors was established at the origin point to represent the x, y, and z axes of the local coordinate system. The axes were oriented in the directions of the optimized planes and were mutually perpendicular to one another.

The optimization procedure used to establish the position of the cube faces, local coordinate systems, and anatomical landmarks was first performed for the intact foot, and was repeated for both the dissected talus and the tibia. Once separate files representing the intact foot (Figure 3.10), tibial surface (Figure 3.11), and talar surface (Figure 3.12) were established, a separate Matlab routine was used to perform a set of matrix transformations in order to describe the position and orientation of the joint surfaces within individual anatomical coordinate systems. These transformations are described by the following equation:

$P_L = [T_{LG}]^{-1} * P_G$

Where:

P_L = A vector (4 x 1) containing 3D coordinates of a point in the local reference system

P_G = A vector (4 x 1) containing 3D coordinates of a point in the global reference system

$[T_{LG}]$ = The transformation matrix (4 x 4) representing the position and orientation of the local Cartesian coordinate system. In this case, the transformation matrix is used to convert global coordinates to local coordinates. Explicitly, the transformation matrix T_{LG} is defined as:

$$\begin{bmatrix} 1 & 0 & 0 & 0 \\ Px & UVx1 & UVx2 & UVx3 \\ Py & UVy1 & UVy2 & UVy3 \\ Pz & UVz1 & UVz2 & UVz3 \end{bmatrix}$$

After the 3D position of the joint surfaces and landmarks were known with respect to local coordinate axes, a new series of transformations were used to find the positions of the joint surface data points within a global space representing the original, intact foot (local to global) using the following equation:

$P_G = [T_{GL}] * P_L$

For visual examination of the transformations, the landmarks that were collected in both the intact foot and dissected conditions were plotted on top of each other. The end result was a plot of two overlapping clouds of points that illustrated the articular surfaces of the bones coming together, as well as overlapping plots of anatomical landmarks (Figure 3.13).

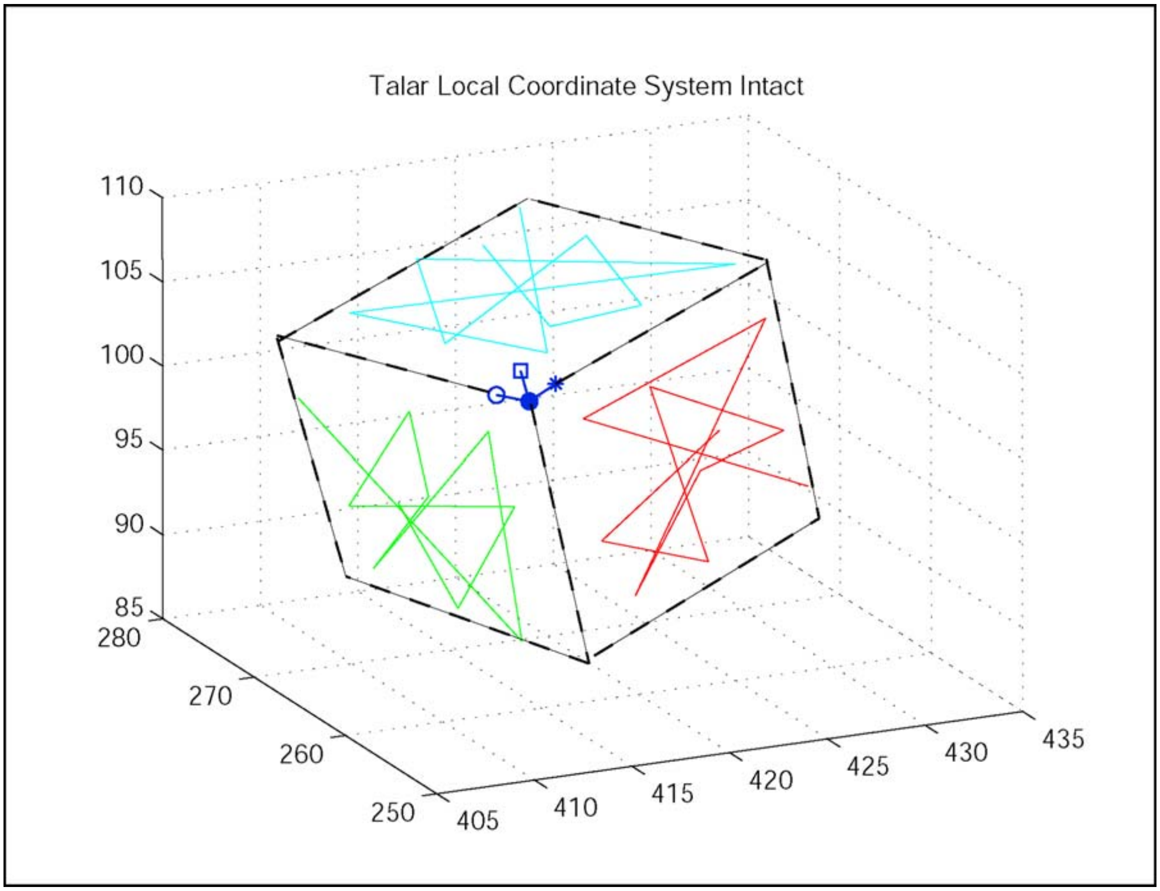

Figure 3.9 A Coordinate system derived from a CS cube. The color traces represent the 10 points digitized points on each cube face. The origin of the unit vectors that represented the local coordinate system was placed at the intersection of the three planes.

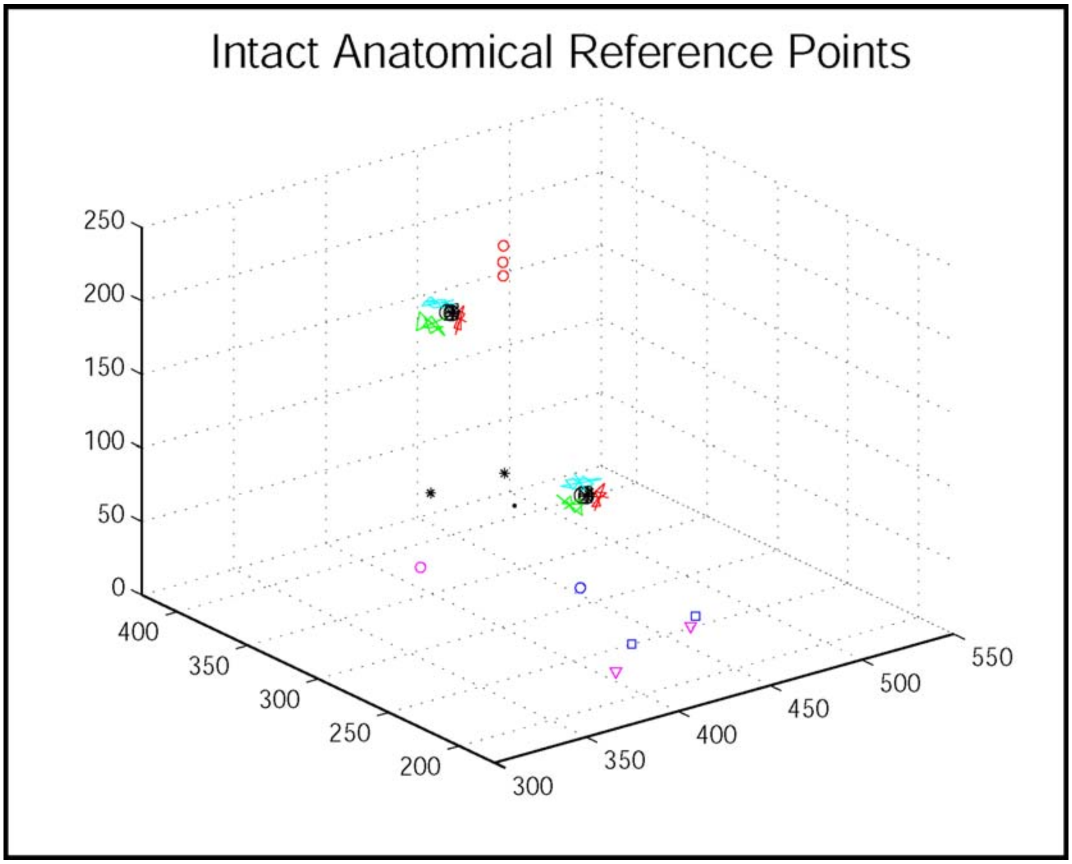

Figure 3.10 Initial plot of the landmarks and local coordinate systems for an intact specimen.

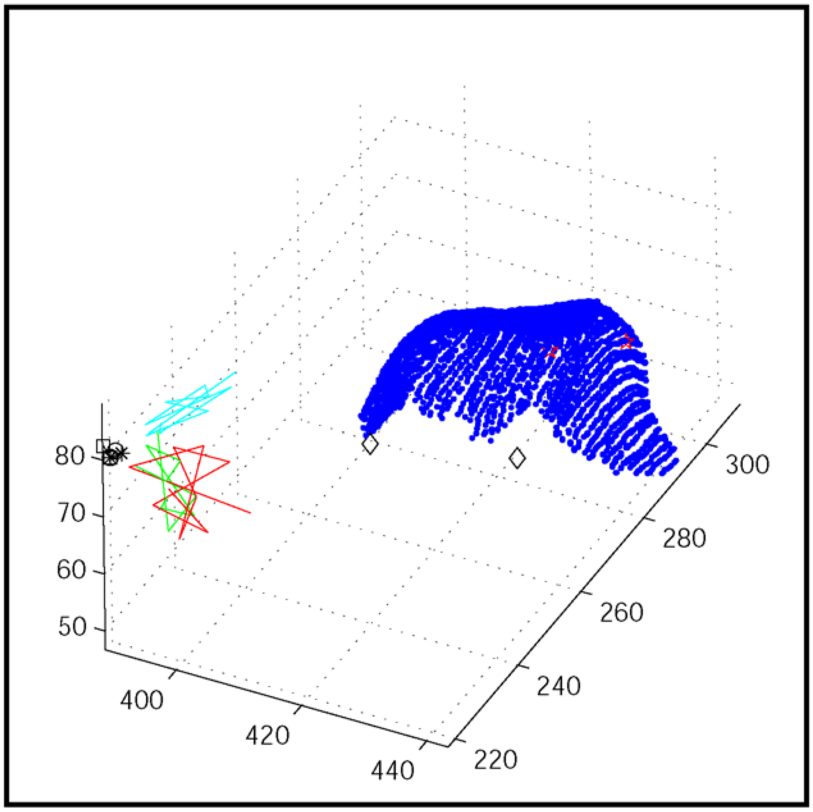

Figure 3.11 Cloud of points, landmarks, and the local coordinate system from a digitized talus. The black diamonds represent the position of the anterior corners of the articular surface. The red dots represent the posterior corners of the articular surface.

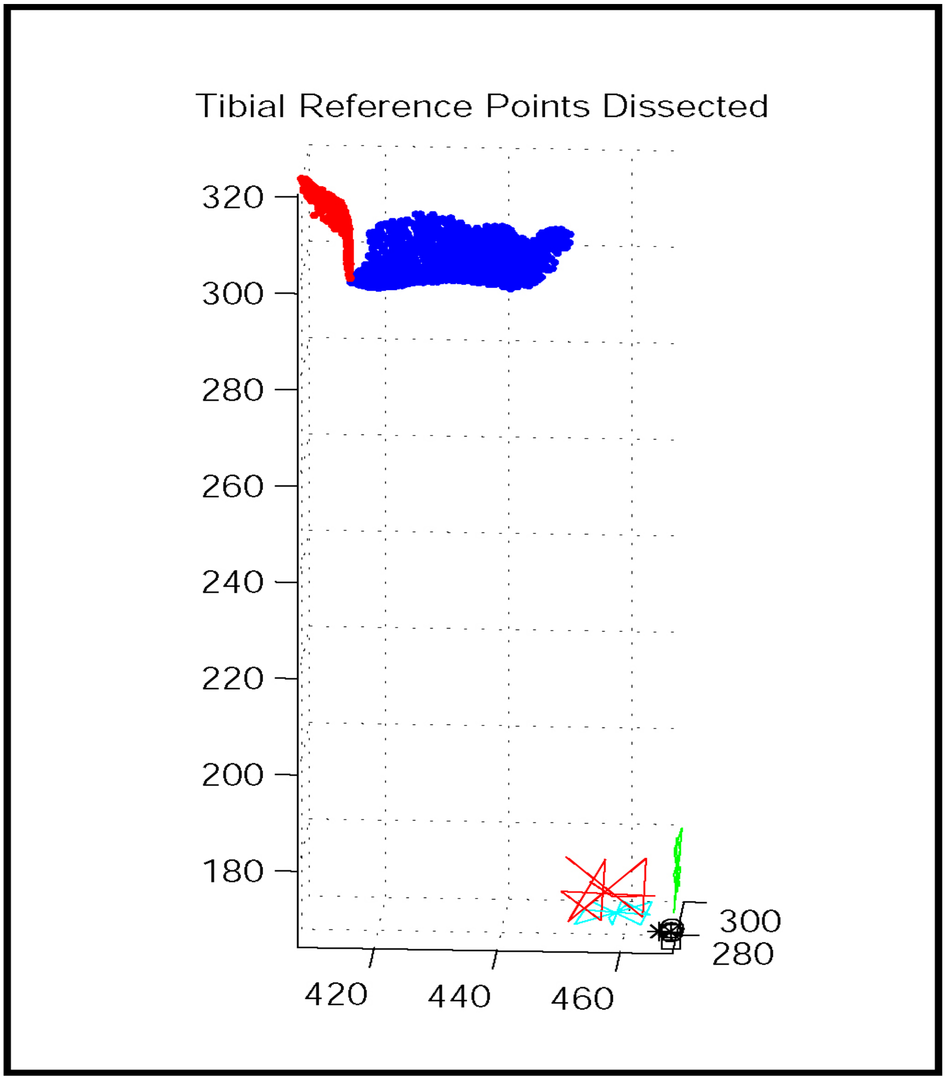

Figure 3.12 Cloud of points and local coordinate system for the tibia-fibula complex. The articular surface of the tibia is in blue, and the articular surface of the fibula is in red. The bone was inverted for surface digitization, hence the registration cube and local coordinate system at the bottom right of the figure.

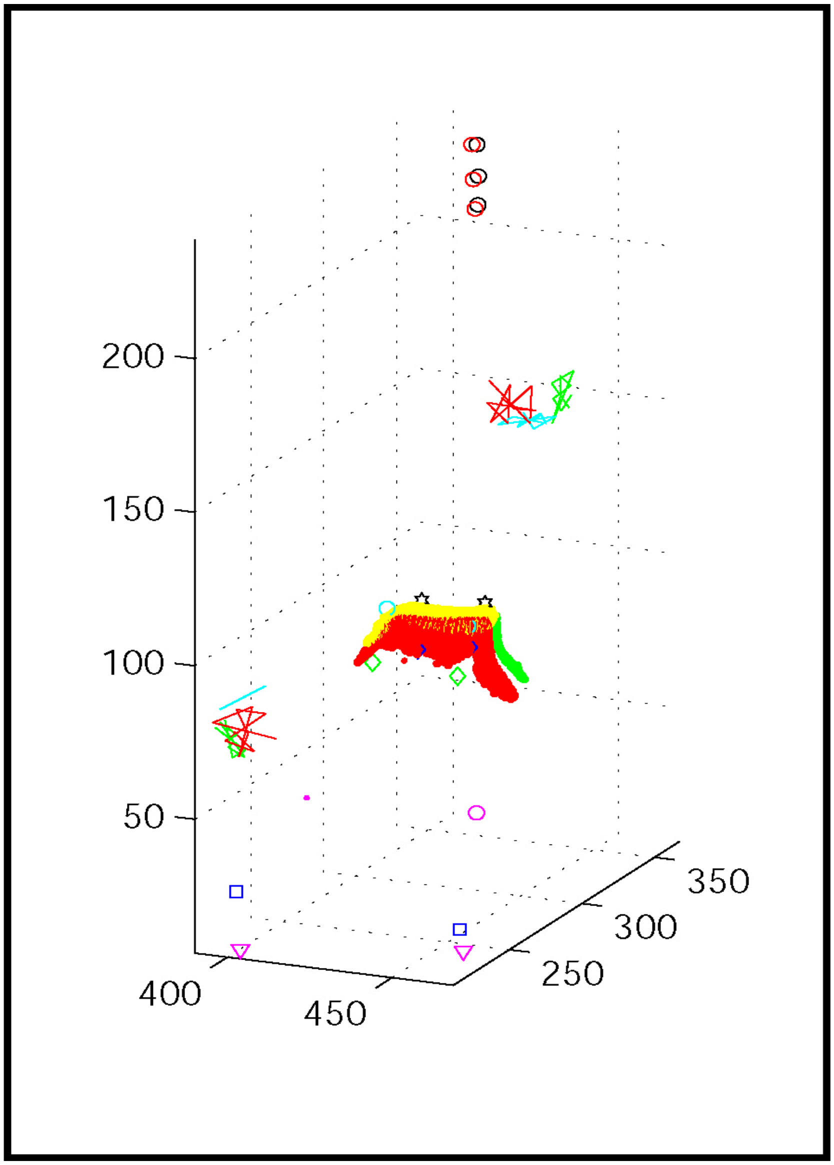

Figure 3.13 Point clouds and landmarks transformed back into their original, intact positions and orientations. The talus is in red, the tibia in yellow, and the fibula in green.

3.5.2 Cylinder Optimizations

In order to describe the position and orientation of the joint surfaces within the intact ankle joint, the surfaces needed to be characterized geometrically. Past research has supported the idea that the talar dome can be represented as a cylinder in the 2D sagittal plane (Fessy et al., 1997; Pappas et al., 1976), so for these experiments, the validity of describing the talocrural articular surfaces as cylinders was explored. First, the digitized points on the superior talar dome were isolated from the point clouds leaving only the superior articular surface, without the sides (Figure 3.14). Similarly, the articular surface of the tibia was isolated from the medial malleolus to only include the portion that articulated with the superior talar dome.

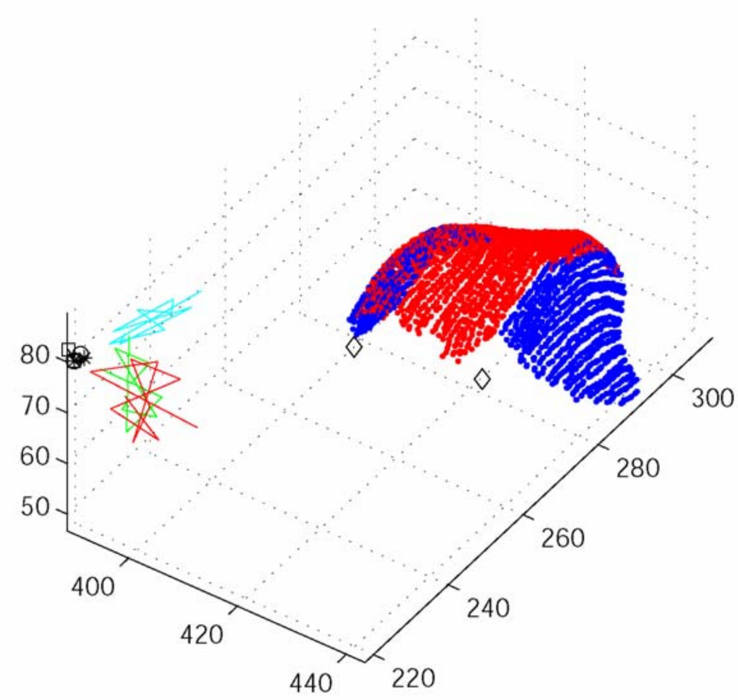

Figure 3.14 A cloud of points representing the articular surface of a talar dome. The red points represent the superior surface of the dome that was used for the cylindrical surface characterizations.

Before a cylinder could be fit to the articular surface points, values for the initial inputs to the optimization routine needed to be established. Several inputs were needed to describe a cylinder including a direction vector for the longitudinal axis, a point on that axis, and a radius. For the initial cylinder axis direction guess, the most superior points were chosen out of the first and last 200 data points, which yielded a medial point, a lateral point, as well as the vector connecting the two points. This vector was then translated inferiorly 15 mm to provide a point and a direction vector for the cylinder longitudinal axis guess. Guesses for the radius were generated randomly between 5 and 15 mm. Sensitivity trials involving different initial guesses for the radius showed that guesses that were too small (less than 5 mm) and guesses that were larger than the actual radius caused the optimization to fail. The upper limit of 15 mm for the random guess was chosen because it was below the actual radius values for both the male and the female specimens.

Once the initial guesses were established, the values were input into a least squares optimization routine in Matlab, similar to the routine used for the local coordinate systems. The objective function was specified to minimize the difference in magnitudes between the fit radius and the distance from the cylinder axis to each point using least squares. The resultant output were the parameters that described the best-fit cylinder including a direction vector for the longitudinal axis, a point on the axis, and a radius (Figure 3.15). The optimized cylinder output data for both the talus and the tibia were stored for later comparisons.

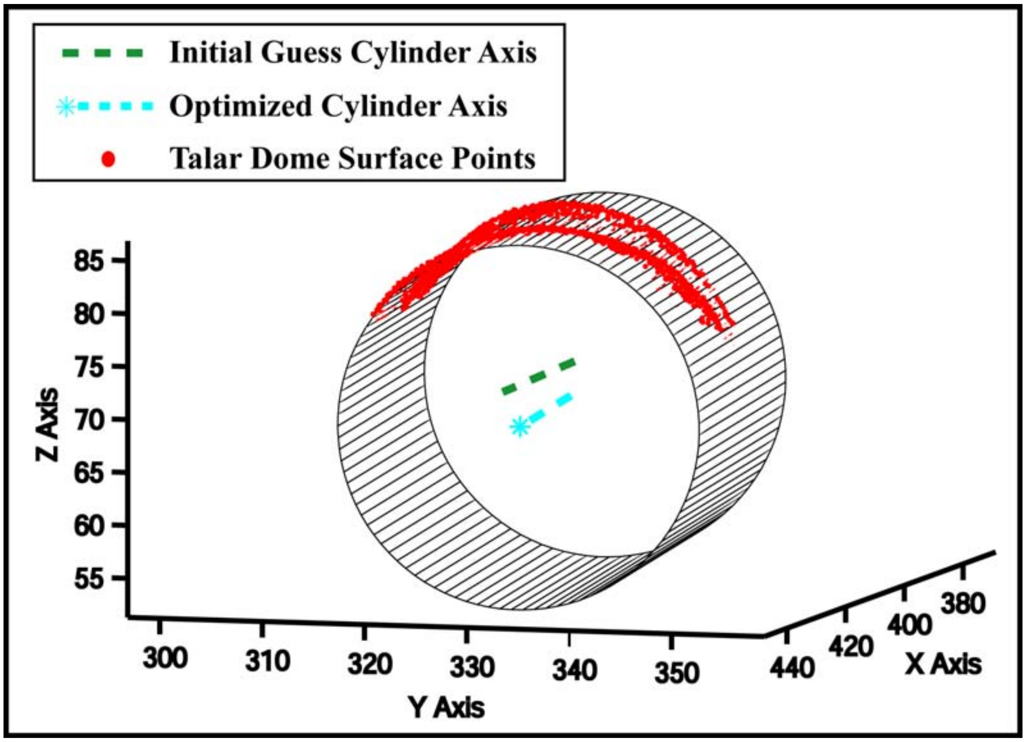

Figure 3.15 A cylinder fit to the digitized points of a superior talar dome by numerical optimization.

In addition to the cylindrical characterizations of the joint surfaces as a whole, additional characterizations were performed in order to address the saddle shape of the talocrural articulation. Since the saddle shape occurs primarily in the coronal plane, the joint surface data were split into medial and lateral halves. Using the same least-squares optimization routines, cylinders were fit separately to the medial and lateral sides of the selected surface points. After the medial and lateral halves of the surface were characterized cylindrically, comparisons were made between cylinder axis locations, orientations, and radii. Statistical comparisons for the talus and tibia were made between male and female radii, medial-fit and lateral-fit radii, as well as between talar and tibial radii for the whole-fits. The position and orientation of the cylinder axes of the talus and tibia were also compared by calculating the minimum distance and angle between respective vectors.

Single-point medial and lateral radius values were also calculated from surface data of the tibia and talus. The most superior data points on the medial and lateral edges of the joint surface data were located, and the perpendicular distances from the points to the optimized cylinder axes were calculated as the radius values on the medial and lateral sides. These acute values were calculated because they represented the maximum medial and lateral radii without the effects of averaging in points from the center of the joint surfaces, which tend to represent smaller radii due to the saddle shape of the bones. These values were considered to be comparable to the 2D estimates of radius of curvature from radiographs.

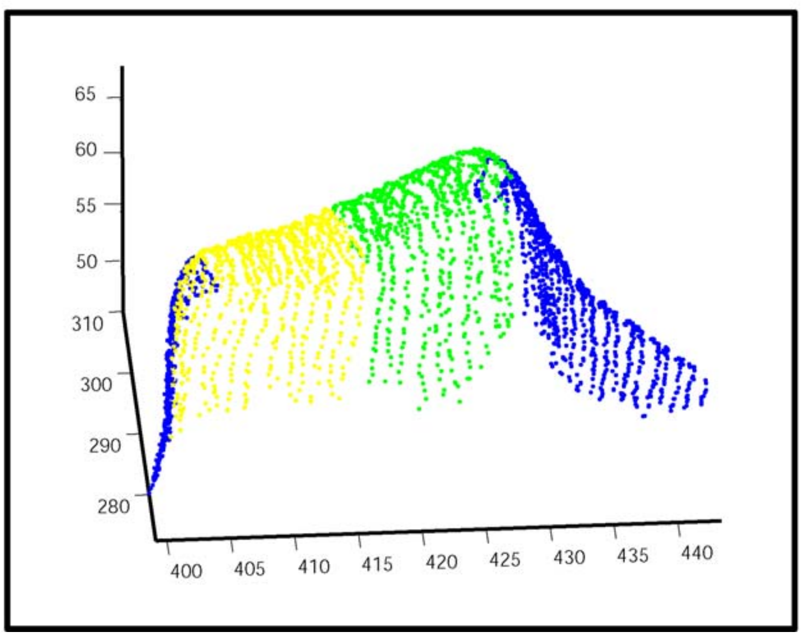

Figure 3.16 A cloud of points representing a digitized talar dome. The yellow points represent those used for the medial cylinder characterization, while the green points are those used for the lateral cylinder characterization.

3.6 Cut Plane Angles

3.6.1 Cut Plane Coordinate System

To examine the spatial relationships between anatomical landmarks and joint surface position and orientation as described by the optimized cylinder axes, a point of reference first had to be established. The point digitized on the dorsal surface of the calcaneus was chosen as the origin for a new, foot-based cut-plane coordinate system (CPCS) that would be used to calculate the orientations of the tibial and talar cylinders (Figure 3.17). The plantar surface of the foot (the ground) was chosen to be the xy plane of the coordinate system (CS). The x-axis of the coordinate system was coincident with the line that connected the origin at the calcaneus with the first metatarsal head. The first metatarsal head was chosen rather than the second or third because of the ease in locating it by palpation, both on the plantar and dorsal sides of the foot. A vector orthogonal to the x-axis was found by calculating the normal vector to the xy plane. This vector was used as the z-axis of the CPCS. The y-axis was computed by taking the cross-product of the z and x-axes. For left feet, the result was a right-handed Cartesian CS with the y-axis pointed laterally. For right feet, a left-handed Cartesian CS was established in order to have the positive y-axis point laterally, rather than medially. This was done by designating the negative of the cross product between the x and z-axes for right feet as the positive y axis. The rationale for using a left-handed CS was to create a system of reference that was independent of side and that would facilitate a design for a potential cutting jig that would be easy to set-up, orientate, and use. Once the CPCS was established, no mathematical calculations were performed that would be influenced by the use of a left-hand CS, such as cross product. Only rotational transformations and dot products were calculated within the left-hand CS space.

The CPCS established new quasi-anatomical reference planes for the ankle joint (Figure 3.18). Normally-defined anatomical planes for the foot are usually established with the AP axis to be between the 2nd and 3rd toes. The CPCS is slightly rotated from that normal convention since its AP axis lies along the 1st toe. As mentioned, the xy plane was equivalent to the plate (or ground), and represented the transverse plane in which internal and external rotations could occur. The yz plane represented the quasi-frontal plane, and the xz plane represented the quasi-sagittal plane. Since these tests were done in a static neutral pose and no movement was analyzed, it was not critical that the CPCS orientation was dictated precisely off of conventional anatomical planes of movement. Rather, only relative orientation angles were calculated between anatomical landmarks from the CPCS, so it was more critical that the convention was consistent across the experiment.

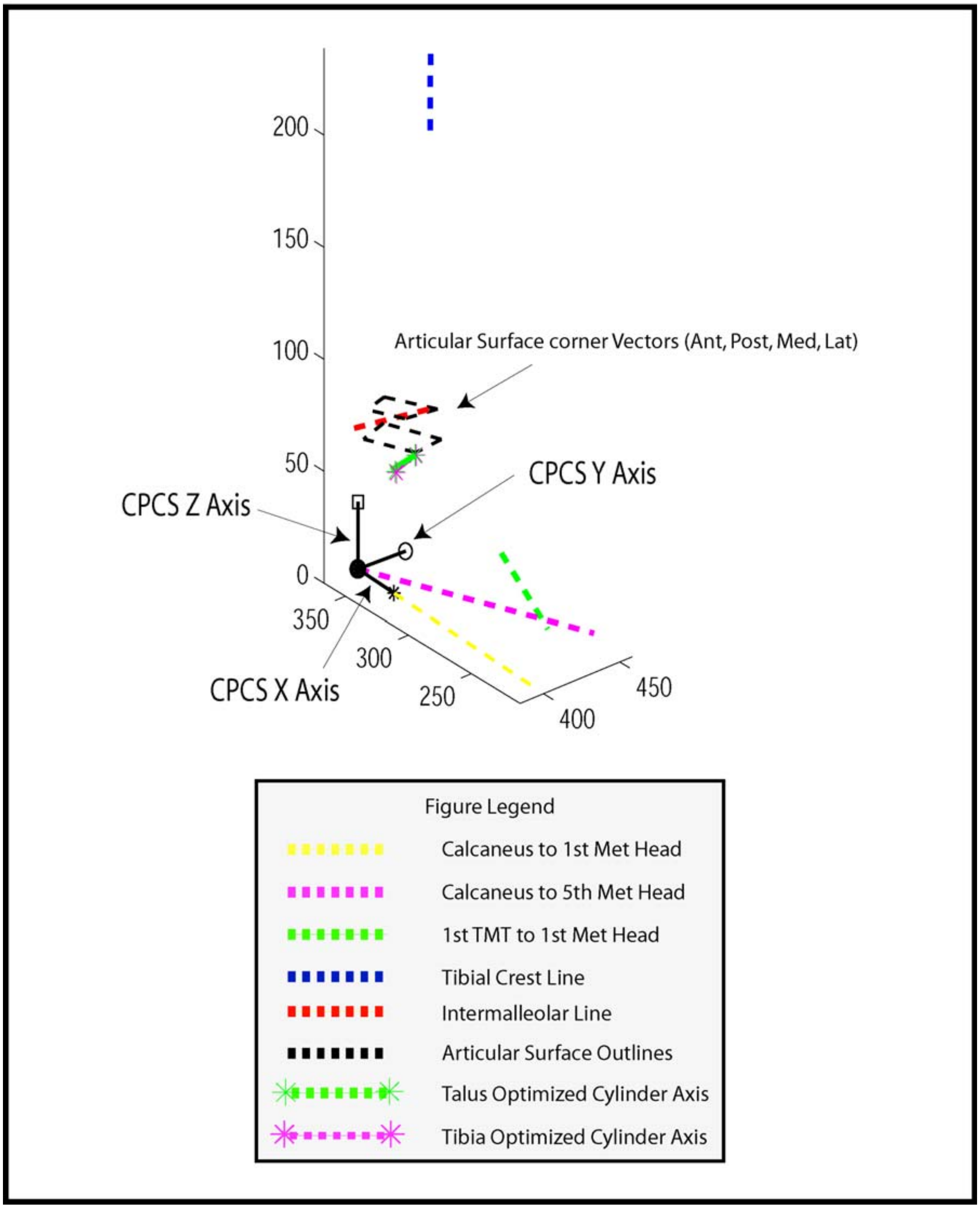

Figure 3.17 Cut Plane Coordinate System (CPCS) for a left foot, and vectors connecting the anatomical landmarks.

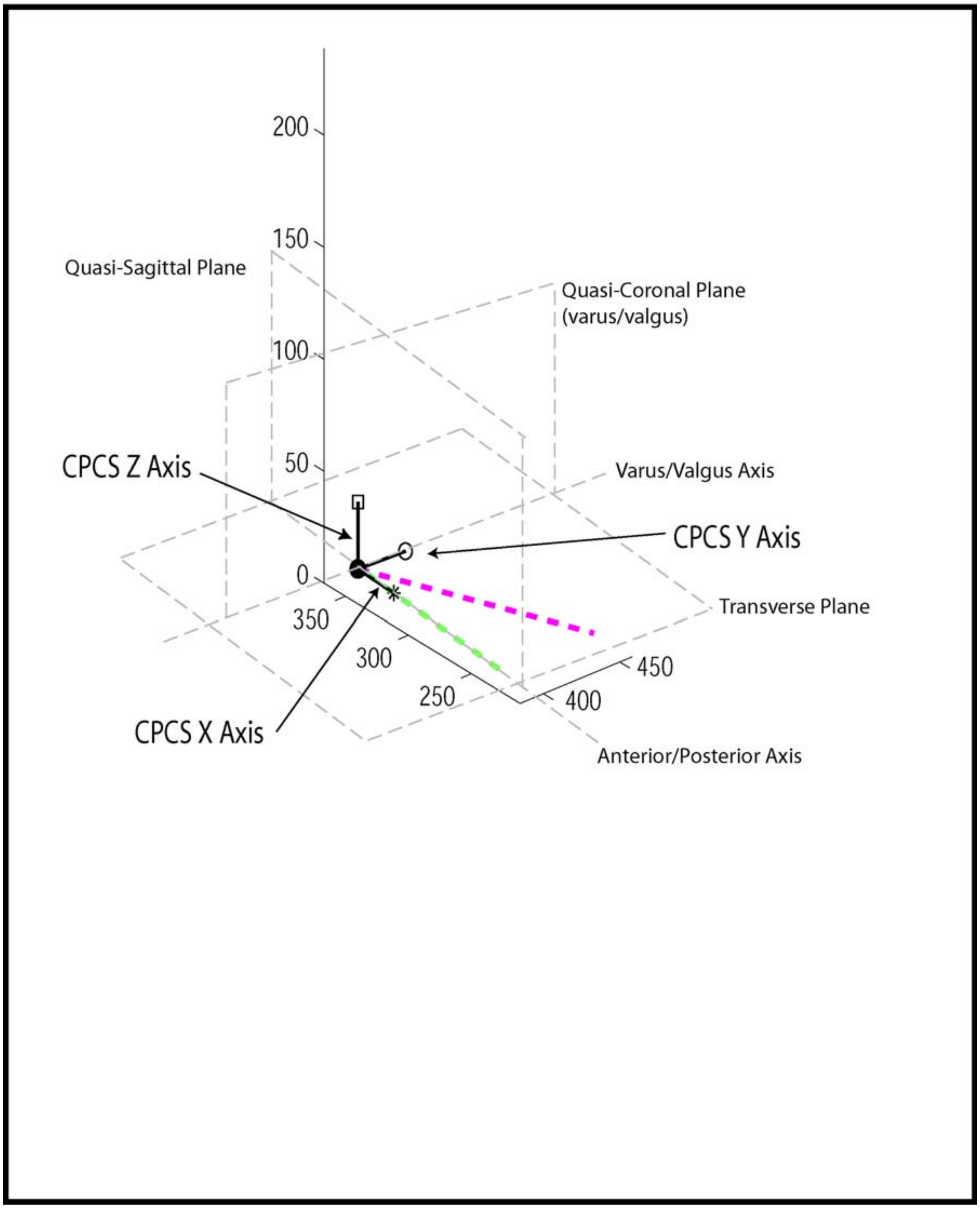

Figure 3.18 The anatomical reference planes defined by the CPCS unit vectors. The AP axis was directed along the first ray, which defines the quasi-sagittal plane (CPCS x-z plane). The CPCS y-axis was the reference for varus/valgus deviations, and the quasi-coronal plane was defined as the CPCS y-z plane. The transverse plane was defined as the CPCS x-y plane and represented the ground.

3.6.2 Orientation Angles

Once the CPCS was established for each specimen, vectors connecting relevant landmarks were plotted, such as the vector connecting the medial and lateral malleoli, the vector connecting the tibial crest points, and the vector connecting the calcaneus and the 5^{th} metatarsal head. The calculated cylinder axes for both the tibia and the talus were also plotted in the CPCS along with the four corner points for each joint surface, and the vectors connecting them. The cylinders were also plotted in the CPCS space for visual reference (Figure 3.19). All the coordinates for the landmarks and cylinder axes were transformed into the CPCS using homogeneous 4x4 transformation matrices. As a result, new rotated direction vectors were calculated for the vectors that connected the landmarks, as well as the cylinder axes.

With the positions and orientations of the landmarks and direction vectors all in the same CS, it was possible to calculate the orientation of the cylinder axes for the tibia and talus within the CPCS, as well as for the anatomical landmark vectors. First, to calculate the quasi-varus/valgus or frontal plane angle, the dot product of each cylinder vector and the z-axis were found using the following calculations:

Cylinder unit vector = cyl_uv [3 x 1]

*1) Dot product = cyl_uv * [0 0 1] * cos θ*

2) Varus/valgus angle = 90 - $cos^{-1}(\theta)$

This calculation provided the angle between the cylinder axes and the CPCS xy plane. Next, the rotations of the tibial and talar cylinder axes in the transverse plane were calculated. The rotation of each axis relative to the CPCS y-axis was calculated by taking the dot product of the cylinder axis and the CPCS x-axis (cyl_uv * [1 0 0] * cos θ) and adding 90 degrees. The result was a value that described the angle between the cylinder axis and the positive CPCS y-axis in the xy plane (the laterally pointing axis). The third orientation angle of the cylinder axes was less straightforward. Since a plane's orientation cannot be completely derived by a vector and two orientation angles, the sagittal orientation angle could not be calculated in the same manner as the varus/valgus and transverse orientation angles. Instead, the vectors on the medial and lateral sides of the joint surfaces that connected the anterior/posterior points were used to calculate the quasi-sagittal orientation, or tilt. The dot products of each of these medial and lateral vectors with the CPCS x-axis were computed in order to determine the angle of the talus and tibia cylinder axes within the CPCS xy plane.

Similar procedures were carried out for the intermalleolar (IM) vector, as well as the vectors connecting the anterior and posterior corners of the articular surfaces. The previously described dot products were computed, with the appropriate vector substituted for the cylinder axes unit vector. Thus, the same orientation angles that were computed for the cylinder axes were computed for these other vectors in the coronal and transverse planes. This allowed for later comparisons between the orientations of the anatomical landmark vectors and the orientations of the tibial and talar joint surfaces. For example, if an angle was calculated for a cylinder axis and the IM axis with respect to the same reference axis, then a simple difference (in degrees) could be found to compare their orientations.

A few of the specimens used for the experiments showed symptoms of hallux valgus upon visual examination. This condition can lead to bunions at the first MTP joint which may cause splaying of the toes, especially the first. If significant splaying of the metatarsals or deformation of the first metatarsal were present in any of the specimens, the orientation of the CPCS x-axis could have been influenced by the condition. Therefore, a second reference line was established in the AP direction to examine any errors in the CPCS x-axis position. The line was established in the xy plane and connected the CPCS origin with the mid-point between the first and fifth metatarsals respectively. This reference line, (AP midline) also represented a more traditional AP axis

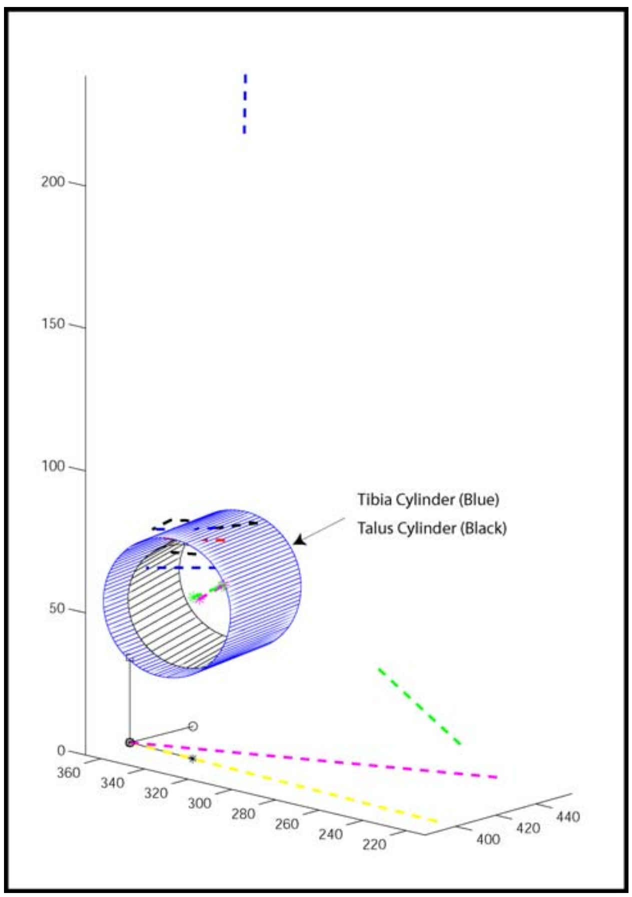

Figure 3.19 CPCS, Landmarks, and optimized cylinder plots for a left foot. Note that the tibia cylinder (blue) has slightly larger radius than the talus cylinder (black).

of the foot. The CPCS x-axis was then directed along the direction of the AP midline, rotating the entire CPCS externally. The orientation of the AP midline was compared to known vector orientation for other landmarks (such as the origin to the 5^{th} toe) to assess whether or not the original x-axis was skewed in any of the specimens due to hallux valgus.

Many current TAA surgical systems rely on the tibial crest as a reference for sagittal and coronal plane alignment, assuming that the tibial crest approximates the vertical line of action of the force in the lower extremity. The orientations of the components are then assumed to be perpendicular to the tibial crest in these planes. To assess whether the tibial crest was actually perpendicular to the ground, the dot product between the CPCS z-axis and the tibial crest was calculated. If the tibial crest is an accurate approximation of the line of force perpendicular to the ground, than the results of the dot product calculation should have been 90 degrees. Additionally, to examine the transverse plane orientation of the tibial crest in these experiments, the intersection of the tibial crest vector with the xy plane of the CPCS was found for each specimen. The vector connecting the origin to this point was calculated, and the angle between this new vector and the CPCS x-axis in the xy plane was computed.

3.6.3 Statistical Analyses

Frequency analyses of the distribution of values such as age, gender, whole radii measurements, and each anthropometric measurement were performed using SPSS (SPSS Inc., Release 11.5.0, Chicago,IL). Output was examined to identify whether or not distributions for each variable were normal (Guassian) or not. Following the frequency analyses, Student's two-tailed t-tests were used to compare the mean values of each measurement variable between gender, and between the talus and the tibia.

Radius of curvature values from the cylinder optimizations for both the tibia and the talus were compared statistically with the anthropometric and morphological data from each specimen. Data representing optimized radii, gender, age, whole foot anthropometric measurements (Section 3.1.3) and bone-specific morphological measurements (Section 3.2.3) were input into SPSS for statistical analysis. Pearson product-moment correlation coefficients were calculated to examine the strength of the relationships between the radius values and the other variables, with significance established at $p < 0.05$. In addition, it was thought that because sex differences were likely to exist in the size of the feet, it could also be possible that associations between radius and the other variables were spurious and caused by sex differences. Therefore, partial correlations were computed between radius and the other variables controlling for sex. Correlation tables can be found in Appendix E.

CHAPTER 4. METHODOLOGY: MOTION ANALYSIS EXPERIMENTS

4.1 Introduction

The following chapter presents a detailed description of the methodology used to perform a set of cadaveric experiments using motion analysis. The goal of these experiments was to further examine the transverse plane orientation of the talocrural joint using novel ankle replacement components. The components replaced the native joint surfaces in an effort to recreate the plantar/dorsiflexion kinematics, while remaining unconstrained in rotation and translation the transverse plane. It was hoped that the natural motion at the talocrural joint would influence the position orientation of the components causing them to move into a repeatable transverse orientation within the joint space. The final orientations of the components were then compared to the orientations of surrounding anatomical landmarks in order to examine any possible similarities across specimens.

4.2 Intact Tests

4.2.1 Preparation

For these experiments, five (5) cadaver lower extremities were used, with a mean age of 65.6 (range 59-79 years). Prior to testing, each specimen was fully thawed and acclimated to room temperature. Palpable landmarks on the foot and ankle were located and marked with 1 mm steel beads. The landmark set was the same set used in the microscribe experiments, with a few modifications. The set included the following landmarks: two points on the tibial crest, the medial and lateral malleoli, the first, second, and fifth dorsal metatarsal heads, the posterior calcaneus, the plantar aspect of the calcaneus, and the anterior medial and lateral corners of both the tibia and talus articular surfaces. The posterior corners of the articular surfaces were not marked with beads as they were in the microscribe experiments, leaving the total number of anatomical landmarks marked with beads to be thirteen.

Following the implantation of the beads, each specimen was radiographed in order to have a record of the intact talocrural joint prior to ankle arthroplasty. Both lateral and AP-oblique views were collected. After radiography, marker clusters were rigidly fixed to the tibial shaft, medial calcaneus, and the neck of the talus using wood screws. The marker clusters were composed of an aluminum mounting plate, aluminum arms, and four 10 mm diameter non-collinear plastic markers covered with reflective tape. Inter-marker distances ranged from 4-8 cm. A tibial cap with a drill rod shaft was secured to the proximal end of the tibia by inserting the distal end of the drill rod into the medullary canal of the tibia and tightening set screws around the outside of the bone in four locations. The fibular shaft was zip-tied to the cap to secure it in place.

The Motion Analysis (MA) camera system (Motion Analysis Corp., Santa Rosa, CA) was calibrated using the static calibration frame and the dynamic calibration wand (Figure 4.1) prior to placing each foot on the MA data collection stand. The calibration volume used for the experiment was approximately 60 x 60 x 60 cm. Mean calibration values used for the experiment were 0.1724 mm ± 0.1663 mm for the marker residuals, and 100.063 mm ± 0.1367 mm for the 100 mm calibration wand. The setup used for the MA experiments was a four camera configuration of Eagle cameras oriented around the specimen from anterior-lateral to posterior-medial. In order to capture a variety of views, the cameras were focused on different areas of the capture volume with focal lengths of 24, 35, 25, and 23 mm respectively. The data collection frequency used for all MA trials was 100 Hz.

4.2.2 Static Testing: Anatomical Landmarks

To begin the testing, each specimen was placed within the MA data collection stand. The stand consists of an aluminum mounting plate atop a frame built from 80-20 aluminum. An abrasive mat was glued to the plate to keep the foot from slipping, and the foot was further secured with duct tape around the forefoot and rear foot. A plate fitted with a drill chuck was secured to the tibial cap via the drill rod (Figure 4.2). This tibial plate had attachment points for the weight lines that passed downwards through guides in the mounting plate used for hanging weights. Each corner of the plate was fitted with a weight line so that the weight was evenly distributed over the tibial plate and

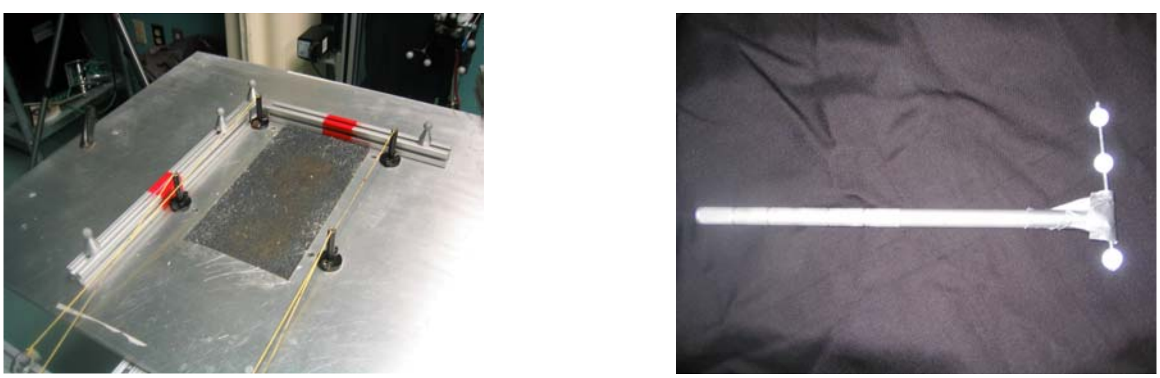

Figure 4.1 The static calibration L-frame and the 100 mm dynamic calibration wand.

the foot. Once the foot was secured on the stand, the weight racks were attached to the lines and weight could easily be added or removed. For the intact tests, 10 lbs were added to each rack for a total of 52 lbs (including the weight of the racks and the tibial plate). The specimens were initially placed in neutral pose as verified by a goniometer (90 degrees between the foot and tibia in the sagittal plane, 0 degrees varus/valgus in the coronal plane). An adjustable and removable 80-20 control arm held the tibia neutral position by securing drill rod just distally to the tibial cap.

The first trial collected with the MA cameras was a static pose of the foot in the neutral position (Figure 4.3). This trial was used to establish the template within the MA software that identifies each marker and groups the markers into their relative clusters. Next, the 3D positions of the previously identified thirteen anatomical landmarks were recorded using a pointer fitted with three 13 mm reflective markers spaced at intervals of 75, 125, and 166 mm from the tip (Cappozzo et al., 1997). In addition, in order to later establish local and global coordinate systems for data analysis, the positions of several other points were also recorded. These points included three non-collinear positions on the mounting plate and one point from each side of the drill rod that was inserted into the tibial medullary canal.

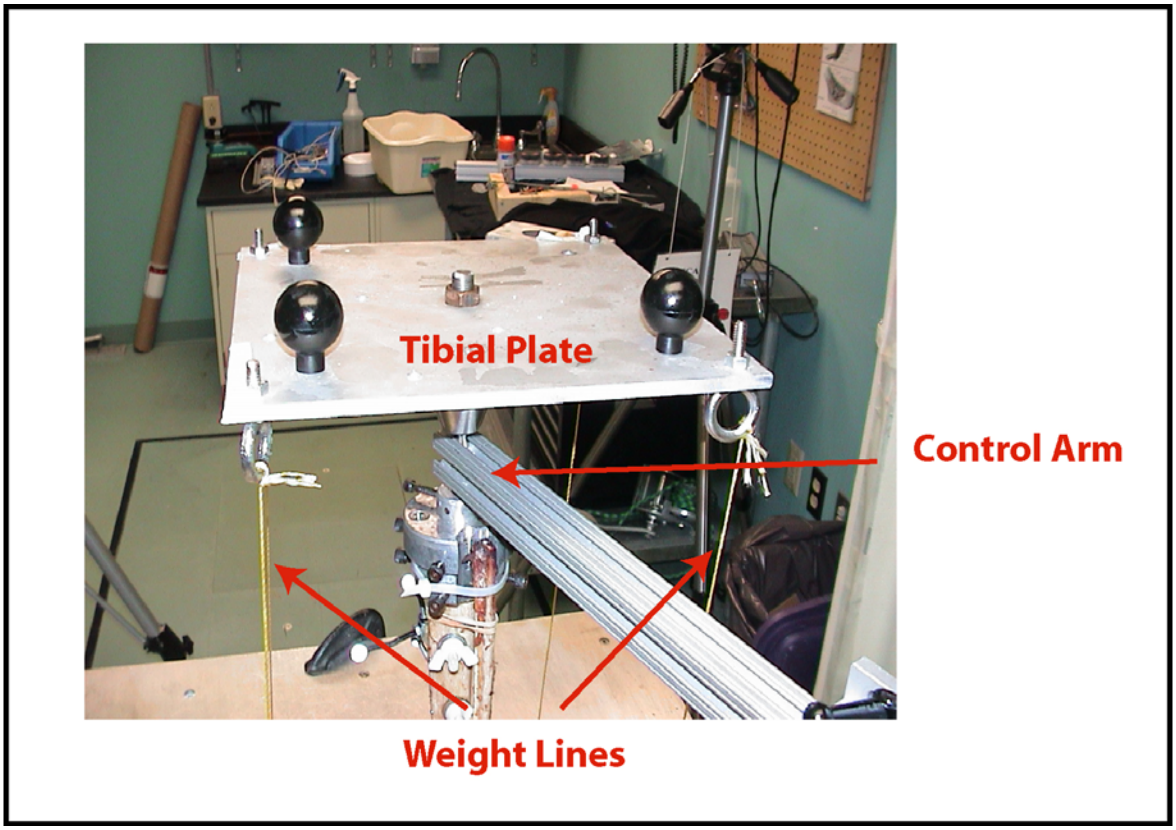

Figure 4.2 The tibial plate attaches to the tibial cap and has a weight line extending down from each corner. The control arm secures the tibia and holds it in the neutral position.

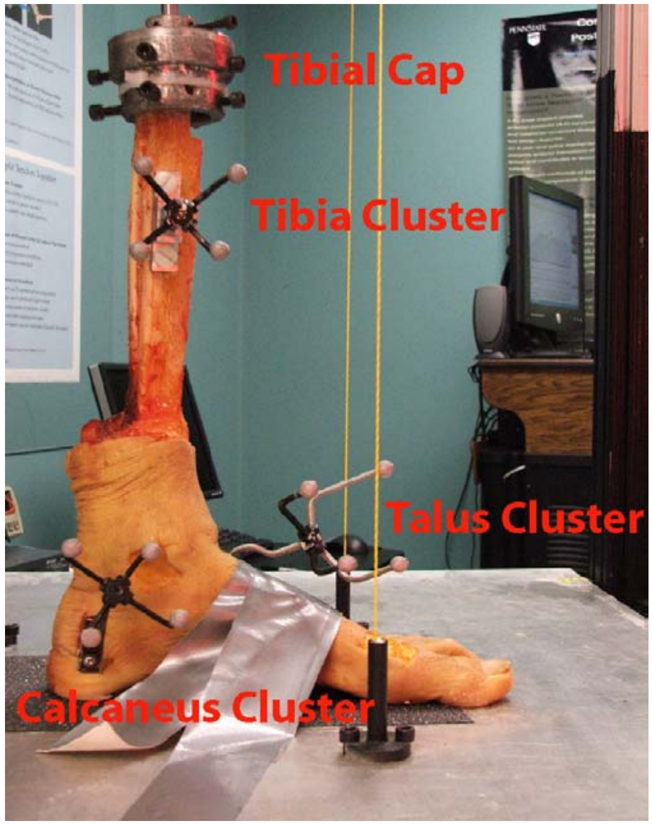

Figure 4.3 A specimen at neutral position, ready for intact testing.

4.2.3 Dynamic Intact Testing

After collecting the static landmark positions, dynamic trials of the intact feet moving through a range of plantarflexion/dorsiflexion (PF/DF) were collected. These trials were collected to have a reference of intact plantar/dorsiflexion kinematics for each specimen before they were compromised by the ankle arthroplasty surgery. At least five twenty-second trials were recorded for each specimen. Each trial began at neutral position, and then the tibia was passively cycled through a range of PF/DF by the experimenter. To move the tibia, the tibial plate was held on the medial and lateral sides and was pushed/pulled in the AP direction by the experimenter. Each trial began at neutral and then moved into DF, followed by PF. The range of PF/DF was subjective for every foot as each foot was moved to its individual maximum range of motion by the experimenter. The end ranges of motion were determined as the points at which resistance to the passive movement was felt, and the motion was reversed. Following collection, all data were post-processed in the MA software (EVaRT 41, V. 4.1.0, Motion Analysis Corp., Santa Rosa, CA) to check for missing markers and proper cluster identification, and was then exported for data analysis in Matlab.

4.3 TAA Tests

4.3.1 TAA Design and Fabrication

A specialized TAA system was designed and constructed to perform the MA experiments after implanting TAA components. The system included an alignment jig to secure the foot and tibia, as well as guide the bone cuts required for arthroplasty relative to the talus and the tibia independently. In addition, the component system was also designed to reproduce the motions of plantar/dorsiflexion while remaining unconstrained in translation and rotation in the transverse plane. These additional degrees of freedom were intended to allow the components to seat themselves in the position and orientation best matched to the kinematics of the talocrural joint. All parts of the new testing device were fabricated in the Biomechanics Lab Machine Shop by either the staff machinist or the experimenter.

The surgical alignment and cutting apparatus was designed and fabricated from a combination of aluminum and existing lower extremity external fixation hardware (Synthes Corp., Pennsylvania, USA). The jig consisted of a base plate fit with blocks drilled to accept surgical pins penetrating and securing the calcaneus, and slots for a Velcro strap used to secure the forefoot (Figure 4.4). By securing the foot in this manner, the base plate was established as a "ground" reference plane for the cut guides. An external fixator rod was rigidly secured to the base plate with a screw, and was fitted with an adjustable mount to secure tibial bone pins. Lastly, two guide-rods extended vertically from the plate and could be adjusted in the AP direction. Both horizontal and vertical cut guides made from slotted aluminum blocks were placed on these vertical rods and adjusted for to achieve the proper vertical positions of the tibial and talar osteotemies.

The cylinder axis orientations obtained in the microscribe experiments indicated relatively consistent orientations in the coronal and sagittal planes, but displayed considerable variance in the transverse plane. To examine the potential of intra-surgical patient specific determinations of transverse orientation, a TAA system consisting of four parts was developed and constructed and consisted of the following: two plates (one for the tibia and one for the talus), one cylindrical talar component, and one congruent tibial component. Initially, prototype pieces were fashioned out of polished aluminum; however, early experimentation revealed that the coefficient of friction of aluminum on aluminum was too, high preventing smooth movement between the components. Therefore, the final component system was constructed from polished stainless steel and oil-impregnated ultra-high molecular weight polyethylene (UHMWPE). The coefficient of friction of UHMWPE on polished steel has been reported to range from 0.10 to 0.25 depending on the presence and type of lubrication (http://www.crownplastics.com). These values are much lower than the coefficient of friction values for aluminum on aluminum, which can range from 1.05 to 1.35 for dry coeffiecient of friction tests, or from 0.3 to 0.6 for lubricated friction tests of aluminum on aluminum http://www.roymech.co.uk/Useful_Tables/Tribology/co_of_frict.htm).

Two implant sizes were initially developed in order to have one system for males, and another for females; however due to restrictions in specimen availability, however, only male feet were used in the experiments and therefore only the implant system sized for males was used. As a result, the size specifications discussed here refer to the system sized for males. Measurements for the system sized for females can be found on the schematic drawings (Figure 4.6). Radius values used for the cylindrical portions of the component system were obtained from the mean optimized cylinder radii calculated in the previously described microscribe experiments.

The two plates were fashioned out of 316 stainless steel and measured 36 mm square (Figure 4.5). On the underside of each plate were stainless steel pegs machined to a point as well as 0.125 inch diameter steel pins 9 mm in length. The tibial component was made from UHMWPE, was flat on the proximal side, and had a concave dorsal surface with a 22 mm radius (Figure 4.6). The anterior and posterior ends were flat and four small divots were machined into the front face to act as fiducial points for MA wanding. The talar (Figure 4.6) component was built from stainless steel and was composed of a cylindrical proximal surface with a 22 mm radius. The height of the stainless portion of the dome was 12 mm. A flat UHMWPE piece 3 mm thick was attached to the underside of the stainless dome. The result of this design was that each interface between component system pieces was always stainless steel on one side, and UHMWPE on the other.

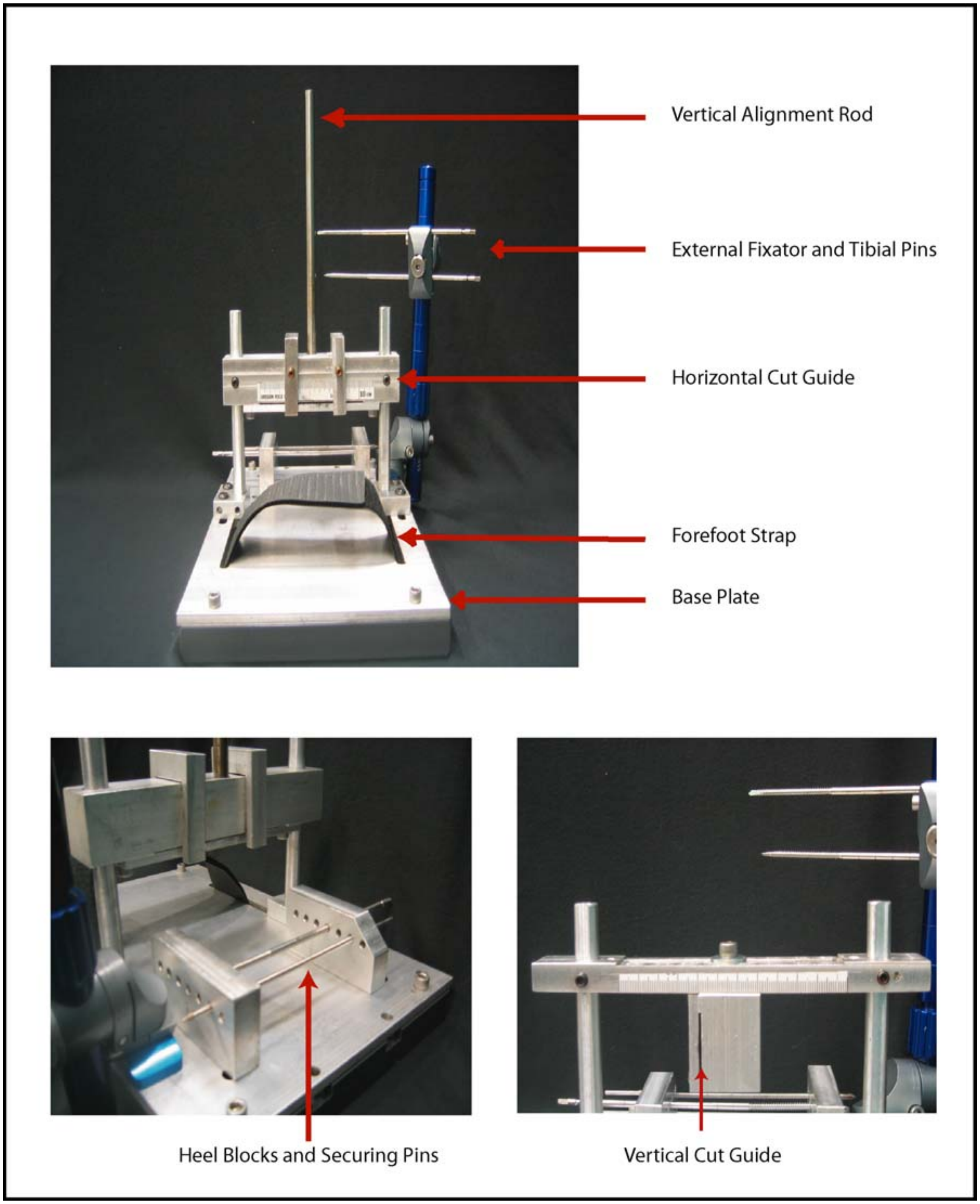

Figure 4.4 The surgical alignment and cutting jig composed of a base plate, adjustable horizontal and vertical cut guides, an adjustable external fixator with tibial pins, and heel blocks/pins to secure the foot.

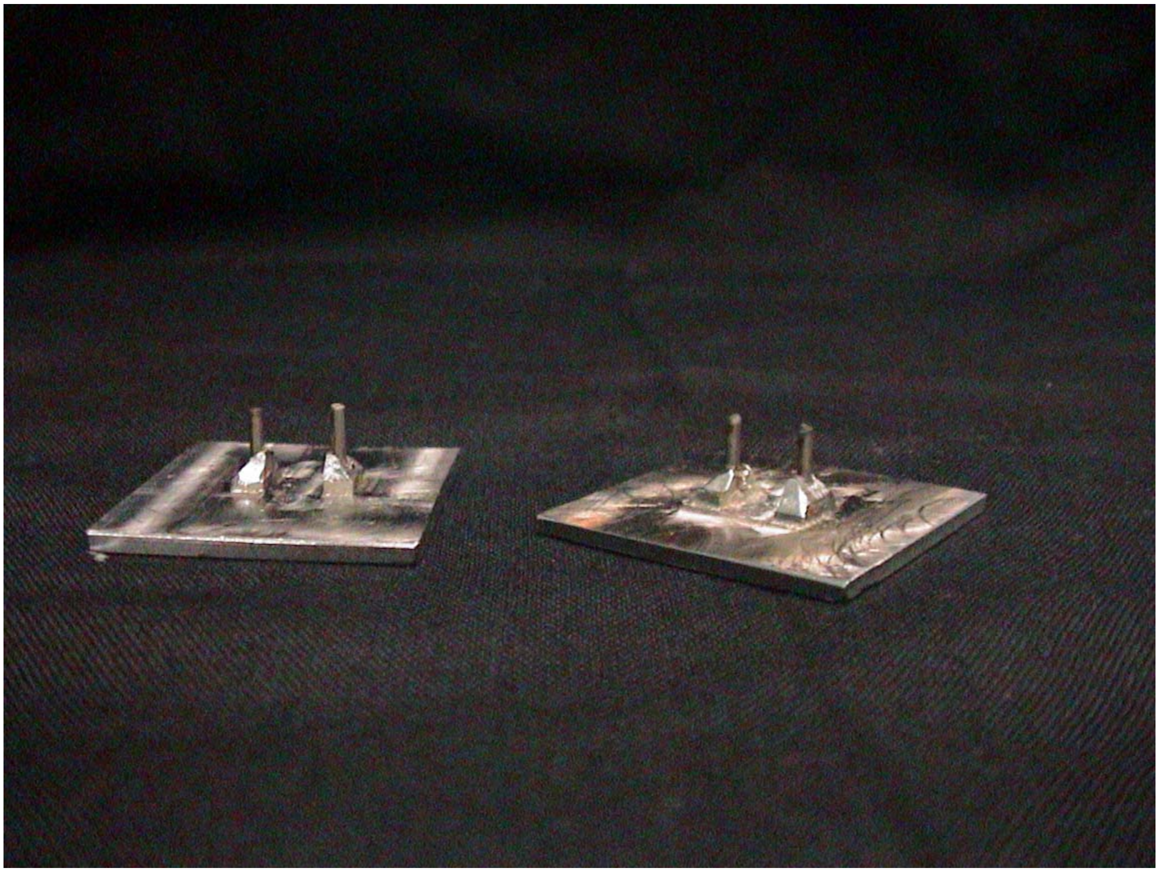

Figure 4.5 The stainless steel plates that are part of the TAA system. 0.125 inch diameter posts extend down from the bottom to secure the plates into the cut bone.

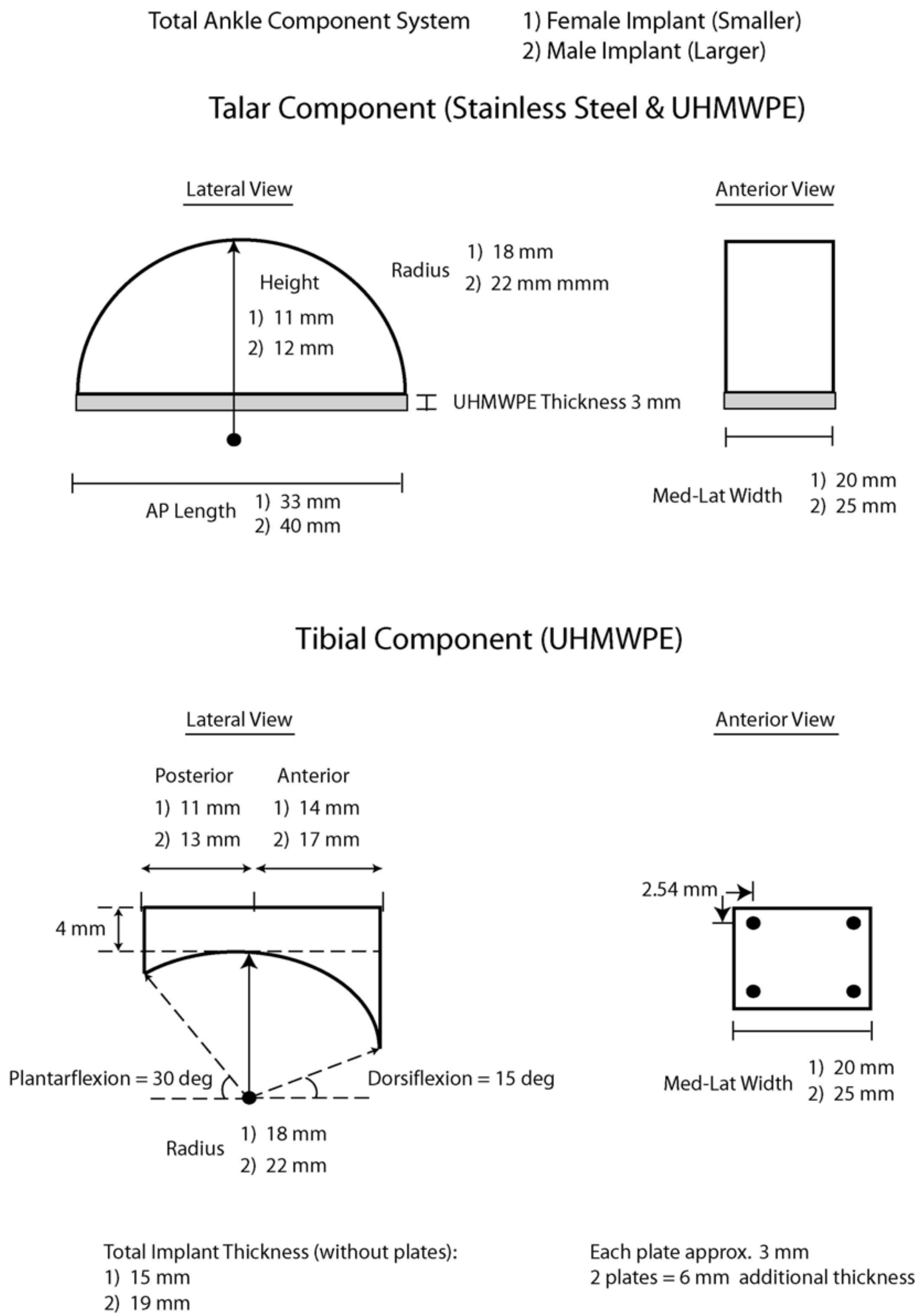

Figure 4.6 Schematic of the cylindrical TAA components for both the male and female sizes.

4.3.2 Total Ankle Surgery

All cadaveric ankle surgeries were done in the presence of, or in consultation with an experienced orthopaedic surgeon in the Biomechanics Lab at Penn State University. To begin the ankle arthroplasty procedure, each specimen was placed in the previously described alignment jig. The plantar surface of each foot was placed on the base plate of the jig and two 4 mm diameter pins were drilled through the calcaneus and the heel blocks on either side to secure the rearfoot to the plate. Next, a Velcro strap was secured around the forefoot to hold it in place. Once the foot was secured to the base plate of the jig, the tibia was aligned and secured. To do this, one 4 mm spade head pin was drilled freehand into the antero-lateral tibial shaft, and then the external fixator mount was clamped around the pin. A second 4 mm pin was then placed through the same external fixator mount and drilled into the bone in line, but below the first pin. At this point, the external fixator was adjusted so that the tibia was in proper alignment.

The alignment goal for the tibia was to make the cut plane both parallel to the base plate of the jig and perpendicular to the long axis of the tibia. To accomplish this, the tibial crest was lined up in the frontal plane with a vertical indicator on the cut guide to insure that the tibial cut would be made at a neutral varus/valgus angle. Next, the shaft of the tibia was visually aligned against the vertical indicator in the sagittal plane to insure that the plane of the tibial cut was parallel to the base plate of the jig. Once the tibia was properly aligned in both the frontal and sagittal planes, all of the adjustment screws on the external fixator were tightened, making the jig rigid and secure.

The talar dome was the site of the first cut. A loose saw blade was placed through the slot in the horizontal cut guide, and the height of the guide was adjusted until the saw blade was at a height just above the anterior edge of the articular surface of the talar dome. The set screws were then tightened to hold the cut guide in place. Once the proper height was determined, the medial and lateral stops were adjusted to limit the width of the horizontal cut. The width of the cut was based on the width of the component system, which was designed to leave the medial and lateral ligaments intact. Therefore, the medial and lateral stops were important in that they prevented unwanted cutting of the ligaments during the surgical procedure. Finally, after all the set screws on the stops were tightened down, the talar cut was made using a sagittal surgical saw (Stryker Instruments, MI, USA). Since the cut guide was fixed parallel to the base plate of the jig, the talar cut was also made parallel to the base plate. After making the cut, the external fixator was distracted slightly to open the joint space, and the free piece of bone was removed from the ankle joint. The ankle was then reversed back out of distraction in preparation for the tibial cut.

After the talar cut was completed, the thickness of the implant system (~25 mm) was measured up from the cut surface of the talus and marked on the anterior tibia with a black marker. The horizontal cut guide was then re-adjusted so that a loose saw blade passed through the block at the level of the mark, and the guide was tightened down again. The placement of the medial and lateral stops were re-verified and adjusted if needed, so that there was no chance of cutting too wide on either side, which could fracture or sever the malleoli. Once the guide and stops were in place, the alignment of the tibia was double-checked and the horizontal cut was made. After sawing completely through from anterior to posterior, the horizontal guide was removed from the jig, and the cut was inspected. If the cut seemed satisfactory (depth and width) then the vertical cut guide was placed on the jig to make the medial and lateral vertical cuts. The medial and lateral vertical cuts were made by sliding the cut block medially and laterally until the slot for the vertical saw blade was in proper location. Once the cuts were made, and the vertical cut guide was removed from the jig. The loose bone stock was removed from the joint leaving a rectangular hole in the distal end of the tibia.

At this point, the stainless steel plates were placed into the new joint space to check the width and height of the cuts. If the cuts were too narrow to accept the plates, then bone was removed either by rasping the medial and lateral walls, or by making additional freehand vertical cuts. Once there was adequate space for both the tibial and talar plates, the external fixator was removed from the tibia and the plates were press-fit into their respective bones. The plate for the talus was inserted by hand, and a small block of wood was placed on top of it to take up the space between the tibia and the plate. The tibial cap was then tapped with a hammer, driving the plate down into the talus. Wood blocks of increasing thickness were then inserted in sequence until the plate was flush with the surface of the bone. The tibial plate was inserted next, and wood blocks of sequentially increasing thickness were again placed between the two plates while hammering the tibial cap in order to drive the tibial plate up into the cut surface of the tibia. Once both plates were press-fit into the two bones, a trial implant was placed into the space between the two plates to verify that enough bone was cut during the surgery. If the trial implant did not fit or the components did not move due to "stuffing" of the joint, than the tibial plate was pulled out and the tibial cut procedure was repeated until the correct amount of bone was removed to facilitate a proper fit for the trial implant. After completing the surgery the foot was removed from the jig and marker cluster mounts for the talus and calcaneus were re-attached to their respective bones in preparation for kinematic testing.

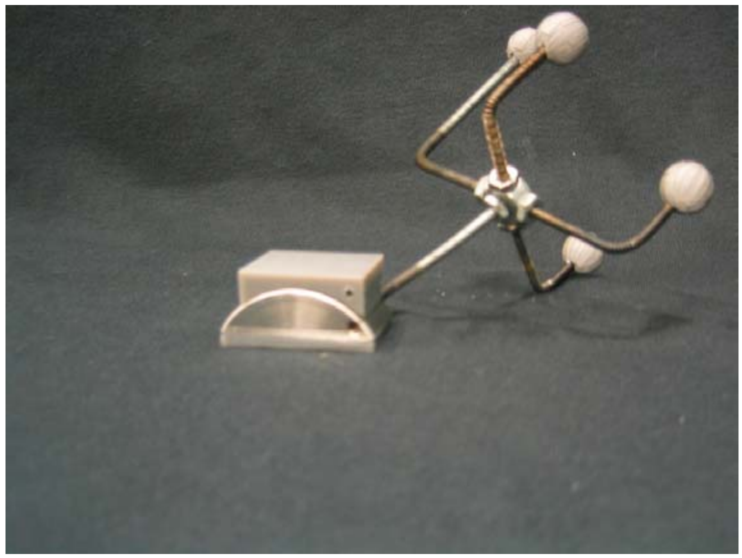

Figure 4.7 The TAA components with marker cluster attached.

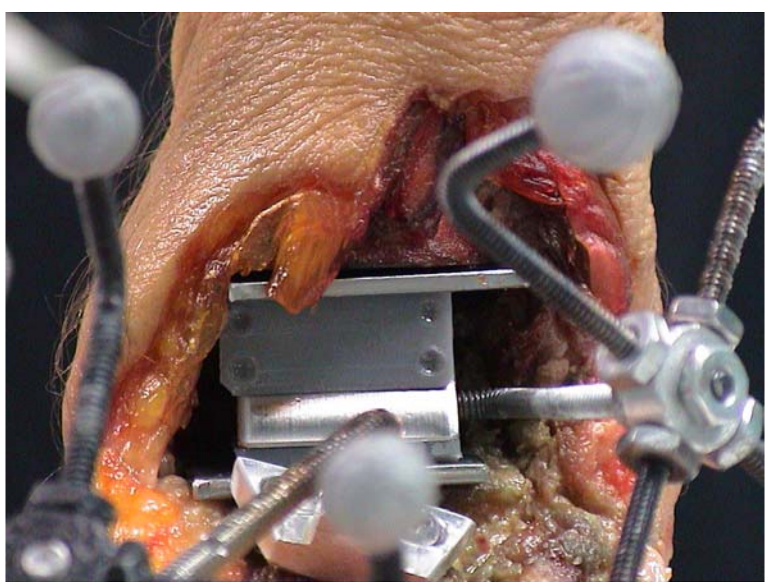

Figure 4.8 Close-up anterior view of the TAA component system. The talar and tibial components are placed between the two stainless steel plates and the marker cluster is attached to the talar component.

4.3.3 Component Kinematic Tests

Kinematic testing of each foot post-surgery was performed on the MA data collection stand as described previously for the kinematic testing of the intact feet. Once each foot was secured to the MA stand, the talar dome component and the congruent tibial component were covered with lubricant and inserted between the two stainless steel plates, whose surfaces were also lubricated. Tri-flow aerosol spray lubricant with Teflon™ was used (Sherwin-Williams, Ohio, USA). A rigid marker cluster with four reflective spheres was attached to the antero-lateral corner of the talar component and extended anteriorly. The tibial piece was placed on top of the dome portion of the talar component so that the face with the four divots was directed anteriorly. The initial orientation of the components before each trial was along the AP axis of the foot.

Static wanding trials were performed to record the position of anatomical landmarks, just as with the intact data collection. The same landmarks and number of reference points were collected for the component trials as in the intact trials, however, instead of recording the anterior corners of the tibial and talar articular surfaces, the location of the four divots on the front of the tibial component were recorded.

After completing all the wanding trials, the weight racks were attached to the lines without adding weight, and the kinematic trials were collected to record the motion of the tibia, calcaneus, talus, and components during plantar/dorsiflexion movements. As mentioned previously, the weight racks and tibial plate weighed 12 lbs (around 53 N). Additional weight was not added during the component tests due to experimental complications that will be discussed later. The trials consisted of sixty seconds of data collection at 100 Hz. Component kinematic trials were longer than the intact trials to allow enough time for the implant system to move and seek its own optimum position and orientation. Due to the unconstrained nature of the components, total ranges of PF/DF during the kinematic testing were significantly less than during the intact trials. As mentioned, the implant was designed to be capable of 40 degrees of total motion, however, in order to prevent the components from dislocating out of the joint, a smaller range of motion, as well as a smaller axial load was observed during the component tests, as compared to the tests of the intact specimens. At the beginning of each trial, the tibia was held in the neutral position and then cycled through PF/DF by the experimenter beginning with DF. Using a goniometer, endpoints of 15 degrees of DF and 25 degrees of PF were noted by marking the weight lines with a felt pen at the respective PF and DF positions in order to provide guides to help judge the amplitude of movement throughout the experiment. While attempts were made to reach these marks, the total range of motion during the experiment was also monitored and limited by visual observation of the components by the experimenter, as well as by subjective feel. The components were monitored throughout the trials so that the maximum travel of the tibial piece on the talar dome was not reached, and motion was reversed if the implant appeared as if it was about to dislocate from the joint space. Despite these attempts to avoid ranges of motion that exceed that capabilities of the implant system, many trials were recorded in which the implant did dislocate due to excessive movement by the experimenter. Whenever this occurred, the implant was re-lubricated, re-positioned, and the location of the four divots were recorded again at a static, neutral pose. As a result, numerous kinematic trials were attempted in order to collect at least five complete, one-minute trials.

4.3.4 Kinematic Data Processing

Following both intact and post-surgical kinematic data collection, all motion tracking data were post-processed in the MA software to check for missing markers and proper cluster identification, and was then exported as Excel files for data analysis in Matlab. For each specimen, a static trial was used to determine the positions of the anatomical landmarks and establish the body-fixed anatomical coordinate systems. In addition, the locations of the marker clusters within the anatomical coordinate systems were determined from the static data.

The body-fixed anatomical coordinate systems were determined similarly to the methods of Lewis (2004). The tibial coordinate system was established by placing the origin at the midpoint of the intermalleolar axis (IM). The z-axis of the tibial coordinate system was orientated along the IM axis and pointed medially, the x-axis was perpendicular to the plane made by the malleoli and the midpoint of the two points wanded on the proximal tibial shaft and pointed anteriorly, and the y-axis pointed superiorly and was orthogonal to the other two axes. The talus coordinate system was established in the same position and orientation as the tibial coordinate system with the foot at neutral position (Figure 4.9). A third anatomical system was established at the calcaneus by positioning the origin at the posterior calcaneus point with the y-axis pointed superiorly and perpendicular to the base plate, the x-axis directed along a vector connecting the calcaneus point to the head of the second metatarsal, and the z-axis orthogonal to the y- and x-axes pointing medially. Date representing the calcaneus markers and anatomical coordinate system were collected in the experiment to allow for the potential calculation of helical axes. For these experiments, helical axis calculations were not done, however the data were collected to have kinematic records of the intact specimens prior to destructive TAA surgery.

For the trials with the TAA component system, a fourth anatomical coordinate system was established. (Figure 4.10) The positions of the divots on the face of the tibial component were used to establish a local coordinate system for the components. The midpoint between the medial and lateral divots in the frontal plane of the implant was calculated, and this point was then offset according the measurement of the implant, first in the posterior direction normal to the frontal plane of the implant, and second, downward in a direction parallel to the frontal plane of the implant. As a result of these offsets, the point was located in the center of the inferior surface of the talar component, which was taken to be the origin of the component coordinate system. The z-axis was directed medially and parallel to the frontal face of the implant, the y-axis was directed superiorly, and the x-axis was directed anteriorly.

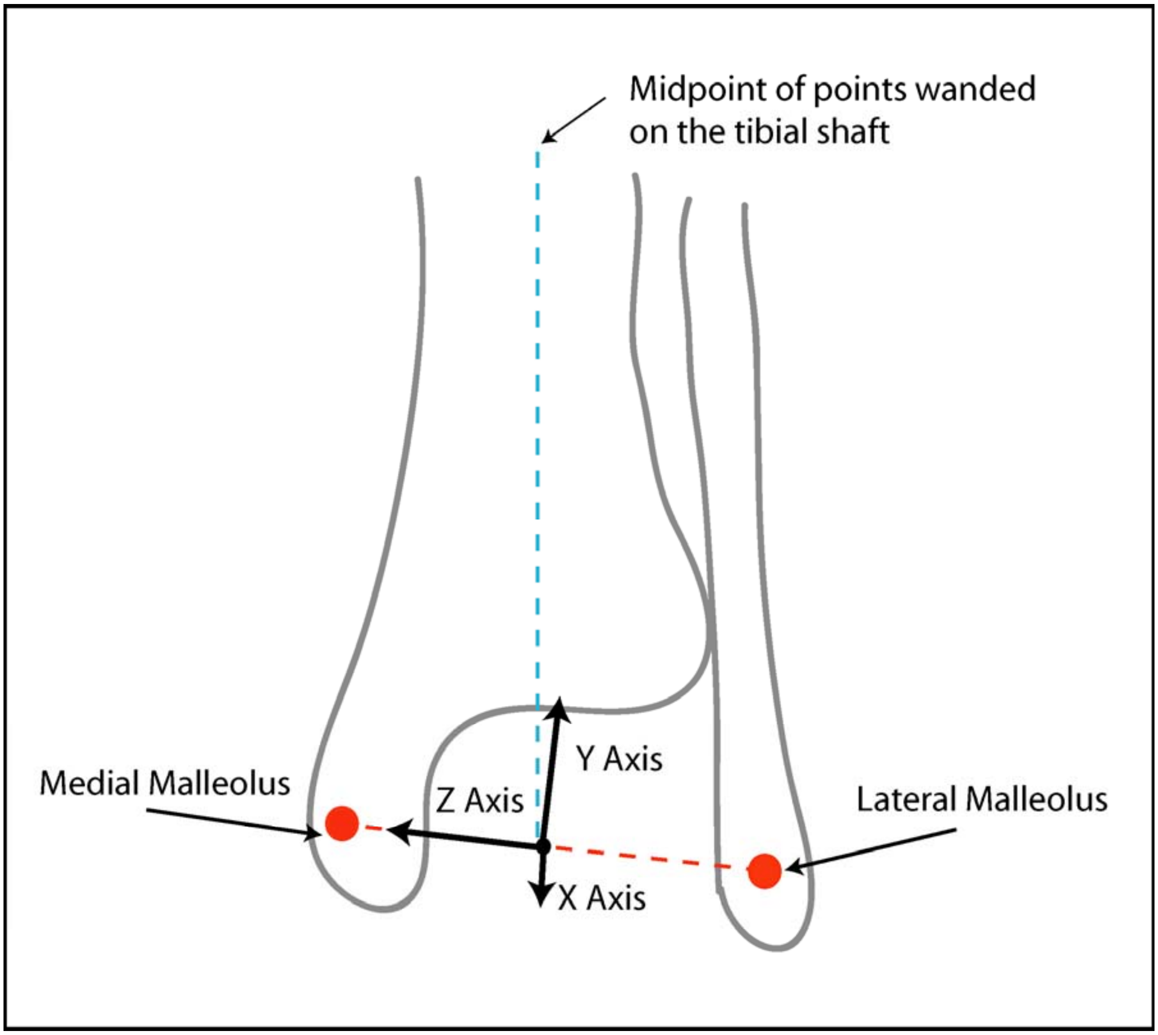

Figure 4.9 Anterior view of the body-fixed anatomical coordinate system used for the tibia and the talus. The z-axis was oriented along the intermalleolar axis and pointed medially. The x-axis was perpendicular to the plane created by the intermalleolar axis and the line passing through the midpoint of the tibial shaft. The y-axis was orthogonal to the x and z-axes, and was directed superiorly.

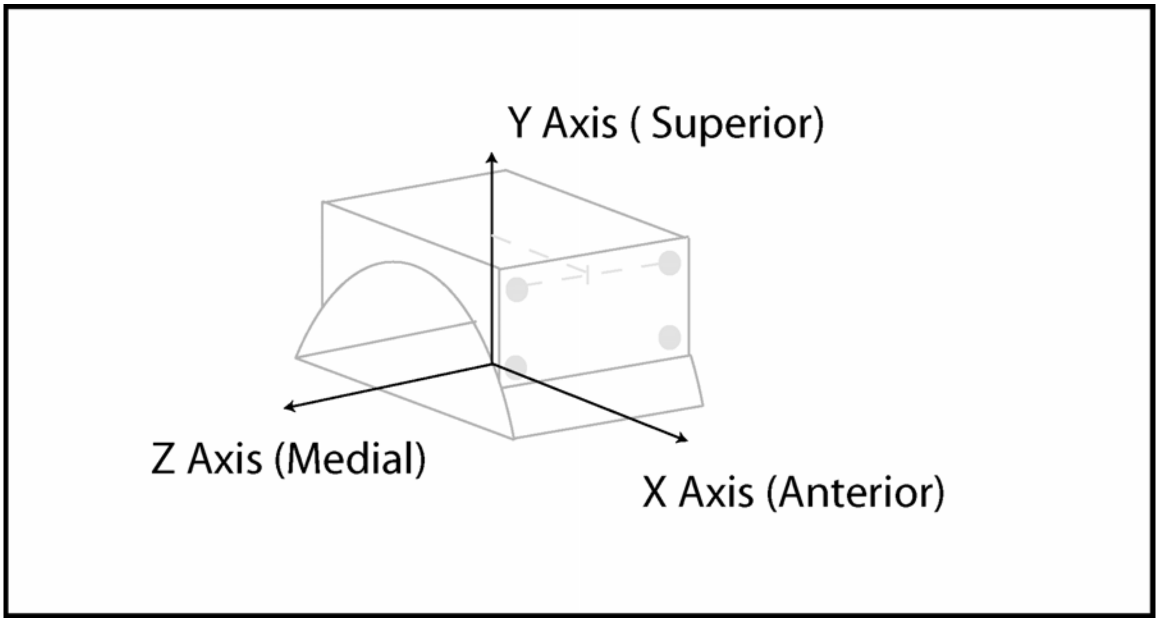

Figure 4.10 The body-fixed anatomical coordinate system for the TAA components. The z-axis was parallel to the face of the tibial component and was directed medially. The x-axis was perpendicular to the anterior face of the tibial component and was directed anteriorly. The y-axis was orthogonal to the x and z-axes and was directed superiorly. The origin was offset to lie on the inferior surfaced of the talar component.

Prior to analysis, the dynamic kinematic data were processed in Matlab using a 4th order low-pass Butterworth filter with a cut-off frequency of 10 Hz. The dynamic data was used to formulate the 4 x 4 homogeneous transformation matrices used to compute the rigid body kinematics of the anatomical coordinate systems. A least squares method was employed for these calculations to account for the redundant fourth marker in each segment marker cluster (Challis, 1995). Rotations about the talocrural joint between anatomical segments such as the talus with respect to the tibia (TIB-TAL), the component with respect to the tibia (TIB-COMP), and the component with respect to the talus (TAL-COMP) were calculated by decomposition of the 3 x 3 rotation matrix obtained from the transformation matrices. Similarly to Lewis (2004), a Z-X-Y fixed angle convention was used to calculate three angles (alpha, beta, and gamma) that described the relative orientation in 3 anatomical planes: sagittal, coronal, and transverse (Craig, 1995). The derivation of the rotation matrix was as follows:

$R_{ZXY}(\alpha, \beta, \gamma) = R_Z(\alpha)R_X(\beta)R_Y(\gamma)$

$$= \begin{bmatrix} 1 & 0 & 0 \\ 0 & \cos\gamma & -\sin\gamma \\ 0 & \sin\gamma & \cos\gamma \end{bmatrix} \times \begin{bmatrix} \cos\alpha & -\sin\alpha & 0 \\ \sin\alpha & \cos\alpha & 0 \\ 0 & 0 & 1 \end{bmatrix} \times \begin{bmatrix} \cos\beta & 0 & \sin\beta \\ 0 & 1 & 0 \\ -\sin\beta & 0 & \cos\beta \end{bmatrix}$$

Translations in each anatomical plane were also computed from the remaining portion of the 4 x 4 transformation matrix. Mean values of initial and final position, as well as total translation of the component in the transverse plane were calculated using the transformation matrix for the TIB-COMP relative motion to find the change in position of the origin of the component anatomical CS.

Values of the relative angular motion between the TIB-COMP, TIB-TAL, and TAL-COMP were compiled for each specimen and were concatenated into matrices representing data from all five trials. In addition, for every variable (i.e. rotation in one plane), data for all specimens were concatenated into grand n x 25 matrices representing the 5 trials for each of the 5 specimens for that specific variable. Mean values for the start-to-finish difference of the relative angles and translations were calculated for each specimen across all trials. Plotting routines in Matlab allowed each variable to be plotted per trial, or per specimen. In addition, variables of specific interest such as transverse plane rotations of the component could be plotted versus PF/DF movement.

To examine the amplitude of any transverse plane oscillations during testing, the data were first divided into individual cycles of plantar/dorsiflexion. A cubic spline interpolation was fit to the PF/DF data (TIB-COMP sagittal rotations) with a resolution of 0.001 degrees. This expanded the original PF/DF data from 600 to almost 60,0000 data points, so that the zero points (neutral orientation) could be accurately located. Once the spline was fit to the data, an index search was used to locate the indices of the zero points across the length of each trial. These points represented the beginning and end of each PF/DF cycle (beginning with dorsiflexion). With the individual PF/DF cycles identified, the minimum and maximum values of component transverse plane rotation were calculated within each cycle, representing the amplitude of rotational oscillations. Using the amplitude values for each cycle, the mean amplitude over each entire trial was also calculated, and the overall specimen mean for all five trials was computed.

4.3.5 Component CPCS Calculations

In order to compare the orientations of the component trials with the cylinder orientations from the microscribe experiments, the data for each experiment had to be compared in the same frame of reference. Therefore, the landmark data from the motion analysis experiments was used to establish the CPCS within the specimens used in both the intact and component MA trials. As described previously, the CPCS was established with the origin at the calcaneus, the x-axis directed in the plane of the ground along the vector connecting the calcaneus and first metatarsal head, the y-axis directed laterally in the plane of the base plate, and the z axis orthogonal to the other two axes pointing superiorly. By establishing the CPCS for the MA specimens, the orientations of the IM axes, anterior tibial axes, anterior talar axes, and TAA component axes could be calculated via dot products and compared between intact and component conditions, as well as with the orientations of the cylinder axes and anatomical counterparts from the microscribe experiments. In addition to addressing the component and landmark orientations for the MA specimens in the transverse plane, the orientations of the TAA components in the coronal plane, and the angle between the tibial crest line and the base plate were calculated using the dot product in an effort to evaluate the accuracy of the alignment jig.

CHAPTER 5. RESULTS: ARTICULAR SURFACE EXAMINATIONS

5.1 Reliability Testing: Digitization Experiments

The following section is a presentation of the data and results from the experiments and calculations described in Chapter 3. This information includes the output from the cylindrical characterizations of the joint surfaces, as well as the quantitative descriptions of the positions and orientations of the cylinders and landmarks with respect to one another.

5.1.1. Wooden Foot Model

Data from the ten digitization test of the wooden foot were analyzed using Microsoft Excel software. Positional data for each landmark were separated by dimension (X, Y, and Z components) resulting in thirty values for each landmark, or ten values per dimension. The mean and median values, standard deviation, standard error, minimum and maximum values, and the range between them were calculated for each landmark in all three dimensions (Appendix C). These data indicated that the microscribe procedure was reliable and consistent in locating the position of the anatomical landmarks. For the majority of the landmarks, the standard deviation for the 10 trials was around 0.01 mm, with a standard error ranging from 0.02 mm to 0.04 mm. Confidence intervals (95%) for almost all landmarks were ± 0.1 mm or less. Overall grand means of the standard deviation and standard error were also calculated for each dimension. For all X component values, the standard deviation of the mean was 0.11 mm, and the standard error was only 0.033 mm. The Y component values exhibited slightly larger values with a standard deviation of 0.13 mm and a standard error of 0.041 mm. The mean Z component values showed the largest range of observations, with a standard deviation of 0.15 mm and a standard error of 0.047 mm.

5.1.2. Palpation Study

Data from the palpation tests were also analyzed in Excel. For each of the nine landmarks collected, basic descriptive statistics were calculated across all ten trials for each component dimension, X, Y, and Z. These values are presented in Table 5-1 A, B, and C. Overall, the landmarks beneath the first and fifth metatarsals showed the largest variances in measured location. For the first metatarsal base, the largest standard deviation was 3.02 mm in the X component direction with a standard error of 0.96 mm. For the fifth metatarsal base, the largest standard deviation was 3.50 mm in the Y component direction, with a standard error of 1.11 mm. The standard deviations of the locations of the other landmarks all ranged between 0.25 mm and 2.0 mm, with standard errors less than 0.62 mm. Overall grand means for the standard deviation and standard error values were also calculated for each dimension. In the X component direction, the grand mean of the standard deviation for all 8 landmarks was 1.98 mm and the grand mean of the standard errors was 0.43 mm. In the Y component direction, the grand mean of the standard deviations was 1.91 mm and the grand mean of the standard error values was 0.60 mm. The Z component direction showed the smallest overall variance; the grand mean of the standard deviations was 1.19 mm, and the grand mean for the standard errors was 0.38 mm.

Table 5-1A Statistical Summary of the X component values for the palpation test.

Values in mm	MMAL	LMAL	1 METH	5 METH	TMT	1 METB	5 METB	CALC
Mean	442.57	376.29	448.85	381.08	433.72	443.59	385.74	416.36
Median	442.55	376.31	449.06	381.07	434.23	444.06	386.11	416.41
Std. Deviation	0.26	0.32	1.50	1.22	1.91	3.02	1.84	0.80
Std. Error	0.08	0.10	0.47	0.39	0.61	0.96	0.58	0.25
Min Value	442.23	375.79	446.12	378.88	429.75	438.41	382.19	414.97
Max Value	442.93	376.79	450.58	383.36	436.15	447.81	388.31	417.61

Table 5-1B Statistical Summary of the Y component values for the palpation test.

Values in mm	MMAL	LMAL	1 METH	5 METH	TMT	1 METB	5 METB	CALC
Mean	350.76	355.86	221.39	233.15	263.92	225.28	221.20	371.99
Median	350.78	355.66	221.27	233.49	263.66	224.83	220.19	372.49
Std. Deviation	1.15	1.59	1.22	1.60	1.97	2.61	3.50	1.64
Std. Error	0.36	0.50	0.39	0.51	0.62	0.82	1.11	0.52
Min Value	349.05	353.63	219.38	230.27	261.67	220.65	217.44	368.75
Max Value	353.10	358.61	223.78	234.81	267.99	229.54	228.11	374.70

Table 5-1C Statistical Summary of the Z component values for the palpation test.

Values in mm	MMAL	LMAL	1 METH	5 METH	TMT	1 METB	5 METB	CALC
Mean	94.71	80.46	30.51	20.29	66.13	1.01	3.79	2.73
Median	94.51	80.81	30.56	20.32	66.36	1.11	4.16	2.64
Std. Deviation	1.57	1.47	1.24	1.23	1.40	1.00	1.12	0.51
Std. Error	0.50	0.46	0.39	0.39	0.44	0.32	0.35	0.16
Min Value	92.17	78.03	28.72	18.36	64.05	-0.76	1.65	2.04
Max Value	98.18	82.32	33.40	22.67	69.22	2.63	5.11	3.83

MMAL = medial malleolus
LMAL = lateral malleoulus
1METH = first metatarsal head (dorsal surface)
5METH = fifth metatarsal head (dorsal surface)
TMT = 1st tarsometatarsal joint
1METB = first metatarsal head (plantar surface)
5METB = fifth metatarsal head (plantar surface)
CALC = calcaneus (plantar)

5.2 Cylinder Optimizations

5.2.1 Whole Surface Cylinder Radii

Cylinders were fit to each articular surface from both the talus and the tibia using the Matlab optimization routine outlined in the Section 3.2.2. Output from these optimization routines included a radius value, a unit vector describing the orientation of the longitudinal axis of the optimized cylinder, and a point on the axis for each optimized cylinder. The fit of each cylinder was evaluated using the mean square error (MSE) values of the optimizations. Error was calculated for each point on the articular surface as the difference between the optimized radius value and the perpendicular distance to that point from the cylinder axis (See objective function, Appendix D). The optimal radius, MSE, root-mean square error RMSE, and min/max error for each talus are displayed in Table 5-2. Values for each tibia are displayed in Table 5-3. The mean talar cylinder radius for all eight specimens was 19.97 ± 2.22 mm, with an overall average MSE of 0.188 ± 0.11 mm. For the tibia, the mean cylinder radius was calculated to be 23.08 ± 2.21 mm with an average MSE of 0.157 ± 0.05 mm.

The mean radius of curvature values from the cylinder characterizations were compared between the tibia and the talus for each specimen. Statistical comparisons of the two means using a Student's two-tailed t-test found that the mean radius value for the tibia was significantly larger than the mean radius for the talus ($t(14) = 2.80$, $p < 0.05$) by an average of 3.1 mm.

Comparisons of the cylinder radii were also made between gender for both the talus and the tibia. The talar radii, MSE, RMS, min/max error values as calculated separately for both men and women are displayed in Table 5-4 A and Table 5-4 B. The corresponding values for the tibia are displayed in Table 5-5 A and Table 5-5 B. The mean radius of curvature for the four male talar specimens was 21.98 ± 0.57 mm while the radii for the female specimens were significantly smaller with a mean of 17.96 ± 0.63 mm ($t(6) = 9.31$, $p < 0.01$). The average MSE for males and females was 0.238 ± 0.138 mm and 0.139 ± 0.05 mm respectively. For the tibia cylinders, the mean radius of curvature for the four male specimens was 24.61 ± 0.88 mm. The radii for the female specimens were significantly smaller with a mean of 21.54 ± 2.01 mm ($t(6) = 2.81$, $p < 0.01$). The average MSE for males and females was 0.183 ± 0.07 mm and 0.134 ± 0.02 mm respectively.

Table 5-2 Summary of the cylinder characterizations for the *talar* articular surfaces.

Specimen	1	2	3	4	5	6	7	8	Mean	Std Dev.
Gender	Male	Male	Male	Male	Female	Female	Female	Female	---	---
Radius (mm)	22.54	22.40	21.30	21.68	17.79	18.12	18.72	17.20	19.97	2.22
MSE (mm)	0.23	0.42	0.20	0.09	0.18	0.09	0.09	0.19	0.19	0.11
RMSE (mm)	0.48	0.65	0.45	0.30	0.43	0.30	0.30	0.44	0.42	0.12
Max Error (mm)	3.46	3.69	2.76	1.27	1.21	1.28	1.66	1.11	2.05	1.08
Min Error (mm)	0.00	0.00	0.00	0.00	0.001	0.00	0.00	0.00	0.001	0.001

Table 5-3 Summary of the cylinder characterizations for the t*ibial* articular surfaces

Specimen	1	2	3	4	5	6	7	8	Mean	Std Dev.
Gender	Male	Male	Male	Male	Female	Female	Female	Female	---	---
Radius (mm)	24.39	25.90	23.91	24.24	20.72	23.56	22.89	18.99	23.08	2.21
MSE (mm)	0.22	0.20	0.23	0.07	0.11	0.14	0.15	0.14	0.16	0.05
RMSE (mm)	0.47	0.45	0.48	0.27	0.34	0.37	0.39	0.37	0.39	0.07
Max Error (mm)	2.74	2.58	3.20	1.87	1.84	5.83	3.68	2.03	2.97	1.33
Min Error (mm)	0.000	0.000	0.000	0.000	0.000	0.000	0.000	0.000	0.000	0.000

Table 5-4 A Summary of the cylinder characterizations for the male tali.

Specimen	1	2	3	4	Mean	Std Dev.
Gender	Male	Male	Male	Male	---	---
Radius (mm)	22.535	22.395	21.304	21.676	21.977	0.586
MSE (mm)	0.234	0.424	0.199	0.093	0.2375	0.138
RMSE (mm)	0.484	0.651	0.447	0.304	0.4715	0.142
Max Error (mm)	3.455	3.691	2.759	1.271	2.0376	1.463
Min Error (mm)	0.0	0.001	0.001	0.0	0.3024	0.603

Table 5-4 B Summary of the cylinder characterizations for the female tali.

Specimen	5	6	7	8	Mean	Std Dev.
Gender	Female	Female	Female	Female	---	---
Radius (mm)	17.793	18.121	18.718	17.199	17.957	0.634
MSE (mm)	0.184	0.092	0.090	0.189	0.1387	0.055
RMSE (mm)	0.429	0.303	0.301	0.435	0.367	0.075
Max Error (mm)	1.208	1.282	1.657	1.113	1.315	0.238
Min Error (mm)	0.0	0.0	0.0	0.002	0.0005	0.001

Table 5-5 A Summary of the cylinder characterizations for the male tibiae.

Specimen	1	2	3	4	Mean	Std Dev.
Gender	Male	Male	Male	Male	---	---
Radius (mm)	24.3914	25.903	23.914	24.235	24.611	0.884
MSE (mm)	0.216	0.200	0.231	0.074	0.183	0.072
RMSE (mm)	0.465	0.448	0.480	0.272	0.416	0.097
Max Error (mm)	2.743	2.576	3.198	1.871	2.597	0.551
Min Error (mm)	0.000	0.000	0.000	0.000	0	0

Table 5-5 B Summary of the cylinder characterizations for the female tibiae.

Specimen	5	6	7	8	Mean	Std Dev.
Gender	Female	Female	Female	Female	---	---
Radius (mm)	20.716	23.5591	22.891	18.987	21.538	2.089
MSE (mm)	0.112	0.135	0.150	0.139	0.134	0.016
RMSE (mm)	0.335	0.367	0.387	0.373	0.3655	0.022
Max Error (mm)	1.844	5.829	3.683	2.032	3.347	1.849
Min Error (mm)	0.000	0.000	0.000	0.000	0	0

5.2.2 Medial & Lateral Cylinder Radii

Output from the cylindrical characterizations of the medial and lateral joint surfaces of the tibia and talus also included radii of curvature values. For the talus, the radii of curvature obtained from the medial and lateral cylinder characterizations and their respective MSE values are presented in Table 5-6. Corresponding values for the tibia are presented in Table 5-7. Values for the whole cylinder characterizations are presented in each table as well, for ease of comparison. The mean radius of curvature of the medial half of the talar dome was 20.00 ± 2.93 mm, while the mean radius of the lateral half was 20.07 ± 1.87 mm. For the tibia, the mean radius of curvature on the medial half was 24.96 ± 3.58 mm, while the mean radius on the lateral half was found to be 23.40 ± 1.85 mm. A two-tailed paired Student's t-test revealed no significant differences between the mean radii of curvature of the medial, lateral, or entire articular surfaces. In order to examine whether or not either the medial or lateral halves of the articular surfaces were better represented by a cylinder, the MSE values of the optimizations were compared. No significant differences were found between the MSE of the medial and lateral optimizations according to the t-test analysis.

The radii of the curvature of the medial and lateral sides of the tibial and talar articular surfaces were also compared across genders. For the male tali, the mean radii of curvature for the medial and lateral halves were 22.59 ± 1.18 mm and 21.59 ± 1.18 mm, respectively. For female tali, the mean radii for the medial and lateral halves were 17.96 ± 0.63 mm and 18.54 ± 0.76 mm, respectively. Although the female values tended to be slightly smaller than the male values, the differences were not statistically significant in this sample.

Table 5-6 Whole-fit, medial-fit, and lateral-fit radii and MSE values for the *talus* obtained from the cylinder characterizations.

Specimen	**1**	**2**	**3**	**4**	**5**	**6**	**7**	**8**	**Mean All**	**Mean ♂**	**Mean ♀**
Gender	Male	Male	Male	Male	Female	Female	Female	Female	---	---	---
Whole Radius	22.54	22.40	21.30	21.68	17.79	18.12	18.72	17.20	19.97 ± 2.22	21.98 ± 0.59	17.96 ± 0.63
Medial Radius	22.55	24.02	22.66	21.14	17.02	17.53	18.58	16.52	20.00 ± 2.93	22.59 ± 1.18	17.96 ±0.08
Lateral Radius	23.07	20.70	20.58	22.02	17.81	18.77	19.48	18.08	20.07 ±1.87	21.59 ± 1.18	18.54 ±0.75
MSE (whole)	0.234	0.424	0.199	0.093	0.184	0.092	0.090	0.189	0.188	0.286	0.142
MSE (medial)	0.306	0.143	0.063	0.073	0.042	0.061	0.035	0.048	0.097	0.171	0.060
MSE (lateral)	0.120	0.478	0.131	0.051	0.087	0.031	0.085	0.060	0.130	0.243	0.075

Table 5-7 Whole-fit, medial-fit, and lateral-fit radii and MSE values for the *tibia* obtained from the cylinder characterizations.

Specimen	**1**	**2**	**3**	**4**	**5**	**6**	**7**	**8**	**Mean All**	**Mean ♂**	**Mean ♀**
Gender	Male	Male	Male	Male	Female	Female	Female	Female	---	---	---
Whole Radius	24.39	25.90	23.91	24.24	20.72	23.56	22.89	18.99	23.07 ± 2.21	24.61 ± 0.88	21.54 ± 2.09
Medial Radius	26.62	30.57	23.97	25.32	20.11	26.30	26.89	19.93	24.96 ± 3.58	26.62 ± 2.85	23.31 ± 3.81
Lateral Radius	25.67	25.02	24.86	24.57	21.72	22.32	22.51	20.57	23.40± 1.85	25.03 ± 0.47	21.78 ± 0.87
MSE (whole)	0.216	0.200	0.231	0.074	0.112	0.135	0.150	0.139	0.157	0.216	0.138
MSE (medial)	0.020	0.067	0.114	0.034	0.022	0.050	0.059	0.026	0.049	0.067	0.055
MSE (lateral)	0.035	0.059	0.045	0.024	0.038	0.039	0.032	0.018	0.036	0.046	0.037

Regarding the tibia, the mean radii of curvature calculated from medial and lateral cylinder characterizations for males were 26.62 ± 2.85 mm and 25.03 ± 0.47 mm respectively. For the female tibiae, the mean value for the medial side radius was 23.31 ± 3.81 mm, and for the lateral side, 21.78 ± 0.87 mm. Although the female radii values tended to be slightly smaller than the male values, these differences were not significant.

In addition to calculating the radii of curvature for cylinders fit to the medial and lateral halves of the talocrural articular surfaces, single-point radius values were calculated by finding the distance from the longitudinal cylinder axis to the furthest points from the axis on both the medial and lateral edges. The medial and lateral single-point radius values for all tali and tibiae are presented in Table 5-8 and Table 5-9 respectively. For the talus, the mean single point radius on the medial side was 20.32 ± 2.66 mm, and the mean value for the lateral side was 20.66 ± 2.14 mm. For the tibia, the mean value on the medial side was 23.74 ± 2.29 mm, and the mean value on the lateral side was 23.64 ± 2.09 mm.

Table 5-8 Medial and lateral single-point radius values for the *talus*.

(mm)	**1**	**2**	**3**	**4**	**5**	**6**	**7**	**8**	**Mean**	**STDEV**
Gender	*male*	*male*	*male*	*male*	*female*	*female*	*female*	*female*	--	--
Medial	23.69	23.45	21.80	21.90	17.56	17.99	18.65	17.51	20.32	2.66
Lateral	22.79	23.16	21.97	22.53	18.57	18.51	19.54	18.25	20.66	2.14

Table 5-9 Medial and lateral single-point radius values for the *tibia*.

(mm)	**1**	**2**	**3**	**4**	**5**	**6**	**7**	**8**	**Mean**	**STDEV**
Gender	*male*	*male*	*male*	*male*	*female*	*female*	*female*	*female*	--	--
Medial	25.05	26.61	25.35	24.25	21.35	24.37	23.44	19.51	23.74	2.29
Lateral	25.30	26.42	24.31	24.75	21.62	23.71	23.12	19.90	23.64	2.09

Statistical comparisons were made between the medial and lateral single-point radius values within the talus and within the tibia. No significant mean differences were found between medial and lateral single-point radius values within the talus or the tibia. The medial and lateral single-point radius values were also statistically compared *between* the talus and the tibia. On the medial side, the radius values for the talus were significantly smaller ($t(14) = 2.75$, $p < 0.01$) than the values for the tibia. On the lateral side, the single-point radius values for the talus were also significantly smaller ($t(14) = 2.81$, $p < 0.01$).

Statistical comparisons of the single-point radius values were also made across gender. For the talus, significant differences were noted across genders for both the medial side ($t(6) = 8.49$, $p < 0.01$) and lateral side ($t(6) = 10.33$, $p < 0.01$) with females having smaller radii of curvature in both cases. For the tibia, similar results were noted with the males having larger radii of curvature for both the medial side ($t(6) = 2.64$, $p < 0.05$), and the lateral side ($t(6) = 3.21$, $p < 0.05$). It is worth noting that the differences between medial and lateral point values for men and women tended to be greater for the talus than for the tibia, which can be inferred from the t-test statistics.

5.2.3 Cylinder Axis Comparisons

Comparisons were made among the longitudinal axes of the different cylinders obtained via the whole, medial, and lateral surface cylindrical characterizations. These comparisons were made between the tibia and talus axes for the whole-fits, as well as between the whole-fit and the medial/lateral-fits for each bone. In order to examine any overall differences in position and orientation between these axes, two values were calculated: the angle between two axes (alpha, in degrees) and the minimum distance between them (beta, in mm). Both values were calculated within the width of the joint space, as determined by the medial and lateral joint edges digitized during the microscribe procedure. Alpha and beta values for comparisons between the tibia whole-fit and the talus whole-fit are presented in Table 5-10. Negative alpha values indicate that the tibial axis was in valgus with respect to the talar axis, while positive values indicate that the tibial axis was in varus with respect to the talar axis. The range of alpha was 9.81 degrees, with a mean of 5.63 ± 3.39 degrees. For beta, the total range of observed values was 18.1, with a mean of 3.98 ± 5.93 mm. Regarding beta values, one specimen (#6) had an uncharacteristically large value (18.41 mm). After excluding this specimen, the range for the remaining 7 specimens was quite smaller at 3.48 mm.

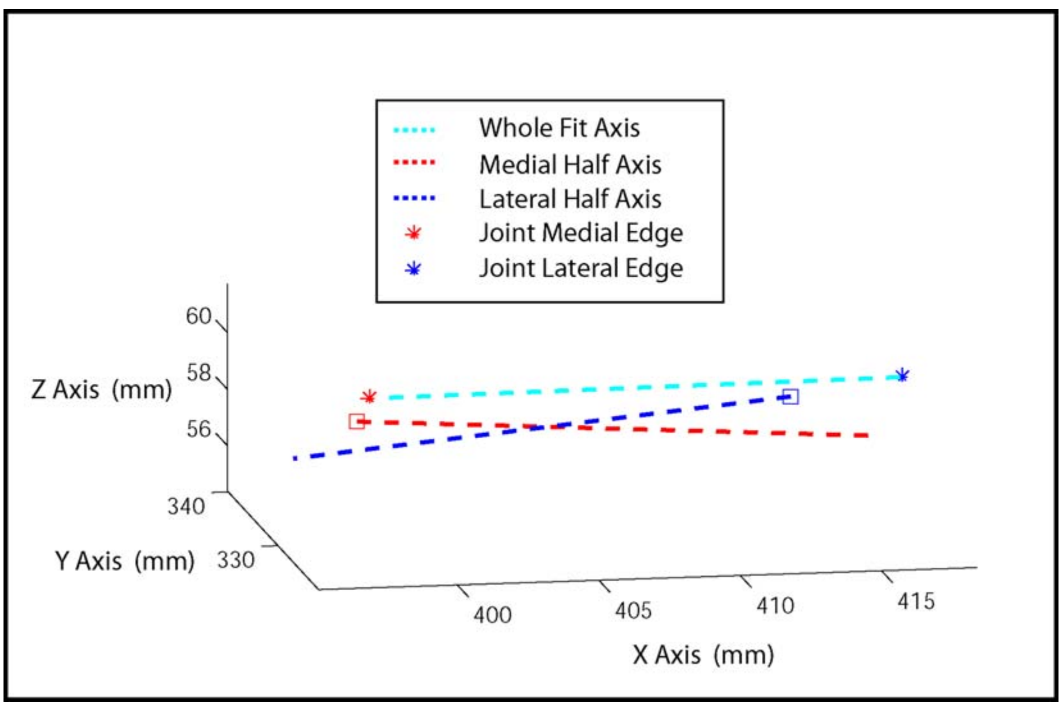

Figure 5.1 Plot of the whole-fit, medial-fit, and lateral-fit cylinder longitudinal axes. The axes were compared by calculating the minimum distance and angle between them, within joint space.

Comparisons were also made between the longitudinal axes for each medial-fit and lateral-fit with the whole fit axes. For the talus, the alpha and beta values between the medial-fit axis and the whole-fit axis, as well as the lateral-fit axis and whole-fit axis are presented in Table 5-11. For the medial-fit versus the whole-fit talus comparison, the range of alpha was calculated to be 6.07 degrees with a mean of 4.87 ± 2.14 degrees. The range of beta was calculated to be 1.6 mm with a mean of 0.67 ± 0.53 mm. For the lateral-fit versus whole-fit talus comparison, the range of alpha was calculated to be 6.01 degrees with a mean of 5.60 ± 2.48 degrees. Beta values for the lateral-fit versus whole-fit talus comparison showed a range of 2.15 mm with a mean of 0.80 ± 0.63 mm.

Table 5-10 Alpha (deg.) and beta (mm) values for the comparisons between the longitudinal cylinder axes for the whole-fit cylinder optimizations of the tibia and talus.

Spec. #	1	2	3	4	5	6	7	8	Mean ± SD
Alpha	9.88	0.51	3.05	4.04	4.63	10.32	5.10	7.54	5.63 ± 3.39
Beta	2.91	3.79	0.31	1.76	1.45	18.41	2.19	1.07	3.98 ± 5.93

Table 5-11 Alpha (deg) and beta (mm) values for the comparisons between the longitudinal cylinder axes of the *talus*. The first values represent the medial-fit vs. whole-fit, and the second values represent the lateral-fit vs. whole-fit.

	Spec. #	1	2	3	4	5	6	7	8	Mean ± SD
Medial vs. Whole	**Alpha**	2.33	4.05	5.40	3.11	8.40	4.48	3.62	7.58	4.87 ± 2.14
	Beta	0.05	1.65	1.19	0.41	0.61	0.85	0.27	0.37	0.67 ± 0.53
Lateral vs. Whole	**Alpha**	2.37	8.38	7.24	3.12	8.80	3.39	5.14	6.40	5.60 ± 2.48
	Beta	0.56	2.19	0.71	0.36	0.04	0.97	0.71	0.85	0.80 ± 0.63

Table 5-12 Alpha (deg) and beta (mm) values for the comparisons between the longitudinal cylinder axes of the *tibia*. The first values represent the medial-fit vs. whole-fit, and the second values represent the lateral-fit vs. whole-fit.

	Spec. #	1	2	3	4	5	6	7	8	Mean ± SD
Medial vs. Whole	Alpha	6.87	8.65	7.73	4.25	9.24	8.39	9.46	10.24	7.80 ± 1.87
	Beta	1.30	4.02	0.39	0.82	0.47	2.32	3.67	0.74	1.85 ± 1.45
Lateral vs. Whole	Alpha	10.32	10.40	11.62	6.28	4.47	5.26	5.01	7.61	7.62 ± 2.81
	Beta	0.89	0.97	0.02	0.31	0.91	0.65	0.04	1.41	0.54 ± 0.49

For the tibia, the alpha and beta values between the medial-fit axes and the whole-fit axes, as well as between the lateral-fit axes and whole-fit axes are presented in Table 5-12. For the medial-fit versus whole-fit tibia comparison, the range of alpha was calculated to be 5.99 degrees with a mean of 7.80 ± 1.87 degrees. The range of beta was calculated to be 3.28 mm with a mean of 1.85 ± 1.45 mm. For the lateral-fit versus whole-fit tibia comparison, the range of alpha was calculated to be 7.15 degrees with a mean of 7.62 ± 2.81 degrees. Beta values for the lateral vs. whole tibia comparison showed a range of 1.41 degrees with a mean of 0.54 ± 0.49 degrees.

In order to evaluate the extent of the saddle-shaped profile of the articular surfaces, the orientations of the axes of cylinders fit to the medial and lateral halves of the talar and tibial surfaces were compared in the coronal plane with their respective whole-fit axes, as well is with each other. These values for the talus are displayed in Table 5-13, while the values for the tibia are presented in Table 5-14. For the talus, the average angle between the medial-fit axis and the whole-fit axis was 4.39 ± 2.01 degrees, with the medial axes at a varus orientation with respect to the whole-fit axis. The average angle between the lateral-fit axis and the whole-fit axis was 3.43 ± 1.64 degrees, with the lateral axis at a valgus orientation with respect to the whole-fit axis. If the medial and lateral axes had the same coronal plane alignment, the angle between them would be 180 degrees. For the talii examined in these experiments, the average angle between the medial-fit axis and lateral fit axis was 172.18 ± 3.20 degrees.

For the tibia, the average angle between the medial-fit axis and the whole fit axis was 6.12 ± 1.52 degrees, with the medial axis at a varus orientation with respect to the whole-fit axis. The average angle between the lateral-fit axis and the whole-fit axis was 4.47 ± 2.78 degrees with the lateral-fit axis at a valgus orientation with respect to the whole-fit axis. Comparisons between the medial-fit axis and lateral fit axis resulted in an average value of 181.54 ± 3.15 degrees. Statistical comparisons between the tibia and talus of the angles between the medial and lateral-fit axes with the whole-fit axes showed no significant differences. The angle between the medial and lateral-fit axes was significantly smaller for the talus than the tibia ($t(16) = -6.54$, $p<.01$), indicating that the talar dome is more saddle-shaped than the tibial articular surface which may imply a lack of conformity between the two bones.

Table 5-13 Coronal plane angular relationships between the medial-fit, lateral-fit, and whole-fit cylinder axes for the *talus*.

Spec. #	1	2	3	4	5	6	7	8	Mean ± SD
Medial vs. Whole	-4.85	-2.80	-5.39	-0.50	-6.08	-3.91	-4.68	-6.91	-4.39 ± 2.01
Lateral vs. Whole	3.33	2.99	5.50	2.48	3.45	2.97	0.79	5.94	3.43 ± 1.64
Medial Vs. Lateral	171.83	174.21	169.11	177.03	170.48	173.12	174.54	167.15	172.18 ± 3.20

Table 5-14 Coronal plane angular relationships between the medial-fit, lateral-fit, and whole-fit cylinder axes for the *tibia*.

Spec. #	1	2	3	4	5	6	7	8	Mean ± SD
Medial vs. Whole	-6.69	-6.17	-4.17	-3.85	-8.06	-5.72	-5.94	-8.41	-6.12 ± 1.52
Lateral vs. Whole	9.04	1.60	7.71	3.27	3.29	4.65	0.32	5.86	4.47 ± 2.78
Medial Vs. Lateral	177.65	184.56	176.47	180.57	184.77	181.07	185.62	182.54	181.66 ± 3.15

5.2.4 Statistical Tests: Distributions, t-Tests, and Correlations

The anthropometric measurements of the cadaver specimens used in the talocrural surface characterization experiments were analyzed statistically along with the radius of curvature data from the cylindrical surface characterizations in order to identify possible relationships between foot size, gender, or age and articular surface radius of curvature.

Distribution

Frequency analyses of the anthropometric and morphological measurements, along with gender, radius values, and age all showed non-Gaussian distributions. The radius values output from both the talus and the tibia cylinder optimizations were bi-modal, and the distributions for the dimensional measurements were skewed from normal. The abnormal distributions were mainly due to the small sample size of only eight specimens. Therefore, interpretation of the following statistical examinations should be exercised with caution, as it is difficult to draw strong conclusions due with such a small sample size. Further discussions of the limitations associated with the experimental sample size and the statistical analyses are presented in the Chapter 7.

T-Tests

The whole foot and bone-specific anthropometric measurements were analyzed using two-tailed Student's t-tests for difference in mean values. Comparisons were made between gender and between each side (left and right) for all measurements. Results showed no significant differences between the mean values for males and females, or between right and left comparisons for all measures.

Talus Correlations

For the talus, the Pearson product-moment correlations (Appendix E) computed in SPSS yielded significant correlations between radius and gender ($r = .96$, $p < .01$) indicating that the radius of curvature of the articular surface of the talus in males is larger than in females. Regarding the whole foot anthropometric measurements, both medial and lateral foot length measurements were also significantly correlated to radius size, with correlations of $r = .744$, $p < .05$ and $r = .708$, $p < .05$, respectively. No other whole foot measures exhibited significant correlations.

Several articular surface morphological measurements of the talus did exhibit significant correlations with radius size. Medial length ($r = .913$, $p < .01$), lateral length ($r = .917$, $p < .01$), and center length ($r = .957$, $p < .01$) all showed significant positive correlations with radius size. In addition, anterior width ($r = .866$, $p < .05$) and center width ($r = .899$, $p < .05$) were also significantly correlated to radius size, while posterior width showed little correlation with radius size. Discrete articular surface measurements such as medial anterior radius (r = .724, $p < .05$) and medial posterior radius (r = .713, $p < .05$) were also positively correlated with radius size as was medial anterior height ($r = .763$, $p < .05$) and overall articular surface width (r = .751, $p < .05$).

Partial correlations were also computed, controlling for gender (Appendix E). The results from these tests showed that out of all the whole foot measurements, only medial foot length remained significantly correlated to radius size (r = .915, $p< .01$) indicating that even after controlling for gender, the length measurement from the calcaneus to the big toe was still significantly correlated to radius size. Regarding the results from the partial correlations of radius size with the articular surface morphological measurements, both medial length (r = .880, $p < .01$) and center length (r = .810, $p < .05$) remained significantly correlated with radius size after controlling for gender. Not surprisingly, the discrete measures of medial anterior and medial posterior radii were also highly correlated with overall radius size, with correlation coefficients of r = .936, $p < .01$, and r = .917, $p < .01$, respectively.

__**Tibia Correlations**__

According to the Pearson product-moment correlations conducted in SPSS for the tibia data, the correlation between overall radius size and gender was not as strong as in the talus, however the association was still significant (r = .742, p< .05) indicating that males have larger tibial radii of curvature. Of all the whole foot anthropometric measurements, medial foot length (heel to big toe) was the only measurement significantly correlated to overall radius size, indicating that longer (or larger) feet have tibial articular surfaces with larger overall radii of curvature. Of the articular surface morphological measurements specific to the tibia, three values were significantly correlated to radius size including center depth (r = .799, $p < .05$), center width (r = .869, $p < .01$), and fibular width (r = .751, $p < .05$).

Partial correlations (controlling for effects of gender) of tibia radius size with all the anthropometric variables revealed only two significant relationships. Medial foot length remained highly correlated with the overall radius size of the tibia (r = .882, $p < .01$), and posterior width of the articular surface was significantly correlated with the size of the radius of curvature of the tibia (r = .756, $p <.05$), even after controlling for gender.

5.3 Landmark Vector Orientations in the CPCS

5.3.1 Cylinder Orientations

As described in Section 3.4.2, the locations of anatomical landmarks and the vectors connecting them, along with the cylinder axes were calculated and plotted within the CPCS. The orientations of relevant vectors with respect to the CPCS axes and planes are presented in this section.

The varus/valgus (coronal plane) and transverse plane orientations of the longitudinal axes of the cylinders fit to both the tibia and the talus were calculated with respect to the CPCS. Orientation angles for the talus are presented in Table 5-15, while values for the tibia are presented in Table 5-16. Positive varus/valgus angles represent a valgus orientation, while negative values represent a varus orientation. Positive transverse values represent internal rotation with respect to the CPCS y-axis, while negative transverse values represent external rotation with respect to the CPCS y-axis.

For the axes of the cylinders fit to the talus, the mean varus/valgus angle (cylinder axis angle with the CPCS xy plane) was 0.08 ± 4.1 degrees with a total range across specimens of 13.3 degrees. All specimens were in a varus orientation except for one, specimen number 6, which also had the largest angle value. Excluding specimen 6, the range for the remaining seven specimens was only 3.51 degrees. The mean transverse orientation of the cylinder axes was -17.41 ± 7.6 degrees, with a total range of 24.8 degrees. All cylinder axes for the talus were externally rotated from the CPCS y-axis.

For the tibia cylinder axes, the mean varus/valgus angle was -1.36 ± 1.28 degrees, with a total range across specimens of 4.0 degrees. All specimens except for one

Table 5-15 Varus/valgus and transverse orientations (in degrees) of the *talus* cylinder axes.

Specimen	1	2	3	4	5	6	7	8	Mean ± SD
Varus/ Valgus	2.91	0.86	1.29	0.23	0.82	-9.54	3.74	0.32	0.08 ± 4.1
Transverse	-31.70	-9.61	-19.47	-20.18	-6.93	-19.97	-14.66	-16.73	-17.41 ± 7.6

Table 5-16 Varus/valgus and transverse orientations (in degrees) of the *tibia* cylinder axes.

Specimen	1	2	3	4	5	6	7	8	Mean ± SD
Varus/ Valgus	-0.64	0.71	-1.47	-2.50	-3.31	-2.20	-0.91	-0.52	-1.36 ± 1.3
Transverse	-22.53	-9.13	-20.76	-17.19	-9.01	-27.54	-12.64	-9.24	-16.00 ± 7.1

(Specimen 2) were in varus. The mean transverse orientation was -16.0 ± 7.1 degrees, with a total range of 18.5 degrees. All tibial cylinder axes were externally rotated with respect to the CPCS y-axis.

5.3.2 Landmark Vector Orientations

The same methods that were used to calculate the orientations of the cylinder axes were also used to calculate the orientations of the vectors connecting the anatomical landmarks within the CPCS. For the intermalleolar (IM) axes, both varus/valgus and transverse rotations were calculated (Table 5-17). Just as with the cylinder axes, positive values represent valgus and internal rotation, while negative values represent varus and external rotation. The mean varus/valgus orientation of the IM axes across all specimens was -12.48 ± 3.2 degrees, with a total range of 9.2 degrees. All IM axes were found to be in a varus orientation. Regarding the transverse orientation of the IM axes, the mean value across specimens was -20.12 ± 6.2 degrees, with a total range of 16.3 degrees. As with the cylinder axes, all IM axes were found to be in external rotation with respect to the CPCS y-axis.

Table 5-17 Varus/valgus and transverse orientations (in degrees) of the Intermalleolar axes.

Specimen	1	2	3	4	5	6	7	8	Mean ± SD
Varus/ Valgus	-7.57	-16.73	-15.20	-14.70	-13.60	-8.97	-11.78	-11.28	-12.48 ± 3.2
Transverse	-22.85	-11.37	-27.41	-22.03	-13.76	-26.35	-23.23	-13.97	-20.12 ± 6.2

The varus/valgus and transverse orientations of the anterior and posterior joint lines for the talus (Table 5-18) were calculated within the CPCS. The mean varus/valgus angle for the anterior line was -4.25 ± 4.5 degrees, with a total range of 14.58 degrees. Six of the eight specimens exhibited talar anterior joint lines that were in varus, while two specimens had joint lines in valgus. The mean transverse orientation for the talar anterior joint lines was -15.46 ± 10.3 degrees, with a total range of 35.2 degrees. All but one specimen (Specimen 2) had anterior joint lines that were externally rotated with respect to the CPCS y-axis. The mean varus/valgus orientation for the talar posterior joint line was calculated to be 0.25 ± 6.7 degrees, with a total range of 19.63 degrees. Half of the specimens had posterior joint lines that were in valgus while the other half were in varus. The mean transverse orientation for the talar posterior joint lines was -14.38 ± 7.1 degrees, with a total range of 22.61 degrees. All of the talar posterior joint lines were externally rotated with respect to the CPCS y-axis.

Table 5-18 Varus/valgus and transverse orientation values (in degrees) for the anterior and posterior talar joint lines.

	Specimen	**1**	**2**	**3**	**4**	**5**	**6**	**7**	**8**	**Mean ± SD**
Ant. Joint Line	**Varus/ Valgus**	0.57	4.20	-6.65	-6.98	-3.39	-8.13	-3.21	-10.38	-4.25 ± 4.5
	Transverse	-33.78	1.42	-9.86	-19.57	-8.46	-18.40	-24.80	-10.21	-15.46 ± 10.3
Post. Joint Line	**Varus/ Valgus**	3.30	10.93	-7.74	8.42	-5.24	-8.70	1.42	-0.38	0.25 ± 6.7
	Transverse	-26.89	-4.28	-18.49	-10.83	-7.76	-22.38	-13.53	-10.91	-14.38 ± 7.1

Varus/valgus and transverse orientation values within the CPCS were also calculated for the tibia anterior and posterior joint lines (Table 5-19). The mean varus/valgus value for the tibia anterior lines was -3.80 (± 2.6) degrees, with a total range of 9.5 degrees. The tibia anterior joint lines for all specimens except one (Specimen 1) were in a varus orientation. The mean transverse orientation for the tibia anterior joint lines was -12.24 (± 5.5) degrees, with a total range of 14.41 degrees. The tibia anterior joint lines for all eight specimens were externally rotated with respect to the CPCS y-axis. Regarding the tibia posterior joint line, the mean varus/valgus orientation was -7.20 (± 4.5) degrees, with a total range of 13.9 degrees. All eight specimens exhibited tibia posterior joint lines that were in a varus orientation. The mean value for the transverse orientation of the posterior line was -25.96 (± 7.2) with a total range of 22.9 degrees. As with the anterior line, all tibia specimens exhibited a posterior joint line that was externally rotated with respect to the CPCS y-axis.

Table 5-19 Varus/valgus and transverse orientation values (degrees) for the anterior and posterior tibial joint lines.

	Specimen	**1**	**2**	**3**	**4**	**5**	**6**	**7**	**8**	**Mean ± SD**
Ant. Joint Line	**Varus/ Valgus**	1.27	-3.33	-3.20	-8.20	-4.70	-4.93	-2.13	-5.16	-3.80 ± 2.6
	Transverse Orientation	-18.82	-5.33	-12.54	-9.12	-8.99	-17.66	-19.74	-5.75	-12.24 ± 5.5
Post. Joint Line	**Varus/ Valgus**	-1.10	-10.88	-15.06	-3.24	-2.47	-6.02	-8.60	-10.20	-7.20 ± 4.5
	Transverse Orientation	-30.70	-18.61	-41.49	-23.82	-19.21	-20.17	-29.57	-24.15	-25.96 ±7.2

For ease of comparison, the following two tables summarize the varus/valgus and transverse orientations for all cylinder axes and landmark vectors.

Table 5-20 Varus/valgus orientations (in degrees) for tibia and talus cylinder axes, IM axes, anterior, and posterior joint lines.

Specimen	1	2	3	4	5	6	7	8	Mean ± SD
Talus Cylinder	2.91	0.86	1.29	0.23	0.82	-9.54	3.74	0.32	0.08 ± 4.1
Tibia Cylinder	-0.64	0.71	-1.47	-2.50	-3.31	-2.20	-0.91	-0.52	-1.36 ± 1.3
Inter-Malleolar	-7.57	-16.73	-15.20	-14.70	-13.60	-8.97	-11.78	-11.28	-12.48 ± 3.2
Anterior Talus	0.57	4.20	-6.65	-6.98	-3.39	-8.13	-3.21	-10.38	-4.25 ± 4.5
Posterior Talus	3.30	10.93	-7.74	8.42	-5.24	-8.70	1.42	-0.38	0.25 ± 6.7
Anterior Tibia	1.27	-3.33	-3.20	-8.20	-4.70	-4.93	-2.13	-5.16	-3.80 ± 2.6
Posterior Tibia	-1.10	-10.88	-15.06	-3.24	-2.47	-6.02	-8.60	-10.20	-7.20 ± 4.5

Table 5-21 Transverse orientations (in degrees) for tibia and talus cylinder axes, IM axes, anterior, and posterior joint lines.

Specimen	1	2	3	4	5	6	7	8	Mean ± SD
Talus Cylinder	-31.70	-9.61	-19.47	-20.18	-6.93	-19.97	-14.66	-16.73	-17.41 ± 7.6
Tibia Cylinder	-22.53	-9.13	-20.76	-17.19	-9.01	-27.54	-12.64	-9.24	-16.00 ± 7.1
Inter-Malleolar	-22.85	-11.37	-27.41	-22.03	-13.76	-26.35	-23.23	-13.97	-20.12 ± 6.2
Anterior Talus	-33.78	1.42	-9.86	-19.57	-8.46	-18.40	-24.80	-10.21	-15.46 ± 10.3
Posterior Talus	-26.89	-4.28	-18.49	-10.83	-7.76	-22.38	-13.53	-10.91	-14.38 ± 7.1
Anterior Tibia	-18.82	-5.33	-12.54	-9.12	-8.99	-17.66	-19.74	-5.75	-12.24 ± 5.5
Posterior Tibia	-30.70	-18.61	-41.49	-23.82	-19.21	-20.17	-29.57	-24.15	-25.96 ±7.2

5.3.3. Sagittal Plane Tilt

In order to examine the tilt of the articular surfaces in the CPCS sagittal plane, the orientation of vectors connecting the anterior and posterior corners of the joint surfaces were calculated with respect to the CPCS xy plane. Values for the sagittal tilt of the talus and the tibia calculated on both the medial and lateral sides are presented in Table 5-22. Positive values indicate a posterior tilt (anterior higher than posterior) while a negative value indicates an anterior tilt (anterior lower than posterior). The mean sagittal tilt was calculated to be between 4.46 and 7.68 degrees across all measures. Total range across all measures was 14.21 degrees. Only one measured value (Specimen 2, talus-medial) exhibited an anterior tilt.

Table 5-22 Sagittal tilt values (deg.) calculated from articular surface corner vectors for the tibia and talus.

	Spec #	**1**	**2**	**3**	**4**	**5**	**6**	**7**	**8**	**Mean ± SD**
Talus	**Medial**	9.56	-0.65	13.33	2.21	0.32	7.82	0.08	2.97	4.46 ± 5.2
	Lateral	9.76	3.06	13.56	9.54	-0.51	9.83	3.92	11.74	7.61 ± 4.9
Tibia	**Medial**	7.76	8.97	12.47	5.04	7.64	6.29	6.25	7.05	7.68 ± 2.3
	Lateral	7.23	6.01	7.93	10.80	11.22	5.53	2.40	6.35	7.18 ± 2.9

5.3.4 AP Midline of the Foot

The AP midline for each specimen was calculated according to the methods described in Section 3.4.2 in order to assess the effects of hallux valgus, which could potentially influence the location of the CPCS x-axis. For all specimens, the angle between the first and fifth metatarsal heads was calculated, and values ranged from 23.5 to 27.7 degrees. Each AP midline axis was created at a point located halfway between the two metatarsal heads, or at half of the angle between them. The x-axis of the CPCS was then oriented along the AP midline, which offset the CPCS an average of 12.5 degrees for the specimens. Since the offset value was very similar for each specimen, it was evident that there were no significant effects of hallux valgus influencing the position of the CPCS x-axis in any of the specimens. Various angles of the IM axis and cylinder axes with the AP-midline and shifted CPCS y-axis are presented in Table 5-23. Despite the lack of significant findings, the AP midline represents a more traditional AP axis of the foot, so its relationships with the anatomical vectors are reported.

Table 5-23 Angular relationships (degrees) between the AP midline axis, the IM axis, and the cylinder axes of the tibia and talus for each specimen. Also presented are the angular relationships between the same landmark vectors and the CPCS y-axis adjusted for the AP midline shift.

Specimen	1	2	3	4	5	6	7	8	Mean	SD
IM axis w/ AP midline	93.07	85.32	106.04	79.14	91.98	101.55	89.75	76.95	90.48	± 10.09
Talus cyl. axis w/ AP midline	101.93	83.56	98.09	77.28	85.16	95.17	81.18	79.71	87.76	± 9.29
Tibia cyl. Axis w/ AP midline	92.75	83.08	99.39	74.30	87.24	102.74	79.16	72.22	86.36	± 11.26
IM with AP midline y-axis	-11.11	0.94	-14.07	-9.63	0.11	-13.98	-10.49	-1.39	-7.45	± 6.30
Talus cyl. w/ AP midline y-axis	-19.97	2.70	-6.13	-7.77	6.94	-7.60	-1.92	-4.15	-4.74	± 8.03
Tibia cyl. w/ AP midline y-axis	-10.79	3.18	-7.42	-4.78	4.85	-15.17	0.10	3.34	-3.34	± 7.37

5.3.5 Tibial Crest Orientation

The orientation of the tibial crest vector in the CPCS was characterized by its relationship to the CPCS z-axis, as well as the talus and tibia cylinder axes as calculated by the dot product. The results for each specimen are presented in Table 5-24. The CPCS z-axis was perpendicular to the ground plane (xy plane), so the angular relationships for the tibial crest versus the CPCS z-axis represent deviations of the tibial crest from a purely vertical orientation. The mean value for the angle between the z-axis and the tibial crest was 5.78 ± 2.2 degrees, with a total range of 5.65 degrees. For the angle calculated between the tibial crest and the talus cylinder axes, the mean value was -94.8 ± 17.4 degrees, with a large total range of 42.1 degrees. For the angle between the tibial crest and the tibial cylinder axes, the mean value was -93.4 ± 18.9 degrees, with an even larger total range of 51.96 degrees. Due to the large range and standard deviations observed for the angles between the tibial crest and the cylinder axes, median values were also calculated. The median values for the angles between the tibial crest and the talus and tibia cylinder axes were calculated to be -86.19 degrees and -83.17 degrees respectively.

.

Table 5-24 Angular relationships (in degrees) between the tibial crest vector and the CPCS z-axis, talus cylinder axis, and the tibia cylinder axis.

Specimen	1	2	3	4	5	6	7	8	Mean ± SD
Tib crest w/ CPCS z-axis	7.14	7.22	7.61	3.24	2.14	6.91	4.20	7.79	5.78 ± 2.2
Tib crest w/ Talus cylinder	-120.32	-82.25	-83.11	-84.93	-93.23	-124.34	-82.79	-87.45	-94.80 ± 17.4
Tib crest w/ Tibia cylinder	-111.14	-81.77	-84.41	-81.94	-95.32	-131.91	-80.78	-79.96	-93.40 ± 18.9

The quasi-transverse orientation of the tibial crest vector was also characterized according to the methods described in Section 3.4.2. After projecting the tibial crest vectors onto the CPCS xy plane and finding the vector connecting these projections with the origin, rotations in the transverse plane of the tibial crest vectors with respect to the CPCS x-axis were calculated (Figure 5.2). These values are presented in Table 5-25. The mean value was 21.59 ± 16.2 degrees. The mean value for right feet was 22.17 ± 17.9 degrees, while the mean value for left feet was 21.02 ± 17.0 degrees. The mean value for male specimens was 24.57 ± 17.9 degrees, while the mean for female specimens was 18.62 ± 20.8 degrees. No significant differences were observed between right and left, or male and female specimens according to a two-tailed Student's t-test. Qualitatively, the majority of the intersection points were found in the antero-medial quadrant (medial to the first ray). One right and one left specimen had intersection points that were just slightly lateral to the first ray.

Table 5-25 Values (in degrees) representing the transverse orientation of the projection of the tibial crest vector on the xy plane with respect to the CPCS x-axis.

Specimen	1	2	3	4	5	6	7	8	Mean
Tibial crest w/ x-axis	15.83	16.50	23.45	42.51	2.90	45.84	1.87	23.85	21.59 ± 16.2

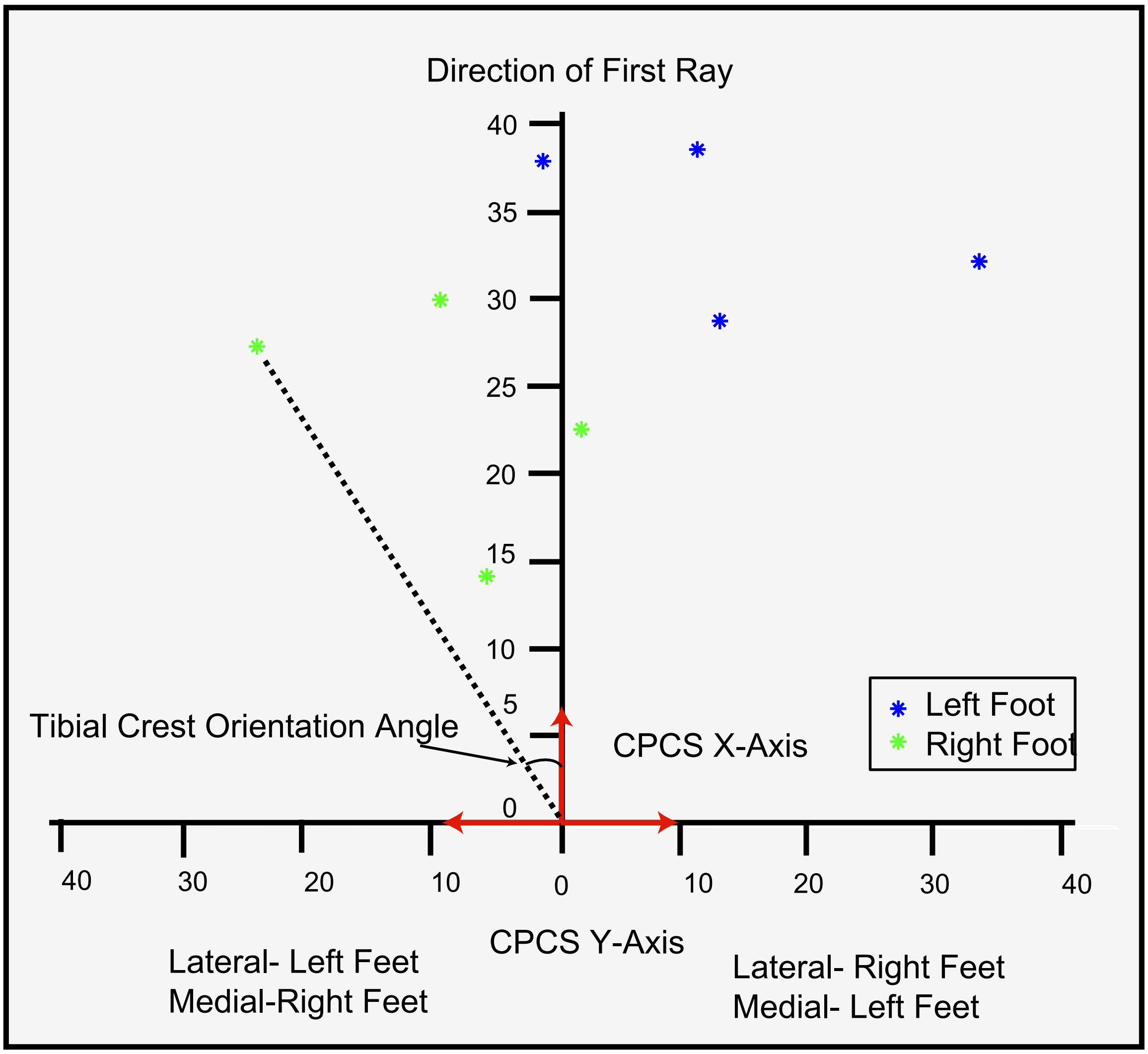

Figure 5.2 The points of intersection of the CPCS XY plane and the tibial crest vectors. The angles between the CPCS x-axis and the vector connecting the origin to each intersection point were calculated in the transverse plane.

CHAPTER 6. RESULTS: MOTION ANALYSIS EXPERIMENTS

6.1 Static Trials and Intact Specimens

The following section is a presentation of the data and results from the experiments and calculations described in Chapter 4 including the motion analysis tests of both intact and post-TAA cadavers, as well as the comparisons of relative translations and orientations in the transverse plane between anatomical segments and the TAA components.

6.1.1 Landmark Orientations

After post-processing, data from the static wanding trials of the five intact specimens were imported into Matlab and the positions of each anatomical landmark were calculated in the global space of the MA test frame. Once these positions were known, the 3D coordinates for each anatomical landmark were transformed into the CPCS space, and the orientation of the vectors connecting the malleoli and the anterior joint lines for the tibia and talus were calculated using the methods described in Section 3.4.2. Varus/valgus and transverse orientations of these vectors for the MA specimens are presented in Table 6-1. As with the microscribe analysis, positive varus/valgus angles represent a valgus orientation, while negative values represent a varus orientation. Positive transverse orientation values represent internal rotation with respect to the CPCS y-axis, while negative transverse orientation values represent external rotation with respect to the CPCS y-axis. For ease of comparison, the corresponding mean and standard deviation values from the eight specimens used in the microscribe experiment are included in Table 6-2.

For the intermalloelar (IM) axes, the mean varus/valgus angle was calculated to be -13.22 ± 2.2 degrees with a total range of 6.5 degrees. The IM axes for all five specimens were in a varus orientation. The mean value for the transverse orientation of the IM axes in the microscribe specimens (-12.48 ± 3.2 degrees) was very similar to the mean value calculated in the MA specimens. The mean transverse orientation angle for the IM axis of the five MA specimens was calculated to be -19.05 ± 3.2 degrees, and all specimens were in external rotation with respect to the CPCS y-axis. Values for the microscribe specimens were quite similar (-20.12 ± 6.2 degrees).

The mean varus/valgus orientation of the anterior joint line of the talus in the MA specimens was -8.46 ± 4.1 degrees, with a total range of 11.1 degrees. The anterior joint lines of all five MA specimens were in a varus orientation, and the mean for the MA specimens was almost twice that of the microscribe specimens, although the difference was not statistically significant ($t(11) = -1.26$, p = *n.s.*). The mean transverse orientation of the talar anterior joint line for the MA specimens was -18.70 ± 3.9 degrees with a total range of 9.9 degrees, which was similar to the mean calculated for the microscribe specimens (-15.46 ± 10.3 degrees). All MA specimens had a talar anterior joint line that was externally rotated with respect to the CPCS y-axis.

Regarding the anterior joint line of the tibia, the mean varus/valgus orientation for the five MA specimens was -8.65 ± 5.5 degrees, with a total range of 14 degrees. All MA specimens had an anterior joint line that was in a varus orientation, and the mean for the MA specimens was twice that of the microscribe specimens, although the difference was only marginally significant ($t(11) = -2.14$, $p < 0.055$). The mean transverse orientation for the MA specimens was -12.41 ± 7.1 degrees, with range of 19.4 degrees. This was similar to the mean for the microscribe experiments which was -12.24 ± 5.5 degrees.

Table 6-1 Varus/valgus and transverse plane orientations of the IM axis, talus anterior joint line, and tibia anterior joint line for the five intact MA specimens.

N=5	**Specimen**	**1**	**2**	**3**	**4**	**5**	**Mean**	**SD**
IM	**Varus/ Valgus**	-12.91	-12.58	-9.61	-16.11	-14.89	-13.22	± 2.22
	Transverse	-16.94	-17.71	-16.99	-18.21	-25.40	-19.05	± 3.21
Ant. Talus Line	**Varus/ Valgus**	-7.33	-7.83	-14.26	-3.12	-9.75	-8.46	± 4.05
	Transverse	-24.02	-22.73	-14.07	-15.93	-16.75	-18.70	± 3.94
Ant. Tibia Line	**Varus/ Valgus**	-12.88	-0.46	-8.23	-14.46	-7.22	-8.65	± 5.50
	Transverse	-16.73	-11.47	-6.08	-4.20	-23.57	-12.41	± 7.10

Table 6-2 Mean ± S.D. varus/valgus and transverse orientation values from the eight specimens used in the microscribe experiments.

N=8	**Specimen**	**Mean**	**SD**
IM	**Varus/ Valgus**	-12.48	± 3.16
	Transverse	-20.12	± 6.18
Ant. Talus Line	**Varus/ Valgus**	-4.25	± 4.50
	Transverse	-15.46	± 10.25
Ant. Tibia Line	**Varus/ Valgus**	-3.80	± 2.56
	Transverse	-12.24	± 5.47

6.1.2 Alignment Verification

To evaluate the orientations of the TAA cuts in the coronal plane, the angle between the anterior joint line of the components and the CPCS xy plane was calculated as described in Section 4.2.5. Based on data from the microscribe experiments in which the cylinder axes of the talus were consistently found to be in a relatively neutral varus/valgus orientation, the goal of the alignment instrumentation and procedure was to make the talar cuts as close to parallel with the xy plane as possible. As a result, the desired angle between the components and the xy plane was zero. Negative values indicate a varus orientation of the cut plane, while positive values indicate a valgus orientation. The resultant angle for each specimen can be found in Table 6-3. As observed from the table, the mean orientation of the components in the coronal plane was -0.34 ± 1.5 degrees, demonstrating that all cuts were made very close to parallel with the xy plane.

The orientations of the components with respect to the tibial crest were also examined, as outlined in Section 4.2.5. According the microscribe experiments, the mean angle between the tibial crest and the cylinder axes was near 90 degrees. Therefore, the goal of the tibial alignment procedure was to make TAA cuts perpendicular to the tibial crest line, so the desired angle for this relationship is 90 degrees. The resultant angles for each specimen are presented in Table 6-4. The mean angle for all five specimens was 90.80 ± 2.14 degrees, indicating the criteria of making TAA cut perpendicular to the tibial crest was met, within a small margin of error.

Table 6-3 Coronal plane angles (deg) of the TAA components with respect to the CPCS xy plane.

Specimen #	1	2	3	4	5	Mean	SD
Tibial Crest vs. xy Plane	1.66	-1.33	-2.00	-0.92	0.89	-0.34	± 1.55

Table 6-4 Angular relationships between the TAA components and the tibial crest in the coronal plane.

Specimen #	1	2	3	4	5	Mean	SD
Tibial Crest vs Comp.	91.03	94.09	89.40	91.01	88.45	90.80	± 2.14

6.2 Relative Motions

6.2.1 Plantar/Dorsiflexion Amplitude

Data from static and kinematic motion analyses of the component trials were processed in Matlab and the relative positions of the tibia, talus, and component were calculated over five trials for each specimen. As described in Section 4.2.4, the data for each trial were separated into individual plantarflexion/dorsiflexion (PF/DF) cycles using a spline interpolation to locate the zero, points (neutral positions) (Figure 6.1). Grand means of PF/DF amplitude calculated over five trials for each specimen were computed by averaging the PF/DF for all cycles in each individual trial, and then finding a specimen mean across trials (Table 6-5). The total mean amplitude of PF/DF for all specimens was 31.32 ± 2.07 degrees.

Table 6-5 Mean plantarflexion-dorsiflexion amplitudes for each MA specimen.

Specimen #	1	2	3	4	5	Mean	SD
PF/DF Amplitude	33.21	28.23	32.08	32.67	30.042	31.32	± 2.07

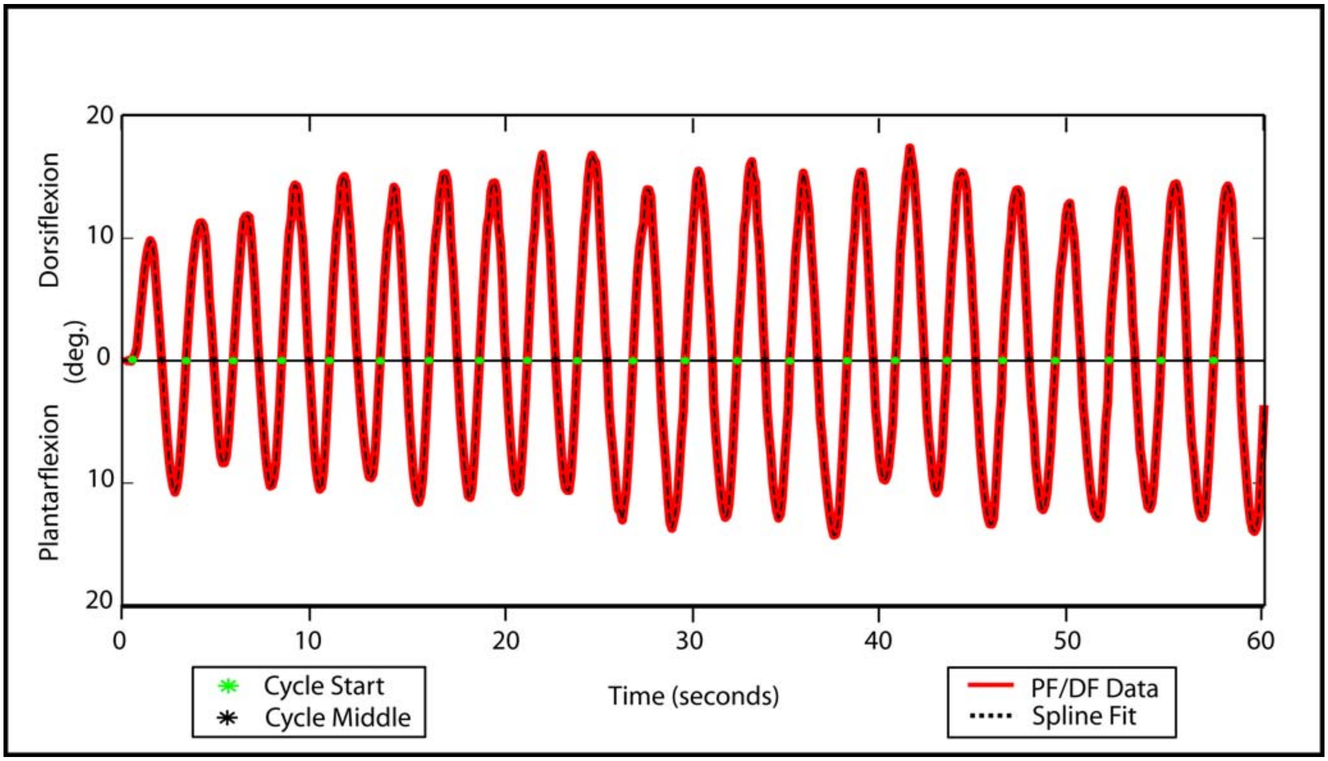

Figure 6.1 Plantarflexion-dorsiflexion data from one example trial. The red line is the PF/DF data, and the dashed black line represents the spline fit. Green asterisks mark the start of each PF/DF cycle, and black asterisks mark the mid-point of each cycle.

6.2.2 Component Transverse Rotations

The transverse orientations of the components with respect to the tibia over the course of the kinematic trails were plotted for all five specimens (Figure 6.2). Total start-to-finish rotations of the experimental TAA components in the transverse plane were calculated by finding the difference between the transverse angles at the first and last neutral points in each trial. Average initial and end orientations for each component are displayed in Table 6-6. The difference values calculated for five trials were averaged to obtain mean transverse orientation changes for each specimen (Table 6-6). Negative transverse orientation values indicate that the components were internally rotated with respect to the tibial anatomical coordinate system (IM axis) while positive values indicate that the components were externally rotated with respect to the tibial anatomical coordinate system. Four of the five specimens were internally rotated with respect to the tibial anatomical coordinate system at both initial and final positions. At their final positions, the mean transverse orientation with respect to the tibia anatomical coordinate system was -8.90 ± 11.1 degrees. The mean absolute value of the start-to-finish difference in the transverse rotations of the components for all five specimens was 4.08 ± 7.17 degrees. All but one component (Specimen 4) externally rotated during the experiment.

In addition to the overall shifts in the transverse orientation of the components, rotational oscillations in the transverse plane were observed. To quantify the amplitude of these oscillations, the minimum and maximum values of component rotations in the transverse plane were calculated for each PF/DF cycle within a trial (Figure 6.3). These values were averaged for every trial, and then grand means were computed for all five specimens (Table 6-7). The amplitudes of the mean rotational oscillations in the transverse plane ranged from 2.16 to 6.12 degrees for the five specimens. The variance in these measurements was low, with standard deviations less than 1.5 degrees for each specimen. Overall, the mean rotational oscillation amplitude across all specimens was 3.37 ± 1.12 degrees.

Table 6-6 Initial and final orientations, as well as total shift in transverse orientation of the TAA components relative to the tibia anatomical CS. All values are in degrees.

Specimen #	1	2	3	4	5	Mean	SD
Initial Orientation	-22.39	5.63	-17.23	-15.96	-14.66	--	--
Final Orientation	-17.79	6.54	-1.15	-18.21	-13.86	-8.90	± 11.05
Start-Finish Difference	4.87	0.90	16.07	2.25	0.80	4.08	± 7.17

Table 6-7 The average amplitude of rotational oscillations in the transverse plane (in degrees) of the components with respect to the tibia anatomical CS. Values for each trial are presented, along with the mean amplitude for each specimen.

	Trial 1	Trial 2	Trial 3	Trial 4	Trial 5	Mean	SD
Specimen 1	5.56	7.21	5.11	7.76	4.94	6.12	± 1.28
Specimen 2	2.13	1.58	2.57	1.73	2.03	2.01	± 0.39
Specimen 3	2.05	3.44	1.95	2.34	2.67	2.49	± 0.60
Specimen 4	4.15	2.25	0.82	2.80	0.78	2.16	± 1.42
Specimen 5	4.36	3.98	3.48	4.84	3.66	4.07	± 0.55
Average Values of Individual Specimen Means =						3.37	± 1.12

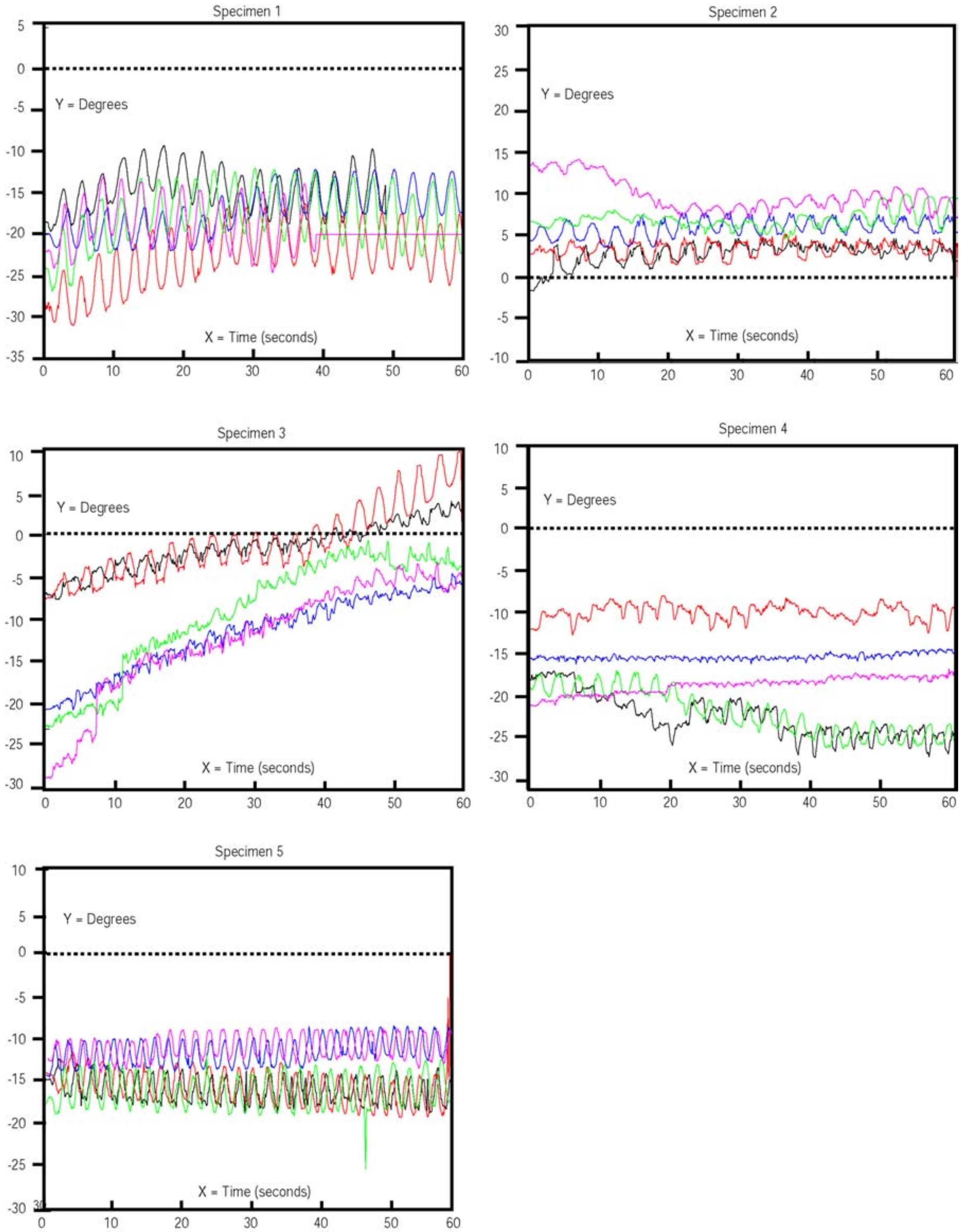

Figure 6.2 Transverse plane rotations of the TAA components with respect to the tibia anatomical CS. Each figure represents 5 trials for a single specimen. The y-axis is the transverse rotation (deg) and the x-axis is time (sec).

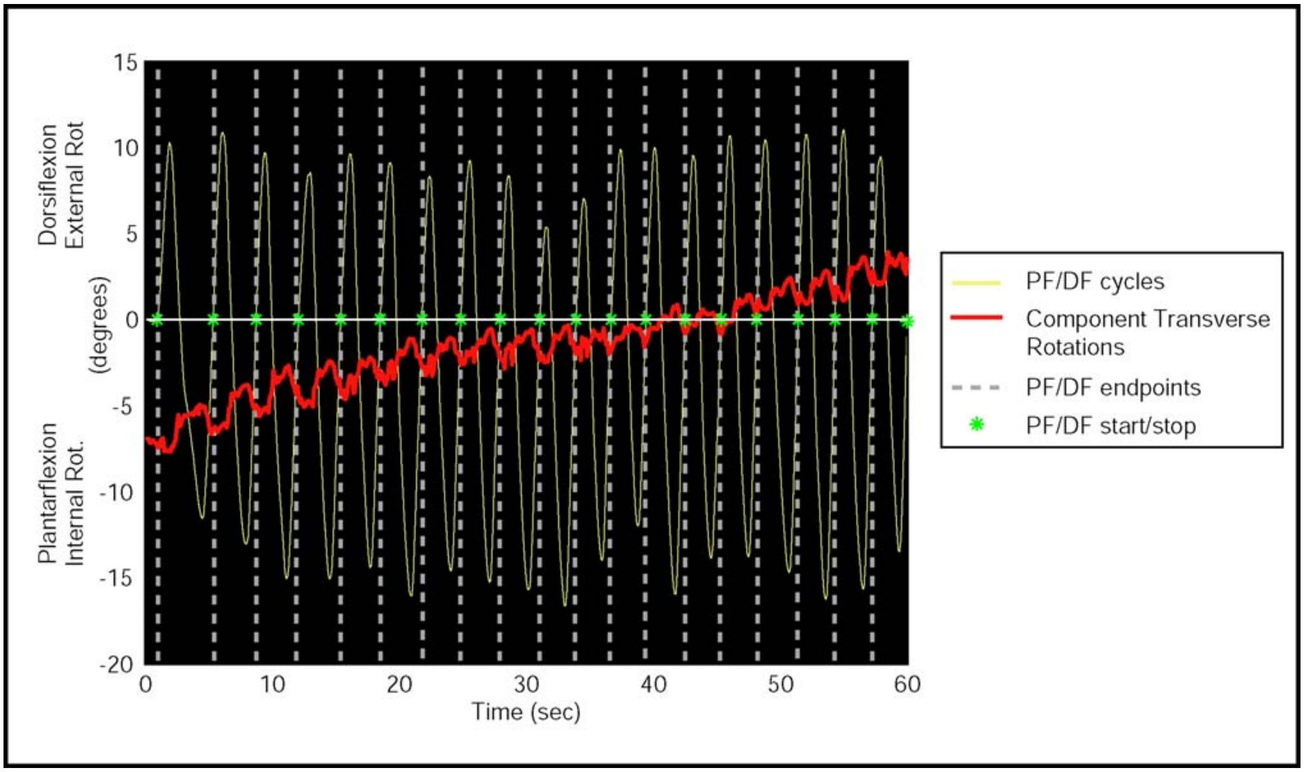

Figure 6.3 Plot of the component transverse rotation and the PF/DF data. PF/DF cycles endpoints were identified and the amplitude of transverse rotation was calculated for each invidual cycle.

The transverse plane rotations of the components with respect to the tibia were also plotted along with the transverse plane rotations of the component with respect to the talus, and the talus with respect to the tibia (Figure 6.4). This was done in an attempt to examine whether or not rotations of the talus were responsible for the transverse plane rotational oscillations or overall rotations of the component. Because of the fixed angle decomposition method used to calculate the relative motion between two anatomical coordinates systems, quantitative calculations could not be performed to compare the motion of the component relative to the tibia with the motion of the talus relative to the tibia. Qualitatively for a single specimen, as observed in Figure 6.4, the rotational oscillations of the component relative to the talus in the transverse plane are similar to the oscillations of the component relative to the tibia, although they appear to be out of phase from one another.

Rotational oscillations in the transverse plane of the talus with respect to the tibia do occur as evidenced by the blue line in Figure 6.4, but the amplitude of these oscillations is smaller than the observed amplitudes of rotation for the component with respect to the tibia. Furthermore, towards the end of the example trial plotted in Figure 6.4, the talus begins to exhibit large rotational oscillation (green and blue lines), but the component rotations with respect to the tibia (red line) are not affected by this. This would suggest that the rotational oscillations of the components were not completely dictated by rotational oscillations of the talus.

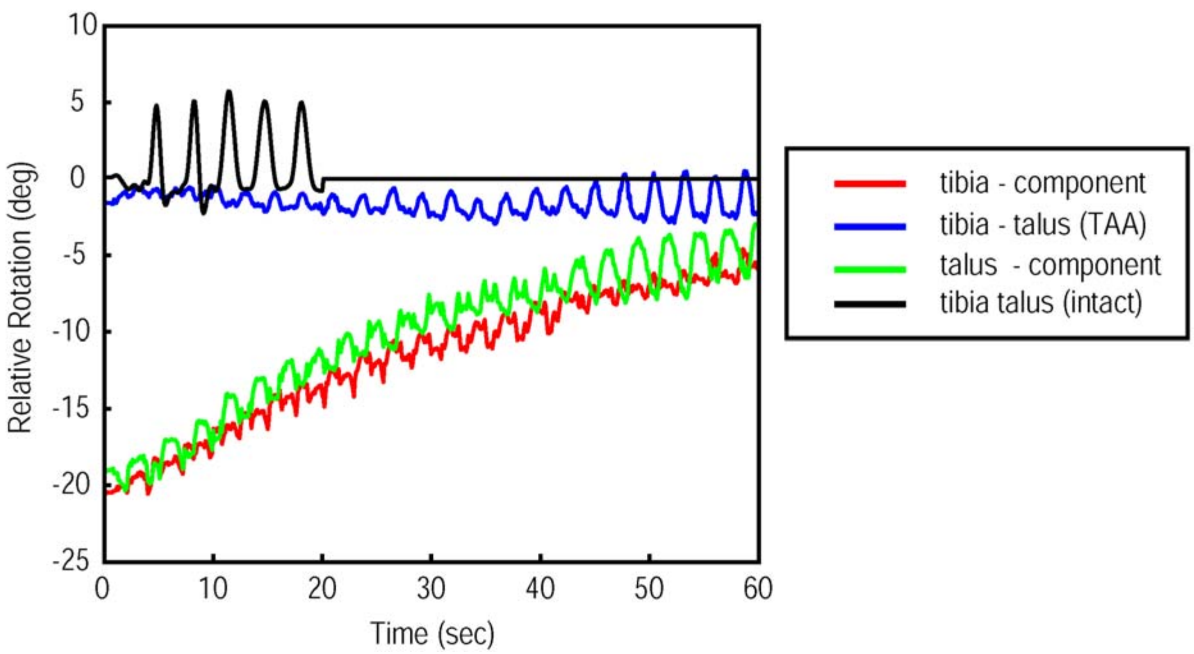

Figure 6.4 A plot of transverse rotations for one example (Specimen 3, Trial 3). The plot includes relative transverse rotations of the talus with respect to the tibia for the TAA trials (blue line), the components with respect to the tibia (red line), and the components with respect to the talus (green line). The black line represents the relative transverse plane rotations of the talus with respect to the tibia for the intact specimen (pre-surgery).

The transverse plane rotations between anatomical segments for the TAA trials differed from the tests of the intact specimen, as indicated by the black line. The plotted relative motion in the transverse plane between the talus and tibia in the intact specimen exhibited larger amplitudes of rotation than in the TAA trials, and the rotation was predominantly external rotation of the talus with respect to the tibia. The amplitudes of the relative rotations for the TAA trials were smaller and more equally distributed between internal and external rotation. It should be noted that the intact specimens were only tested for a duration of 20 seconds, therefore the data is only comparable for a few trials of movement. This is evident in Figure 6.4 by the black line at zero degrees rotation after 20 seconds.

6.2.3 Transverse Orientation Comparisons

Endpoint orientations of the components in the transverse plane were compared to the transverse plane orientations of the anterior tibial and talar joint lines, as well as the tibial and talar optimized cylinder axes from the microscribe experiments (Table 6-8). Comparisons were made relative the CPCS as described in Section 3.4.1. To facilitate comparisons with the cylinder axes and respective anatomical counterparts from the microscribe specimens, the microscribe values are presented again in Table 6-9.

Table 6-8 Transverse plane orientations in the CPCS for the TAA components, IM axes, and anterior joint lines for the MA specimens.

Specimen	1	2	3	4	5	Mean	S.D.
TAA Component	0.85	-24.24	-15.83	0.00	-11.54	-10.15	±10.69
Intermal. Axis	-16.94	-17.71	-16.99	-18.21	-25.40	-19.05	± 3.25
Talus Ant. Joint Line	-24.02	-22.73	-14.07	-15.93	-16.75	-18.70	± 3.94
Tibia Ant. Joint Line	-16.73	-11.47	-6.08	-4.20	-23.57	-12.41	± 7.16

Table 6-9 Transverse orientations of the cylinder, IM, anterior, and posterior axes for the digitized specimens.

Specimen	1	2	3	4	5	6	7	8	Mean	SD
Talus Cylinder	-31.70	-9.61	-19.47	-20.18	-6.93	-19.97	-14.66	-16.73	-17.41	± 7.6
Tibia Cylinder	-22.53	-9.13	-20.76	-17.19	-9.01	-27.54	-12.64	-9.24	-16.00	± 7.1
Inter-Malleolar	-22.85	-11.37	-27.41	-22.03	-13.76	-26.35	-23.23	-13.97	-20.12	± 6.2
Anterior Talus	-33.78	1.42	-9.86	-19.57	-8.46	-18.40	-24.80	-10.21	-15.46	± 10.3
Posterior Talus	-26.89	-4.28	-18.49	-10.83	-7.76	-22.38	-13.53	-10.91	-14.38	± 7.1
Anterior Tibia	-18.82	-5.33	-12.54	-9.12	-8.99	-17.66	-19.74	-5.75	-12.24	± 5.5
Posterior Tibia	-30.70	-18.61	-41.49	-23.82	-19.21	-20.17	-29.57	-24.15	-25.96	±7.2

Comparisons of the transverse orientation of the TAA components to the IM axes and anterior joint lines in the CPCS revealed that the components were internally rotated from the other vectors. Regarding the mean values across specimens, the TAA components were internally rotated around 10 degrees with respect to the IM axes, almost 10 degrees with the talus anterior joint lines, and around 3.5 degrees with the tibia anterior joint lines. Comparisons made between the mean component transverse orientations and the mean transverse orientations of the cylinder axes calculated in the microscribe experiments revealed that the TAA components were internally rotated in the CPCS around 7 degrees from the mean talus cylinder axis, and around 6 degrees from the mean tibia cylinder axis. In fact, the TAA components were internally rotated from all measures of transverse orientation including the IM axis and the anterior/posterior joint lines of the microscribe specimens. It is worth noting, however, that the standard deviation of the mean TAA component orientation was quite large, therefore the mean value may not be an optimum representation of specimen-specific component orientation.

Individually, a few of the specimens tended to display TAA component transverse rotations that converged towards a repeatable orientation across trials (Specimens 1, 2, and 3) while others exhibited more random behavior. For two specimens, the TAA components showed convergence for some, but not all of the trials (Specimens 3 and 4). Regarding the endpoint orientations, there seemed to be two separate orientation groups. Three specimens (1, 4, and 5) had endpoint orientations between 13 and 18 degrees of external rotation, which is in the orientation range of the anterior joint lines and the IM axis. The remaining two specimens (2 and 3) had endpoint orientations that were closer to the CPCS y-axis (between 1 degree of external rotation and 6 degrees of internal rotation). Interestingly, these were also the specimens that exhibited the smallest and largest total change in transverse orientation.

6.2.4 Component Translations

Translations of the TAA components in the transverse plane were calculated for each experimental trial, and mean start-to-finish translation values were compiled for all five specimens. Initial and final positions of the TAA components are displayed in Figure 6.5. Total translation of the component in the xz plane was computed by calculating the difference between the initial and final positions for each direction (x and z) independently (Table 6-10). For x-axis translations, positive values represent anterior translation, while negative values represent posterior translation. For the z-axis, positive values represent medial translation, while negative values represent lateral translation. Mean total translations in the x-axis direction ranging from -4.43 mm to 7.48 mm were observed, while mean total translations in the z-axis direction ranged from -3.52 mm to 2.09 mm. Three out of five specimens (specimens 1, 2, and 5) translated posteriorly and laterally and the other two specimens (specimens 3 and 4) translated medially and anteriorly.

Table 6-10 Mean TAA component translation values in the x and z directions for each MA specimen. Positive/negative x values represent anterior/posterior translation, while positve/negative z values represent medial/lateral translation respectively.

(Values in mm)	**X Direction (ant/post)**		**Z Direction (med/lat)**	
	Mean	**SD**	**Mean**	**SD**
Specimen 1	-3.34	3.26	-3.52	1.06
Specimen 2	-4.43	4.08	-2.23	2.06
Specimen 3	7.48	5.37	0.40	1.59
Specimen 4	1.21	2.78	2.09	1.74
Specimen 5	-2.42	4.08	-2.17	0.66
Overall Mean	-0.30	3.91	-0.11	1.42

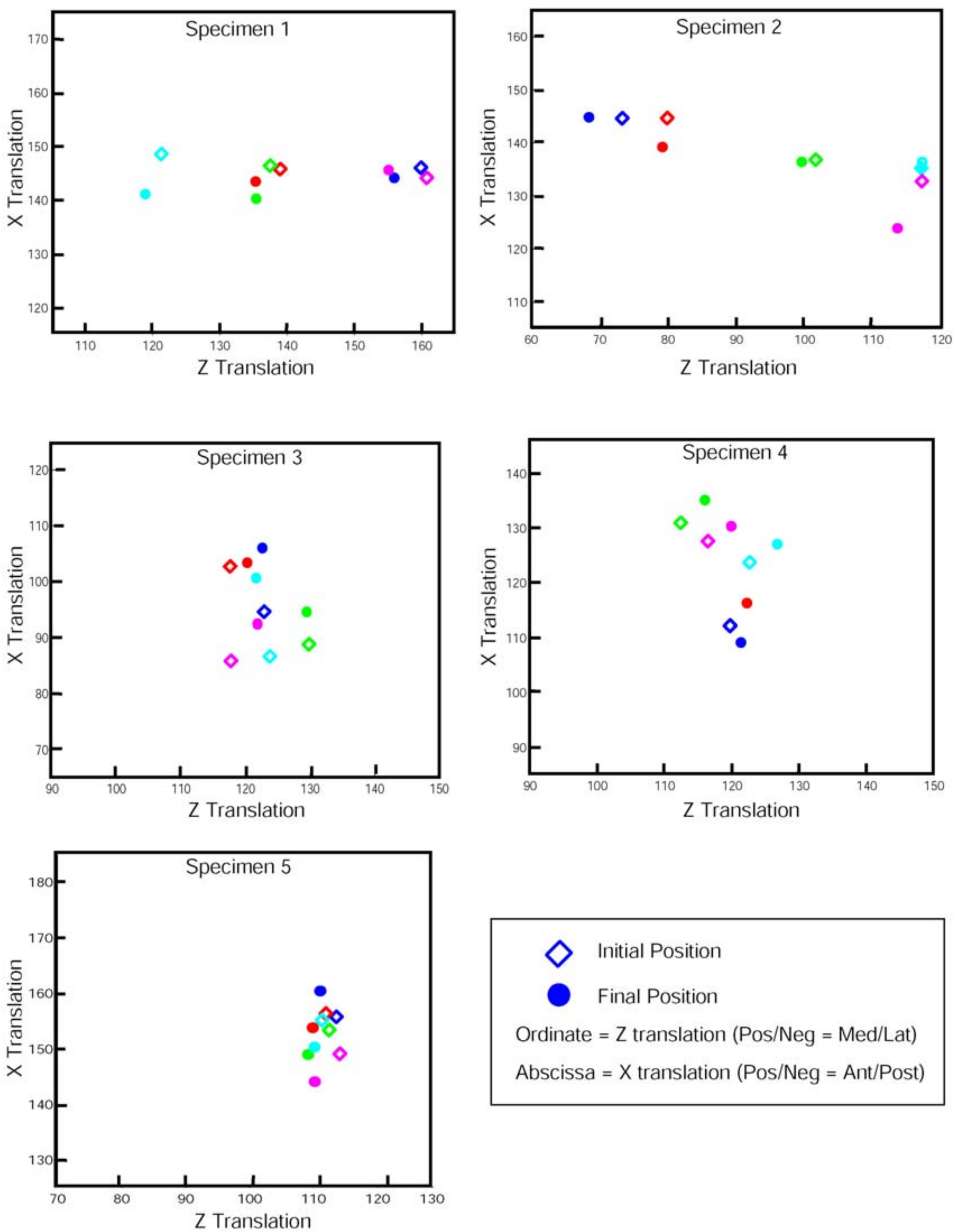

Figure 6.5 Initial and final positions of the origin of the TAA components for each trial of the MA experiments. Open diamonds represent initial positions, while solid dots represent final positions. Total translation was calculated as the difference between the initial and final positions in both the X and Z directions.

CHAPTER 7. DISCUSSION AND CONCLUSIONS

Overview

This chapter addresses the findings from both the 3D digitization experiments and the TAA motion analysis tests. A discussion of the cylinder charcterizatoins for both the talus and tibia articular surfaces, as well as the examinations of landmark and cylinder axis orientations is presented first, followed by a discussion of the TAA kinematic experiments and their relevance to the ankle joint and TAA. Next, the limitations and considerations associated with each experiment are discussed, followed by an evaluation of the hypotheses from Chapter 1. The implications of this work and recommendations for future research are presented in the final sections.

7.1 3D Digitization Experiments

7.1.1 Cylinder Characterizationss

Data from the digitization experiments and cylinder characterizations provided unique information regarding the geometry and static orientations of the articular surfaces of the talus and the tibia. While the idea that the articular surface of the talar dome represents a cylinder in a sagittal profile is not novel, there have been few, if any, studies in which the *entire* articular surface of the talus has been characterized in 3D. As mentioned previously, a variety of authors have reported estimates of the radius of curvature for the talus ranging from 18 mm to 28 mm, however, all of these values are calculated from 2D sagittal profiles (Barnett and Napier, 1976; Fessy et al., 1997; Leardini et al., 1999; Pappas et al., 1976; Reimann et al., 1986, Waugh et al., 1976).

Both the 2D (single-point) and the 3D values calculated in this study via the cylinder optimizations were in the range of these previous estimates. The radius values described by Medley et al. (1983), in which multiple AP radial lines were measured across the width of the talar dome are probably the most similar to the 3D values calculated in this study. The mean radii of curvature calculated in that study was 20.8 mm, which is close to agreement with the mean of 19.97 mm calculated in the current experiments. In the study by Medley and colleagues, the sample size was only three, and there was no mention of specimen gender making it difficult to compare their values with the current values for male and female radii of curvature.

The 3D estimates of the radii of curvature for the tibia in this experiment were significantly larger than the estimates for the talus. Tibial articular surfaces from previous experiments have also been noted to be larger than their counterparts on the talus, and estimates for the tibial radii of curvature in the literature range from 22.1 mm to 27.8 mm (Medley et al., 1983; Stagni et al., 2005). The mean radius of curvature of the articular surface of the tibia calculated in the current experiments was 23.1 mm, which is in agreement with these previous estimates. The difference in size of around 3 mm between the radii of curvature of the tibia and talus has been postulated to be a result of the talocrural joint's similarity to a hydrodynamic bearing, in which the convex surface often has a slightly smaller radius of curvature than the mating concave surface, in order to aid in entrainment of the lubricant (in this case, synovial fluid) (Medley, et al., 1983).

According to the cylinder characterizations for the medial and lateral halves of the articular surfaces, there were no statistical differences between the mean radii of curvature of the tibia or talus between medial and lateral sides. These data differ from previously reported results, which have noted significant deviations (about 5 %) in the 2D radii of curvature from medial to lateral sides (Barnett and Napier, 1952; Medley et al., 1983; Waugh et al., 1976). There were no statistically significant deviations between the medial and lateral single-point radius measures in the current experiments that would support this idea either, although experimental methods or error may account for this.

The gender comparisons of the data from the 3D digitization experiments also showed that males had significantly larger tibial and talar radii of curvature than females. Examinations of correlations with radius of curvature values yielded significant correlations between medial foot length and radius, however, it could be argued that this relationship only reflects an inherent difference in foot length between men and women. Unfortunately, the specimens used in this study did not represent a broad range of sizes, therefore it is difficult to draw any concrete conclusions regarding foot size differences between gender. Nevertheless, partial correlation examinations controlling for gender also indicated that strong correlations between medial foot length and radius size remained for both the talus and the tibia. Based on these results, it may be possible to estimate the curvature of the talar dome using medial foot length. Data from additional specimens is needed before this approach can be applied. Estimates of the radii of curvature for both the talus and tibia in the literature have little mention of gender, so it is difficult to compare these results with previously reported values. Stagni and colleagues (2005) did report a trend of male specimens having larger radii of curvature than females, although no statistical analyses were reported. To the knowledge of this author, the data presented in these experiments representing 3D male and female radii of curvature are the first of their kind.

The comparison of the position and orientation of the longitudinal cylinder axes of the tibia and talus yielded mean angles of around 5 degrees and distances of around 4 mm between the two axes, indicating acceptable agreement between the two optimizations. If the articular surfaces of the tibia and the talus are predominantly congruent at a position of neutral plantar/dorsiflexion, then they should exhibit similar orientations. Deviations in orientation between the two axes may be due to experimental error, or may be a reflection of slight non-conformity between the articular surfaces. The talocrural joint has been postulated to be somewhat incongruent, a fact that is thought to account for changes in its rotational axis during movement (Deland et al., 2000; Inman, 1976; Lundberg et al., 1989). The distance between axes may also be due to the natural space between the two articular surfaces, which has been reported to be around 2-3 mm (Fessy et al., 1997; Stagni et al., 2005).

Comparisons of the coronal plane orientation of each medial-fit and lateral-fit cylinder axis with the whole-fit cylinder axis for each specimen yielded angles between the axes ranging from 0-6 degrees, supporting the idea that there are slight differences in the orientations of articular surfaces from medial to lateral. These small differences in orientation between the medial and lateral sides support the presence of a saddle-shaped talar dome noted in previous morphological examinations of the talus (Barnett and Napier, 1952; Inman, 1976). This finding may seem to contradict the idea that a cylinder fit to the entire surface is an accurate representation of the geometry of the talar dome, however, MSE values from the cylinders fit to the whole surface were quite small (less than 0.2 mm). The medial and lateral halves of the tibial surface were also shown to differ less from one another in their coronal plane orientations as compared to the medial and lateral halves of the talar dome, which seems to implicate that the tibial articular surface is flatter in the coronal plane as compared to the talus. These differences also imply that a degree of non-conformity exists between the tibial and talar articular surfaces which may be responsible for the coupled motions that have been shown to occur in previous research (Michelson and Helgemo, 1995; Michelson et al., 2000; Siegler et al., 1988). Regarding the cylinder optimizations however, the mean MSE values for the medial and lateral cylinder fits tended to be smaller than the MSE values for the whole cylinder fits, although the differences were not significant. The current data suggest that a cylinder fit to the entire superior articular surface is a good approximation of the geometry of the talar dome insofar as describing the general orientation of the articular surface, however, constriction of the tibial and talar surfaces to congruent cylinders may ignore or over-simplify the conformity and kinematics of the native joint.

7.1.2 Landmark and Cylinder Axis Orientations

One of the major motivations of this research, prior to the onset of the microscribe experiments, was to gain a better understanding of the spatial relationships between the talocrural joint surfaces and surrounding landmarks in order to develop repeatable alignment criteria that could be used for TAA surgery. Due to anatomic variability, we were unable to establish reliable and potentially useful relationships between talocrural joint orientations and easily palpated landmarks. Despite the fact that a novel alignment protocol was not developed, valuable information was discovered regarding the alignment of the joint surfaces, as well as landmark positions and orientations. In addition, a reference coordinate system was developed (CPCS) that was independent of side and that could potentially facilitate an intra-operative alignment procedure that is simple and easy to use.

The orientations of both the talus and tibia cylinder joint axes were analyzed in three anatomical reference planes in order to identify similarities and repeatability between specimens. Orientation in the sagittal plane was identified by examining the AP tilt of vectors connecting the anterior and posterior corners of the articular surface. Values for AP tilt across specimens were somewhat variable with a range of around 0-14 degrees, which agrees with previously reported data (Barnett and Napier, 1952). This variance in sagittal orientation is not of great concern. Sagittal plane orientation is the least important of the three principle orientations because joint motion occurs in this plane. Traditional TAA presumes that the implant should be placed orthogonally to the line of action of force in the lower extremity, which is assumed to be vertical with respect to the ground (Gill 2002; Waugh et al., 1976). Therefore, in both existing TAA as well as the TAA motion analysis trials in the current work, the sagittal orientation is assumed to be zero degrees with respect to the ground (parallel).

The cylinder axes for the talus and tibia demonstrated that the varus/valgus orientation of the joint surfaces was very repeatable among the eight specimens examined in the microscribe experiments. The mean ranges for the articular surfaces of both bones were very near zero, with only small variances found across specimens. The variances found in the experiment may have even been a result of experimental error in positioning the foot. These findings suggest that native joint surfaces are at neutral alignment in the coronal plane. Deviations in coronal plane that might occur in TAA surgery may have serious implications for the success of the procedure. Variation in coronal plane alignment has been noted to be a major cause of complications and failure in TAA, leading to pain, gutter impingement, sub-fibular impingement, pronation deformities, edge loading of polyethylene, and bone in-growth inhibiting micro-motion (Conti and Wong, 2001; Gittens, 2002). While existing TAA systems usually aim for neutral coronal plane alignment, the idea is based on implied joint lines from 2D radiographs, not 3D characterization of the articular surfaces as a whole. The current data verifies this previous assumption with regard to both the talus and the tibia using 3D whole surface characterizations.

The transverse plane orientation (internal/external rotation) of the cylinder axes exhibited large variability between specimens due to an array of orientation angles that spread over a range of around 25 degrees. The intermalleolar (IM) axes exhibited even higher variability, with a range of values spanning almost 39 degrees. Some current TAA systems such as the Agility address the transverse orientation by incorporating 20 degrees of external rotation into the alignment of the talar component during surgery, in an effort to approximate the IM axis (Saltzman and Alvine, 2002). Others have shown that the IM axis is a good predictor of the kinematic axis of the talocrural joint in the transverse plane (Inman, 1976). The current data suggests that the IM axis may not be a good predictor of transverse plane orientation for total ankle surgery. While the mean IM axis was located around 20 degrees of external rotation in this study, individual values tended to deviate substantially from the mean, as evident by the high variance in measurements. Furthermore, the mean cylinder axis orientations in this study were around 16 degrees of external rotation, which was quite different from the mean IM axis orientation of 20 degrees of external rotation.

The IM axis may be a good general, qualitative estimation of the talocrural movement axis, but for the purposes of determining the precise transverse joint orientation for an individual, approximating the IM axis could introduce large errors. It is also worth noting that the estimation of 20 degrees of external rotation for the orientation of the IM axis is based on conventional reference systems which place the AP axis of the foot along the second metatarsal (Saltzman and Alvine, 2002), while the CPCS used in this study was orientated along the first ray, slightly more internally rotated from these traditional reference systems. This means that transverse orientation values calculated via the CPCS would actually be more internally rotated in traditional reference systems and would differ even more from the 20 degrees of external rotation guideline that is traditionally assumed. The orientations of the IM and cylinder axes with respect to the AP midline y-axis in these experiments might be more comparable to their orientations in more traditional reference frames. The values for these relationships were quite small though, as each axes was only slightly in external rotation (-4 to -7.5 degrees). It is clear from these results that a better understanding of the relationship between the orientation of the joint surfaces and the IM axis is needed before any further predictions are made regarding this use of the IM axis in TAA alignment procedures.

Orientation angles of the tibial crest with respect to the CPCS were also analyzed, in order to assess its validity as a landmark used for alignment in ankle replacement surgery. As described previously, the tibial crest is traditionally used to position alignment jigs in the coronal and sagittal planes because it is believed that the crest is a good approximation of the line of action of force in the lower extremity (Agility video, DePuy; Pyevich et al., 1998; Saltzman and Alvine, 2002). For the specimens analyzed in the microscribe experiments, the tibial crest vectors were found to deviate around 6 degrees from the CPCS z-axis, on average. In other words, according to this study, alignment procedures that rely on the tibial crest as a predictor of a vertical reference (orthogonal to the ground) may be introducing an average error of 5 degrees. Despite these errors, the tibial crest still seems to be a fairly repeatable approximation of a vector that is orthogonal to the plane of the ground, and deviations during these experiments may be due to errors in bead placement, specimen positioning, or digitization. Also, the dot product relationship between the tibial crest and the CPCS z-axis only provides a general angle between two unit vectors. Qualitatively, the tibial crest tends to deviate posteriorly as the bone thins from proximal to distal in the sagittal plane. Therefore, it may be that the tibial crest is a good predictor of coronal plane alignment, but is less robust in determining sagittal plane orientation.

The cylinder axes were found to be in a neutral varus/valgus orientation in the coronal plane with respect to the ground. If the tibial crest vectors were indeed orthogonal to the ground in the coronal plane, then the angle between them and the cylinder axes should have been 90 degrees. Evaluations of the dot product between these vectors revealed that, on average, this was the case. The mean angles between the tibial crest vector and the talus and tibia cylinder axes were 94.8 degrees and 93.4 degrees. These results should be interpreted with caution however, as there was a great deal of variance in these measurements. Total ranges for the observed values were 42 degrees for the talus, and 52 degrees for the tibia, indicating that while the mean is near the expected value of 90 degrees, individual specimens displayed considerable deviations from the mean value.

Quasi-transverse examinations of the tibial crest position were performed in an effort to seek repeatable relationships between specimens that could be used for the development of alignment criteria. These examinations showed interesting trends in that the projections of the tibial crest vector onto the CPCS xy plane tended to be medial to the first ray, although the variance in the position of these projections was quite large. Ideally, if the tibial crest line is to be used as a reference for varus/valgus cut guide or component alignment, than the vector should project to a repeatable position along the AP axis (CPCS x-axis) of the foot.

7.2 Motion Analysis Experiments

7.2.1 TAA Component Orientations

During the Motion Analysis (MA) experiments, the mean PF/DF amplitude was around 30 degrees. While this is far below the reported total range of motion for the talocrural joint of approximately 70 degrees (Boone and Arzen, 1979; Sammarco et al., 1973), it is similar to the total talocrural range of motion reported to occur during gait (Kadaba et al., 1989). Therefore, despite some of the limitations on the PF/DF amplitude in the current experiments, the MA tests were a good representation of the range of motion required for effective locomotion.

One of the main motivations for pursuing the TAA motion analysis experiments was to address the large variance in the transverse orientations of the cylinder axes computed in the microscribe experiments. It was assumed that by allowing the TAA components to remain un-constrained in the transverse plane, the components would seat themselves in a transverse orientation best suited to the natural kinematics and anatomy of the specimen when the ankle joint was moved through a range of repeated plantarflexion/dorsiflexion movements.

Analysis of the TAA component transverse orientation data revealed mixed results. Since two very different, general endpoint orientation ranges were identified in the experiment, it may be that there is no single approximation of transverse orientation that can be used for TAA component alignment. In three of the specimens, the components aligned themselves in a range of external rotation that was in the same general orientation range of the anterior joint lines. This range was also similar to the mean range of external rotation calculated in the microscribe experiments for the tibia and talus cylinder axes. The second group of specimens was much more internally rotated than the first group, and was in a range of transverse orientation that was much different from any of the other vector orientations, such as the anterior lines or the IM axis. Again, due to the observed variance in the transverse orientation measurements, it is difficult to judge whether the mean values of transverse orientations for any of the axes obtained across specimens is an accurate approximation. Clearly, further testing is needed before any concrete conclusions can be made. Others have also reported variability of the transverse plane orientation values for ankle joint helical axes (Lundberg, et al., 1993). Nevertheless, there is a possibility that with the testing of additional specimens, separate categories might be established for component transverse orientations. If separate categories could be clearly identified for a range of specimens, then perhaps the position and orientation of some of the anatomical landmarks could be used as predictors of which category an individual specimen might belong to.

Another result of particular interest is the degree to which the TAA components in these experiments oscillated during the PF/DF movement cycles. The amplitude of the rotations varied from specimen to specimen, but the mean amplitude was over three degrees, suggesting that the interaction of the tibia and talus during PF/DF motions does not occur in a single plane, nor is it a purely cylindrical movement pattern. The qualitative examinations of relative motion in the transverse plane between the tibia, talus, and the components seemed to indicate that the component oscillations were occurring independently of any rotations of the talus during the PF/DF cycles. While rotations of the talus relative to the tibia in the transverse plane did occur during the trials and may have some influence on the component rotations, the talar rotations do not seem to be the cause of the component oscillations. Nevertheless, the fact that the rotations of the talus with respect to the tibia were out of phase with the rotations of the components with respect to the tibia may indicated that coupled motions may have occurred between the components and talus, but friction in the system caused the component rotations to lag behind. It may also be the case that the amplitude of transverse plane oscillations of the TAA components may be directly proportional to the load applied to the specimen during testing. This point will be discussed further in the limitations section to follow.

Rotational oscillation data from the current experiments suggest that a small amount of rotational freedom needs to be incorporated into ankle replacement components if the relative motion between the tibia and talus is replicated with simple, single planar motion (i.e. cylindrical motion, as used in the current experiment).

Lundberg et al. (1989) analyzed the discrete helical axes of eight normal ankle joints and found that although the projections of the helical axes in the transverse plane clustered around the tips of the malleoli, there was substantial variance in these projections (up to 13 degrees) depending on the degree of plantar or dorsiflexion (see Section 2.1.1, Figure 2.3). Attempts to ignore this motion in TAA by over-constraining motion may result in the generation of shearing forces either at the implant-bone or implant-implant interfaces (Henne and Anderson, 2002). The Agility implant is designed so that the tibial component is larger than the talar component, allowing for gross transverse plane rotations between the tibial and talar implants (Saltzman and Alvine, 2002). It is not clear, however, if the oscillations that were observed in these experiments would introduce complications such as undesirable edge loading and stress concentrations in designs like the Agility which could ultimately lead to complications including polyethylene wear, micro-motion, and implant loosening (Neufeld and Lee, 2000; McIff, 2002).

Since the tibial and talar articular surfaces were replaced with simple artificial components designed to move in a single plane, there are two possibilities for the multi-planar movement patterns exhibited in the MA experiments that caused the components to shift and oscillate in the transverse plane. The first possibility is that the ligaments surrounding the talocrural joint are dictating the motion. This idea agrees with previous descriptions of ankle motion proposed in the literature (Leardini et al., 1999; Leardini et al., 2000; Leardini et al., 2002). Leardini and colleagues have proposed that the ankle joint behaves as a single-degree-of-freedom mechanism that can be modeled as a four-bar linkage. According to the model, the medial and lateral ankle ligaments, when tensioned properly, act as a 4-bar mechanism that dictates the movement of the ankle joint, resulting in both rolling and sliding movements. While the importance of ligament tensioning with respect to successful outcomes in TAA has also been repeatedly confirmed in the literature by others (Beuchel et al., 2002; Conti and Wong, 2001; Henne and Anderson, 2002; Gould et al., 2000) the model proposed by Leardini and colleagues deals only with sagittal plane motion in an unloaded state. Furthermore, this sagittal plane model assumes perfectly congruent cylindrical surfaces, and does not account for any transverse rotations that might occur (Leardini et al., 2002).

The second possible explanation that would cause shifts and oscillations of the components in the transverse plane is related to the bony articulations between the malleoli and the sides of the talus. The TAA procedure in these experiments did not remove or disturb the articulations of the medial and lateral malleoli with the talus. Therefore, it is possible that these articulations are responsible for the variance in the movement axis over the duration of the PF/DF trials. Several authors have noted that the articular surfaces of the malleoli are fairly congruent with the medial and lateral walls of the talar dome, however, the orientations of these surfaces differ between the medial and lateral side. For example, Barnett and Napier (1952), and Inman (1976) noted significant wedging of the talar articular surface from anterior to posterior. Inman (1976) also noted that despite posterior wedging of the talar dome, the malleolar and talar facets appeared to remain in contact throughout the entire range of ankle joint motion. Inman, however, noted that the medial and lateral talar facets varied in orientation by about 7 degrees, and that the talus fits snugly in the tibial mortise on the lateral side, but loosely on the medial side, resulting in a few millimeters of play. Also, the distal fibula has been shown to exhibit small motions with respect to the tibia, especially at large angles of dorsiflexion (Inman, 1976). Fessy and colleagues (1997) also reported that the mean angles of inclination for the medial and lateral articulations in the frontal plane differ by about 14 degrees, which would introduce substantial deviations in the motion over a range of PF/DF.

Both the ligamentous and bony articulation explanations are possibly valid. Overall talocrural motion is probably dictated to some degree by the orientation and congruency of the medial and lateral articulations between the talar facets and the malleoli, as well as by the soft tissues surrounding the joints. A plausible explanation is that the two work in concert with one another; the bony articulations dictate the overall movement pattern, but exhibit variance depending on the degree of ligament tension at various points throughout the PF/DF movement cycle. It is worth noting that the relative transverse rotations in the TAA trials differed from those observed between the talus and tibia in the intact trials. The difference in the observed rotations may be due to a "de-coupling" effect in the TAA trials that occurred as a result of removing the articular surfaces. In other words, the different rotations observed in the intact trials may have occurred primarily as a result of the interaction between the articular surfaces, while the transverse rotations in the TAA trials occurred as a result of extraneous influences such as the ligaments and medial/lateral facets. These data indicate that further investigation is warranted to fully explore the relative motion and "coupling" between anatomical segments in the ankle and their influence on TAA.

7.2.2 Component Translations

The position of the TAA components within the joint space during these experiments may have also influenced their observed motion. While no repeatable overall position was found for all specimens, individual trends, although small, were noticed for each specimen. For most specimens, more motion occurred in the anterior-posterior direction which may have been a function of the components sliding back-and-forth as the direction of applied force changed with plantarflexion and dorsiflexion. Specimens 3 and 4 tended to exhibit component translations that were both anterior and medial, while Specimen five showed the opposite behavior, exhibiting component translations that were posterior and lateral. Individual trends in specimen translations are also a function of initial component position, therefore only the final position could indicate an optimum location. Overall, while it is recognized that the position of the components within the surgically altered joint space have the potential to influence the kinematics, examinations of the component translations and endpoints did not reveal any repeatable relationship from which conclusions could be made regarding an optimum component position.

7.3 Limitations and Considerations

As with any cadaveric tests, there are limitations to the validity of the experimental results. First, the majority of the specimens used for both the microscribe and MA experiments were from older adults with relatively unknown histories. Thus, the results from these experiments could potentially be different from the results obtained in experiments using younger specimens. With the exception of the correlation tests reported in Section 5.2.4, specimen age was excluded from all analyses, therefore, few assumptions about the effects of specimen age can be made. The testing of human tissue can also present limitations regarding experimental validity. A general assumption must be made that the freezing and thawing of the cadaveric tissues used in these experiments did not compromise the integrity of the results, which has been supported by previous research (Black et al., 1981). Additionally, because of the financial expense and inherent nature of cadaver work, only a small number of specimens were able to be analyzed for each experiment. The low sample size, combined with the large variability in individual feet, necessitates the need for caution when generalizing the findings of the current work to the larger population.

3D Digitization Experiments

In the 3D digitization experiments, the articular surfaces were exposed for long periods of time during digitization, which may have caused dehydration of the articular cartilage. While this can lead to shrinkage of the cartilaginous surfaces, it was assumed that these effects were negligible. The results of the microscribe digitization were also limited by the intrinsic error of the data collection procedure, itself. The steel beads marking the positions of the anatomical landmarks were placed using a combination of palpation and visual location, both of which are subjective procedures. Therefore, the landmarks used in the experiment may not be truly accurate representations of the actual landmarks. Furthermore, the microscribe is not a perfect measurement tool. According to the manufacturer specifications, the digitizer has a precision of ± 0.4 mm (Immersion Corp., San Diego, USA). This error in precision may have also been compounded with error in placing the pointer on the steel beads, although the repeatability data from the wooden foot tests demonstrated that these additional errors are probably quite small, around 0.02 mm to 0.04 mm.

The optimization procedures used to locate the anatomical reference frames as well as the cylinders fit to the joint surface data were also subject to mathematical errors. Data from in-house experiments suggest that the accuracy of using the microscribe to approximate a plane approaches the inherent error of the digitizer when ten or more points are used, such as in this experiment. Nevertheless, rounding errors and small errors in the determination of spatial positions may have been compounded in the transformation operations, leading to errors in calculations of the positions and orientation of anatomical landmarks and vectors.

TAA Motion Analysis Experiments

The MA tests involving the TAA components were also subject to limitations. While the novel alignment system was designed to improve the accuracy of the orientation of the cut-planes for the TAA surgery, there was still some subjectivity involved in the procedure that may have lead to small errors in alignment. This would explain the small deviations reported in the angle between the tibial crest and the components in the coronal plane. Although the cuts were guided by cutting blocks, tiny deviations in the orientation of the blade may have occurred, introducing errors in either the flatness or the orientation of the cuts. While the surgeries were performed in consultation with an experienced orthopedic surgeon, they were carried out by the author who is not formally trained in orthopedic surgery. Although, this may have also introduced errors, the fact that the cuts were made as accurately as they were is a testament to the simplicity and ease of operation associated with the novel alignment jig.

The MA kinematic experiments were subject to several limitations. Since the TAA components were unconstrained between the stainless-steel plates, both the range of motion and the ability to test under load were limited. The force vector on the components was predominantly vertical, however, at ranges of plantarflexion or dorsiflexion beyond 15-20 degrees, the orientation of the force vector would shift and tended to cause the components to dislocate in either the anterior or posterior directions. The addition of weight only exacerbated this problem, so all testing was done with only the mass of the tibial plate and the empty weight racks which amounted to about 12 lbs (53.4 N). Therefore, testing was not performed under loads representative of normal walking. Dislocation of the TAA components may not have been a problem if the skin and surrounding tissue would have been closed around the anterior talocrural joint after implanting the components, as in a normal surgery, but it was necessary to leave the anterior joint space open to track the motion of the components using the marker cluster. Another potential limitation is the resolution of the Motion Analysis system. Errors might have occurred in location the reflective markers by the high-speed cameras at any point during the test. Calibration values for the MA tests indicated that any errors in resolution were small, however, so the effects of MA system errors on these experiments were probably negligible.

Regarding the TAA components, there were a few limitations that had the potential to influence the observed results. The components were lubricated between each trial to reduce the friction between the tibial and talar pieces, as well as between the components and the plates. Despite the use of low-friction materials and lubrication, the experimental results, especially the transverse rotation values, may have been affected by the presence of friction in the system. In addition to the effects of friction, the motion of the components could have been influenced by the marker cluster attached to the anterior corner of the talar piece. Attempts were made to reduce the mass of the cluster as much as possible by using small-sized aluminum thread rods instead of steel, and the overall mass of the cluster was quite small compared with the mass of the stainless steel talar component. Nevertheless, the moment of inertia of the cluster may still have been a factor. Finally, the lack of realistic loading may have also influenced the motion of the components during the kinematic trials, especially the rotational oscillations. If testing under normal loading conditions could have been performed, the increased vertical load may have compressed the components between the plates more and limited these oscillations.

7.4 Evaluation of Hypotheses

3D Digitization Experiments

Hypothesis #1: *The articular surfaces of the talar dome and the distal tibia can be described by a simple geometric shape, such as a cylinder.*

After performing the numerical optimizations in the microscribe experiments, this hypothesis was confirmed. The articular surfaces for both the tibia and the talus were characterized by fitting cylinders to clouds of points representing the articular surface. Errors for these fits were quite low, with MSE values of 0.188 mm for the talus and 0.157 mm for the tibia, which are well within the precision limits of the digitizing device.

Hypothesis #2: *A repeatable relationship across specimens can be found for the position and orientation of the talar articular surface with respect to palpable anatomic landmarks on the foot and leg.*

This hypothesis was rejected due to the variance in the transverse plane orientations of the cylinder axes among individual specimens. It was not possible to identify a single, repeatable relationship that could be used to predict the position and orientation of the talocrural joint surfaces. Although this hypothesis was rejected, repeatable orientations between the joint surfaces and anatomical landmarks were identified in both the sagittal and coronal planes. In addition, novel information regarding the relationship between the orientation of the joint surfaces with respect to the intermalleolar axis and the anterior and posterior joint lines was discovered.

<u>TAA Motion Analysis Experiments</u>

Hypothesis #1: *Simple cylindrical components, unconstrained in translation and rotation in the transverse plane, will seat themselves in an optimum and repeatable position and orientation after being subjected to a series of cyclical plantar/dorsiflexion movements.*

This hypothesis could not be accepted, due to inconclusive data. The results of the MA experiments did show a tendency of the components to move towards a repeatable orientation in three of the five specimens, but not in all. In addition, some specimens had some trials that converged to a similar orientation, while other trials for the same specimen rotated in the opposite direction. The results indicate that more testing is necessary to identify whether or not the components will self-align themselves during PF/DF cycles. Longer tests, coupled with a re-designed component system that limits translation, more trials, and a larger sample size may provide results that would further address this hypothesis. Translation data from the MA experiments was inconclusive, although some specimens did exhibit a tendency for the components to move in a common direction.

Hypothesis #2: *The cylindrical components will exhibit a cyclical rotation in the transverse plane relative to plantar/dorsiflexion of the tibia.*

This hypothesis was confirmed. Component transverse plane data for all five of the specimens tested showed rotational oscillations ranging from 2 to 6 degrees. These rotations may be due to the shape and orientation of the articulations between the malleoli and the talar facets, the influence and tension of soft tissues such as the medial and lateral ligaments, or a combination of both. While rotational oscillations of the tibia with respect to the talus were also noted, these were not thought to be causing the component rotational oscillations.

7.5 Implications and Future Work

7.5.1 Implications

These experiments have numerous implications. First, although several 2D sagittal characterizations of the talar dome have been reported in the literature, there are few, if any, characterizations of the talocrural joint surfaces in 3D. While the general assumption has been that the talar dome can be represented by a cylinder in 2D, the data from these experiments confirms this assumption in 3D. The surprisingly low MSE values associated with the cylinder fits may have implications regarding the shape and design of components for TAA. Past research has suggested that purely cylindrical component systems can be over-constrained and lead to failure (Sodha et al., 2000; Henne and Anderson, 2002), but the data from these experiments suggest that cylindrical surfaces are indeed good approximations of the articular surfaces. If nothing else, these experiments indicate that perhaps an implant system incorporating congruent cylindrical surfaces in concert with built-in degrees of freedom in the transverse plane to allow multi-planar movements is necessary. Current total knee systems incorporate rotational degrees of freedom by using rotating tibial platforms. Future designs of TAA components may benefit from similar design considerations in which the talar component is actually 2 separate pieces that are allowed to rotate in the transverse plane with respect to one another.

The results from the cylindrical joint surface-fits also revealed the importance of the relationship between gender and sizing. Since the male tali in these experiments were characterized by significantly larger radii of curvature, it is evident that TAA component systems should account for variance caused by size and/or gender in their designs. The different sizes of the implants should not only vary in length and width, but the implants used for males may need to have a different radius of curvature than the implants used for females. While the difference in radius size may have merely been a result of overall foot size and not gender, the small sample size and relatively similar foot size observed between the male and female specimens in the current experiments make it difficult to draw statistical conclusions regarding foot size. These issues should be examined in further studies.

There were several implications from these studies regarding the orientation of the talocrural joint surfaces. Coronal plane orientation was quite repeatable among specimens, confirming current practices of TAA surgery in which a neutral alignment in the coronal plane is the goal. In contrast to the coronal plane, these experiments revealed extremely high variability in the transverse plane alignment of the joint surfaces, as well as in the IM axes. While current TAA systems such as the Agility strive for a transverse orientation that is thought to be in line with the IM axis at about 20 degrees of external rotation, the data from these experiments suggest that this may not be correct. According to the cylinder axes, the orientations of the joint surfaces across specimens differed from the orientations of the IM axes, and both varied from 20 degrees of external rotation. Mal-alignment of TAA components in the transverse plane has been shown to cause rapid loosening, pain, and early failure of TAA components (Gill et al., 2002). It is evident that a better, more precise understanding of the transverse orientation of the joint surfaces is needed before TAA can be completely successful.

Current TAA systems do incorporate some alignment instrumentation, however, the placement of these instruments are still left primarily to subjective observation by the surgeon, which can lead to errors. TAA research over the last 10-20 years has focused primarily on implant designs and post-operative clinical evaluations, while little attention has been given to issues of correct alignment and surgical guidance. Clearly, if TAA is to become a successful procedure, major improvements need to be made in the alignment systems use to make the surgical cuts and implant the components. With existing systems such as the Agility, both the tibial and the talar are cut from the same guide that is aligned only with the tibia (Pyevich et al., 1998). It may seem logical that both cuts should be made according to the same orientation, however, deviations of the foot from a neutral position can lead to errors in placement of the talar component, even though the jig may be properly aligned with the tibia. The novel system developed for this study relied on rigid fixation of the foot with respect to a plantar plate that simulated the ground, which led to precise talar cuts that were parallel to the plate. Although alignment of the tibia was still somewhat subjective in these experiments, the results showed good accuracy of the tibial cut (perpendicular to the long axis of the bone). Overall the novel alignment jig performed very well, and small improvements made to its design in future versions may help to reduce intra-operative error.

The cylindrical components also performed favorably in the MA experiments. PF/DF motion was replicated within normal ranges of gait (Kadaba et al., 1989) and the use of low friction materials such as polished stainless steel and UHMWPE facilitated smooth motion. The design of TAA components can dramatically influence the success or failure of an implant system. Gittens and Mann (2002) described four goals for the design of TAA components in order to improve function and reduce pain, which are as follows: preserve the axis of movement, maintain as much of the anatomy as possible, avoid constrained designs, and reproduce cylindrical motion. It is clear from both this study and current TAA designs that components with cylindrical surfaces help to replicate the natural PF/DF motion of the talocrural joint. Today's modern TAA systems also do a fairly acceptable job at preserving the natural anatomy around the joint, although some systems are more destructive than others (Rippstein, 2002). The data from the current study suggest that the most difficult aspect of TAA is preserving the natural movement axis of the joint. As demonstrated by the large variance in joint surface orientations calculated in this study, it is evident that current systems may rely too heavily on assumptions of axis positions and orientations that may be incorrect.

One potential solution to address the considerable anatomical variance of the transverse joint axes is to design an intra-operative procedure whereby a patient's individual joint axes orientation can be determined. This could be done by inserting a trial implant system that replicates cylindrical motion, but allows for transverse plane rotations and translations. The patient's ankle could then be moved through a range of plantarflexion/dorsiflexion using the trial implant to determine the patient's specific transverse orientation demands. Once the proper orientation is found and recorded, a permanent implant could be chosen from a range of models that vary in size and orientation design that would correctly match the anatomy and kinematics of the patient.

7.5.2 Future Work

This study has only just begun to address the most relevant issues of TAA. There is clearly room for improvement with the procedure, and data from the current experiments have increased the general understanding of issues related to talocrural joint alignment and TAA. While the results of these experiments did not facilitate the development of a rigorous alignment formula or protocol, this still remains a viable goal in TAA research. If a solid understanding of the orientation of the talocrural joint surfaces is to be realized, then future work should strive to increase the number of specimens analyzed. Cadaver work is slow and expensive, but *in vivo* methods such as MRI could be implemented to examine the relationship between the joint surfaces and surrounding anatomical landmarks in large numbers, which might elucidate trends or categories among patients and would also increase statistical power. The addition of more anatomical landmarks to the examinations may also be worthwhile. The landmarks used in this study were selected because they were easily identifiable and/or palpable. The inclusion of more landmarks, which may or may not be palpable, may be helpful in identifying more basic predictors of joint surface position and orientation. Another possibility for future work would be to incorporate osteometric scaling. Osteometric scaling applied to the bones of the ankle, although difficult to implement within the foot, might facilitate more accurate assessments of landmark and joint surface positions.

The recommendation of increasing the sample size also applies to the TAA motion analysis experiments. While some specimens showed a tendency to converge towards a repeatable transverse orientation, there was not enough data to draw any significant conclusions. More specimens need to be tested over longer trials in order to assess whether or not the components reach an consistent specimen-specific orientation. Additional studies with modified components that limit translation but allow rotation may provide a means by which experiments with more realistic loading can be performed, without the risk of component dislocation. There is also a great deal of potential to examine different component designs that might better simulate the PF/DF motion while at the same time allowing for the natural transverse plane rotations and deviations that were observed in the current study.

7.6 Summary

To summarize, the current study has provided valuable insight into some of the issues of TAA that continue to hinder the procedure. In this research, the talocrural joint surfaces were accurately characterized and their orientations with respect to the surrounding anatomical landmarks were calculated. The findings from these calculations have helped to confirm existing TAA alignment practices in the sagittal and coronal planes, and they have also raised new questions regarding the transverse plane orientation of the joint surfaces. Current TAA surgical practices and alignment guidelines in the transverse plane have been shown to rely largely on assumptions that may lead to significant errors in the implantation and orientation of ankle replacement components, which may be contributing to the high failure rates noted in the literature.

Furthermore, this study has demonstrated that while simple, cylindrical components can be used to replicate PF/DF motion, the motion at the talocrural joint does not occur in a single plane, as evident by the rotations and oscillations observed in the transverse plane. This multi-planar movement has important implications regarding the design and alignment of TAA components. If TAA is to surpass arthrodesis and become a mainstream procedure, then a great deal of future work is needed to better understand the relationship between ankle kinematics and the orientation of TAA components.

REFERENCES

Abidi, N. A., Bruen G. S., and Conti, S. F. (2000) Ankle Arthrodesis: Indications and Techniques. *Journal of the American Academy of Orthopaedic Surgeons* **8,** 200-209.

Allinger, T.L. and Engsberg, J.R. (1993) A method to determine the range of motion of the ankle joint complex, in vivo. *J Biomech* **26,** 69-76.

Andriacchi, T.P., Anderson, G.B.J., and Fernier, R.W. (1980) A study of lower-limb mechanics during stair climbing. *J Bone Joint Surg* **62,** 749-757.

Barnett, C.H. and Napier, J.R. (1952) The axis of rotation at the ankle joint in man. Its influence upon the form of the talus and the mobility of the fibula. *Anatomy* **86,** 1-9.

Belegundu, A.D. and Chandrupatla, T.R. (1999) *Optimization Concepts and Applications in Engineering*. Prentice Hall, New Jersey.

Black, J.D., Matejczyk, M. B., and Greenwald, A. S. (1981). Reversible cartilage staining technique for defining articular weight-bearing surfaces. *Clin Orthop and Rel Res*. **159** 265-267.

Boone, D.C. and Azen, S.P. (1979) Normal range of motion of joints in male subjects. *J Bone Joint Surg. Am* **61,** 756-759.

Buechel, F.F., Pappas, M. J., and Iorio, L.J. (1988) New Jersey low contact stress total ankle replacement: Biomechanical rationale and review of 23 cementless cases. *Foot Ankle* **6,** 279-290.

Buechel, F. F. Sr., Buechel, F. F. Jr., and Pappas M. J. (2002) Eighteen year evaluation of cementless meniscal bearing total ankle replacements. *AAOS Instructional Course Lectures* **51,** 143-151.

Calderdale, P.M., Garro, A., Barbiero, R., Fasolio, G., and Pipino, F. (1983) Biomechanical design of the total ankle prosthesis. *Eng Med* **12,** 69-80.

Cappozzo, A., Cappello, A., Della Croce, U., and Pensalfini, F. (1997) Surface-marker cluster design criteria for 3-D bone movement reconstruction. *IEEE Trans Biomed Eng* **44,** 1165-74.

Caron, M., Kron, E., and Saltrick, K.R. (1999) Tibiotalar joint arthrodesis for the treatment of severe ankle joint degeneration secondary to rheumatoid arthritis. *Clin Podiatr Med Surg* **16,** 337-61.

Challis, J.H. (1995) A procedure for determining rigid body transformation parameters. *J. Biomechanics* **28,** 733-737.

Conti, S.F. and Wong, Y.S. (2001) Complications of total ankle replacement. *Clinical Orthopaedics and Related Research* **391,** 105-114.

Craig, J.J. (1995) *Introduction to robots: mechanics and control*. Pearson Prentice Hall, New Jersey.

Deland, J.T., Morris, G. D, and Sung ,I. H. (2000) Biomechanics of the ankle joint. A perspective on total ankle replacement. *Foot Ankle Clin* **5,** 747-759.

Fessy, M.H., Carret, J.P., and Bejui, J. (1997) Morphometry of the talocrural joint. *Surg Radiol Anat* **19,** 299-302.

Gill, L. H. (2002) Principles of joint arthroplasty as applied to the ankle. *AAOS Instructional Course Lecture* **51,** 117-128.

Gittins, J. and Mann, R. A. (2002) The history of the STAR total ankle arthroplasty. *Foot Ankle Clin N Am* **7,** 809-816.

Gould, J.S., Alvine, F.G., Mann, R.A., Sanders, R. W., and Walling, A.K. (2000) Total ankle replacement: A surgical discussion. Part I. Replacement systems, indications, and contraindications. *American Journal of Orthopaedics* **8,** 604-609.

Guralnik, J.M. (1989) Aging in the eighties: The prevalence of co-morbidity and its association with disability. *Advanced Data for Vital and Health Statistics, National Center for Health Statistics* **170**.

Henne, T. D. and Anderson, J. G. (2002) Total ankle arthroplasty: A historical perspective. *Foot Ankle Clin N Am* **7,** 695-702.

Hicks, J.H. (1953) The mechanics of the foot. *J Anatomy* **87,** 345-357.

Inman, V.T. (1976) *Inman's Joints of the Ankle*. Williams and Wilkins, Baltimore.

Jaakola, J.I. and Mann, R.A. (2004) A review of rheumatoid arthritis affecting the foot and ankle. *Foot and Ankle Int* **25,** 866-874.

Kadaba, M.P., Ramakaishnan, H.K., Wooten, M.E., and et al. (1989) Repeatability of kinematic, kinetic, and electromagnetic data in normal adult gait. *J Orthop Res* **17,** 849-860.

Kofoed, H. (1999) The evolution of ankle arthroplasty. *Orthopade* **9,** 804-11.

Kofoed, H. (2004) Scandanavian total ankle replacement (STAR). *Clin Ortho and Rel Research* **424,** 73-79.

Kofoed, H. and Sorensen, T.S. (1998) Ankle arthroplasty for rheumatoid arthritis and osteoarthritis. *J Bone Joint Surg (Br)* **80-B,** 328-332.

Leardini A. (2001) Geometry and mechanics of the human ankle complex and ankle prosthesis design. *Clinical Biomechanics* **16,** 706-709.

Leardini, A. and Moschella, D. (2002) Dynamic simulation of the natural and replaced human ankle joint. *Med Biol Eng Comput*. 40[2], 193-199.

Leardini, A. and O'Connor, J. J. (2002) A model for lever-arm length calculation of the flexor and extensor muscles at the ankle. *Gait and Posture* **15,** 220-229.

Leardini A., O'Connor, J. J., Catani, F., and Giannini, S. (1999) A geometric model of the human ankle joint. *J. Biomechanics* **32,** 585-591.

Leardini, A., O'Connor, J. J., Catani, F., and Giannini, S. (1999) Kinematic of the human ankle complex in passive flexion: a single degree of freedom system. *J. Biomechanics* **32,** 111-118.

Leardini, A., O'Connor, J. J., Catani, F., and Giannini, S. (2000) The role of the passive Structures in the mobility and stability of the human ankle joint: A literature review. *Foot and Ankle Int.* **21,** 602-615.

Leardini, A., Rapagna, L., Ensini A., and Catani, F. (2002) Computer-assisted preoperative planning of a novel design of total ankle replacement. *Computer Methods and Programs in Biomedicine* **67,** 231-243.

Lewis, G.S. (2004) Non-Invasive methods for locating ankle joint axes of the human ankle complex. *Masters Thesis*. Penn State University.

Lundberg, A., Svensson, O.K., Nemeth, G., and et al. (1989) The axis of rotation of the ankle joint. *J Bone Joint Surg Br* **71,** 94-99.

Martin, R.B. Burr, D.A., and Sharkey, N. A. (1998) *Skeletal Tissue Mechanics*. Springer-Verlag Inc., New York.

McIff, T. (2002) Design factors affecting the contact stress patterns in a contemporary mobile bearing total ankle replacement. Proceedings from the IV Biomechanics World Congress, 2002.

Medley, J.B., Dowson, D., and Wright, V. (1983) Surface geometry of the human ankle joint. *Eng Med* **12,** 35-41.

Michelson, J. D., Checcone, M., Kuhn, T., and Varner, K. (2001) Intra-articular load distribution in the human ankle joint during motion. *Foot and Ankle Int* **22,** 226-233.

Michelson, J. D., Clarke, H. J., and Jinnah, R. H. (1990) The effect of loading on tibiotalar alignment in cadaver ankles. *Foot and Ankle Int* **10,** 280-284.

Michelson, J. D. and Helgemo, S. L. (1995) Kinematics of the axially loaded ankle. *Foot and Ankle Int* **16,** 577-582.

Michelson, J. D., Schmidt, G. R., and Mizel, M. S. (2000) Kinematics of a total arthroplasty of the ankle: comparison to normal ankle motion. *Foot and Ankle Int* **21,** 278-283.

Michelson, J. J., Easley, M., Wigley, F. M., and Hellmann, D. (1994) Foot and ankle problems in rheumatoid arthritis. *Foot and Ankle* **15,** 608-613.

Murray, M.P., Drought, A. B., and Kory, R. C. (1964) Walking patterns in normal men. *J. Bone Joint Surg.* **46-A,** 335.

Myerson, M. S. and Mroczek, K. (2003) Perioperative complications of total ankle arthroplasty. *Foot and Ankle Int* **24,** 17-21.

Neufeld, S. K. and Lee, T. H. (2000) Total ankle arthroplasty: indications, results, and biomechanical rationale. *American Journal of Orthopaedics* 593-602.

Newton, S.E. 3rd (1982) Total ankle arthroplasty. Clinical study of fifty cases. *J Bone Joint Surg Am* **64,** 104-11.

NIH. 2002. Handout on Health: Osteoarthritis. Accessed January, 2003: http://www.niams.nih.gov/hi/topics/arthritis/oahandout.htm.

NIH. Handout on Health: Rheumatoid Arthritis. 1989. Accessed January, 2003: http://www.niams.nih.gov/hi/topics/arthritis/rahandout.htm#ra_3.

Pappas, M., Buechel, F.F., and DePalma, A.F. (1976) Cylindrical total ankle joint replacement. *Clinical Orthopaedics* **118,** 82-92.

Pappas, M.J. and Buechel, M.D. (2002) Biomechanics and design rationale: The Buechel-Pappas ankle replacement.

Pyevich, M.T., Saltzman, C.L., and Callaghan, J.J. (1998) Total ankle arthroplasty: A unique design. *J Bone Joint Surg (Am)* 80**-A,** 1410-1420.

Rippstein, P. (2002) Clinical experiences with three different designs of ankle prosthesis. *Foot and Ankle Clin* **7,** 817-831.

Roas, A. and Andersson, G. B.J. (1982) Normal range of motion of the hip, knee and ankle joints in male subjects 30-40 years of age. *Acta Orthop Scand* **53,** 205-208.

Rockett, M.S., Ng, A., and Guimet, M. (2001) Posttraumatic ankle arthrosis. *Clin Podiatr Med Surg* **3,** 515-35.

Saltzman, C. L. (1999) Total ankle arthroplasty: state of the art. *AAOS Instructional Course Lectures* **48,** 263-268.

Saltzman, C. L. and Alvine, F. G. (2002) The agility total ankle replacement. *AAOS Instructional Course Lecture* **51,** 129-133.

Saltzman, C.L., Amendola, A., Anderson, R., Coetzee, J.C., Gall, R. J., Haddad S.L., Lian G., Sanders R. W., Scioli, M., and Younger, A.S. Surgeon Training and complications in total ankle arthroplasty. *Foot Ankle Int* 24[6], 514-518. 2003.

Saltzman, C.L., Tochigi, Y., Rudert, M.J., McIff, T.E., and Brown, T.D. (2004) The effect of agility ankle prosthesis misalignment on the peri-ankle ligaments. *Clin Ortho and Rel Research* **424,** 137-142.

Sammarco, G.J., Burstein, A.H., and Frankel, V.H. (1973) Biomechanics of the ankle: a kinematic study. *Orthop Clin North Am* **4,** 75.

Scott, S.H. and Winter, D.A. (1991) Talocrural and talocalcaneal joint kinematics and kinetics during the stance phase of walking. *J. Biomech* **24,** 743-752.

Shih, L., Wu, J., and Lo, W. (1993) Changes in gait and maximum ankle torque in patients with ankle arthritis. *Foot and Ankle* 97-103.

Siegler, S., Chen, J., and Schneck, C. D. (1988) The three-dimensional kinematics and flexibility characteristics of the human ankle an subtalar joints- Part 1: Kinematics. *J Biomech. Eng.* 110: 364-373.

Sodha S., Wei S. Y., and Okereken E. (2000) Evolution of total ankle arthroplasty. *UPOJ* **13**.

SooHoo, N.F. and Kominski, G. (2004) Cost-effective analysis of total ankle arthroplasty. *Journal of Bone and Joint Surgery* **86-A,** 2446-2455.

Stagni, R., Leardini, A., Ensisi, A., and Cappello, A. (2005) Ankle morphometry evaluated using a new semi-automated technique based on X-ray pictures. *Clinical Biomechanics* **20,** 307-311.

Stamatis, E. D. and Myerson, M. S. (2002) How to avoid specific complications of total ankle replacement. *Foot and Ankle Clinic* **7,** 765-789.

Stauffer, R.N. and Segal, N.M. (1981) Total ankle arthroplasty: four years' experience. *Clin Orthop* 217-21.

Stauffer, R. N., Chao, E.Y., and Brewster, R.C. (1977) Force and motion analysis of the normal, diseased, and prosthetic ankle joint. *Clin Orthop* **127,** 189-196.

Takakura, Y., Tanaka Y., Sugimoto K., Tamai, S., and Masuhara, K. (1990) Ankle Arthroplasty: A comparative study of cemented metal and uncemented ceramic prosthesis. *Clinical Orthop* **252,** 209-216.

Waugh, T.R., Evanski, P.M., and McMaster, M.D. (1976) Irvine ankle arthroplasty: Prosthetic design and surgical technique. *Clinical Orthop***114,** 180-184.

Weseley, H.S., Kaval, R., and Kleiger, B. (1969) Roentgen measurement of ankle flexion-extension measurement. *Clin Orthop* **65,** 167.

Wood, P.L. and Deakin, S. Total ankle replacement. The results in 200 ankles. *J Bone Joint Surg Br*. 85[3], 334-341. 2003.

Wood, P. L. R., Clough, T. M., and Jari, S. (2000) Clinical comparisons of two total ankle replacements. *Foot and Ankle Inter* **21,** 546-550.

Wright, D.G., Desai, S.M., and Henderson, W.H. (1964) Action of the subtalar and ankle joint complex during the stance phase of walking. *J Bone and Joint Surg* **46-A,** 361.

APPENDIX A: Whole Foot Anthropometrics

Specimen Anthropometric Measurements (Microscribe Experiments)

* All Measurements in mm

Specimen	1	2	3	4	5	6	7	8	Mean	STD
Gender	*male*	*male*	*male*	*male*	*female*	*female*	*female*	*female*	--	--
Foot Length (heel-1st toe)	240.0	245.0	232.0	235.0	225.0	230.0	240.0	210.0	232.1	10.2
Foot Length (heel-5th toe)	195.0	215.0	200.0	200.0	180.0	190.0	190.0	195.0	195.6	14.2
Heel Width	85.0	60.0	45.0	46.0	45.0	45.0	43.0	55.0	53.0	11.8
Forefoot Width	60.0	94.0	100.0	83.0	84.0	87.0	80.0	80.0	83.5	3.5
Arch Height	11.0	17.0	9.0	10.0	10.0	6.0	15.0	9.0	10.9	3.4
Malleoli Height-Medial	75.0	76.0	75.0	80.0	85.0	80.0	78.0	76.0	78.1	6.0
Malleoli Height-Lateral	70.0	68.0	65.0	65.0	82.0	75.0	70.0	65.0	70.0	6.4
Inter-malleolar Width	65.0	75.0	61.0	57.0	60.0	58.0	58.0	55.0	61.1	11.0

APPENDIX B: Morphological Measurements of Articular Surfaces

Morphological Measurements of the Talar Dome (Microscribe Experiments) (All measurements in mm)

Specimen	1	2	3	4	5	6	7	8	Mean	STD
Gender	*male*	*male*	*male*	*male*	*female*	*female*	*female*	*female*	--	--
Length Medial Side	39.50	39.90	33.00	38.30	28.90	32.30	33.70	28.80	34.30	4.47
Length Lateral Side	39.30	34.70	37.50	34.90	30.20	28.60	31.40	28.70	33.16	4.04
Length Center	38.60	39.90	34.80	35.50	30.30	29.70	32.30	30.00	33.89	3.96
Width Anterior	31.50	35.90	29.70	31.70	26.80	27.40	30.00	26.10	29.89	3.21
Width Posterior	19.00	24.20	25.10	25.40	22.30	23.80	23.30	16.70	22.48	3.08
Width Center	31.30	34.80	30.60	28.90	26.20	25.90	27.90	25.30	28.86	3.24
Lateral Radius Ant.	24.80	28.30	17.80	23.90	21.40	23.40	18.80	21.10	22.44	3.39
Lateral Radius Post.	30.30	25.60	18.70	25.40	23.70	23.20	19.50	21.00	23.43	3.77
Lateral Radius Center	30.70	26.00	19.30	24.10	23.10	22.90	18.10	21.10	23.16	3.98
Medial Radius Ant.	19.40	18.20	15.40	17.04	13.10	14.70	19.10	11.40	16.04	2.90
Medial Radius Post.	19.40	18.20	15.40	17.04	13.10	14.70	19.10	12.60	16.19	2.64
Medial Radius Center	12.50	12.20	11.30	9.50	8.70	11.70	9.90	7.60	10.43	1.77
Medial Height Ant.	17.60	17.00	12.90	12.40	9.90	10.90	14.10	11.90	13.34	2.75
Overall Width	49.40	49.30	39.80	44.90	37.10	40.10	29.40	38.60	41.08	6.68

Morphological Measurements of the Tibia/Fibula Articular Surface (Microscribe Experiments)
(All measurements in mm)

Specimen	**1**	**2**	**3**	**4**	**5**	**6**	**7**	**8**	**Mean**	**STD**
Gender	*male*	*male*	*male*	*male*	*female*	*female*	*female*	*female*	--	--
Medial Depth	28.55	23.88	24.83	23.57	22.16	19.00	19.37	19.43	22.60	3.31
Center Depth	33.35	32.29	28.97	30.50	24.82	24.17	24.81	22.83	27.72	4.06
Lateral Depth	22.55	28.35	32.69	26.03	25.45	24.20	24.93	26.03	26.28	3.08
Anterior Width	34.28	34.00	28.72	26.57	24.36	22.40	29.32	26.56	28.28	4.24
Center Width	29.18	29.93	29.06	26.34	24.77	25.59	27.58	23.24	26.96	2.37
Posterior Width	23.22	25.26	26.19	20.68	21.37	26.96	24.65	20.18	23.56	2.60
M Mal. Narrow Width	13.44	13.88	9.00	12.61	9.24	9.50	12.98	11.21	11.48	2.01
M Mal. Wide Width	28.09	24.25	18.92	23.93	19.95	20.83	19.61	21.28	22.11	3.10
M Mal. Height	17.07	14.59	9.29	26.04	14.12	15.91	14.66	14.76	15.81	4.71
Fib Width	19.20	24.71	20.41	19.66	18.78	19.90	20.66	17.77	20.14	2.07
Fib Height	23.33	31.95	19.47	22.42	21.56	22.93	15.94	18.33	21.99	4.76

APPENDIX C: Wooden Foot Repeatability Data

Reliability Statistics for the 10 Wooden Foot Trials: X Values

(values in mm)	**Mean**	**Std Error**	**Std Dev**	**Range**	**95% C.L.**
TC1	419.427	0.024	0.076	0.222	0.054
TC2	418.245	0.032	0.103	0.285	0.073
TC3	417.180	0.045	0.141	0.400	0.101
MMAL	450.517	0.030	0.094	0.279	0.067
LMAL	383.267	0.029	0.091	0.254	0.065
1st METT	436.937	0.030	0.094	0.288	0.067
5th METT	392.271	0.033	0.106	0.296	0.076
TMT	435.798	0.045	0.143	0.408	0.102
TALMA	437.103	0.029	0.091	0.272	0.065
TALLA	394.223	0.026	0.084	0.268	0.060
TALMP	437.935	0.033	0.105	0.301	0.075
TALLP	394.369	0.016	0.051	0.154	0.037
TIBMA	438.716	0.023	0.072	0.215	0.051
TIBLA	393.409	0.027	0.085	0.248	0.061
TIBMP	442.346	0.029	0.093	0.296	0.067
TIBLP	390.612	0.030	0.095	0.293	0.068
1st METB	444.848	0.022	0.070	0.223	0.050
5th METB	398.317	0.068	0.214	0.715	0.153
CALC	417.503	0.065	0.206	0.549	0.148

Grand Means (across all landmarks)

Standard Error = 0 .033 mm

Standard Deviation = 0.106 mm

Range = 0.314 mm

95 % Confidence Level = 0.076 mm

Reliability Statistics for the 10 Wooden Foot Trials: Y Values

(values in mm)	**Mean**	**Std Error**	**Std Dev**	**Range**	**95% C.L.**
TC1	331.631	0.039	0.123	0.416	0.088
TC2	332.088	0.024	0.075	0.229	0.054
TC3	332.430	0.024	0.077	0.228	0.055
MMAL	357.223	0.078	0.247	1.001	0.176
LMAL	353.962	0.090	0.285	0.972	0.204
1st METT	235.937	0.024	0.075	0.222	0.054
5th METT	234.666	0.018	0.058	0.168	0.042
TMT	264.603	0.055	0.173	0.509	0.124
TALMA	337.061	0.020	0.064	0.190	0.046
TALLA	336.081	0.020	0.063	0.197	0.045
TALMP	374.176	0.025	0.078	0.242	0.056
TALLP	373.270	0.015	0.048	0.147	0.034
TIBMA	337.547	0.019	0.061	0.210	0.044
TIBLA	336.448	0.025	0.078	0.271	0.056
TIBMP	375.245	0.016	0.049	0.157	0.035
TIBLP	373.431	0.046	0.147	0.447	0.105
1st METB	215.359	0.026	0.084	0.227	0.060
5th METB	216.045	0.058	0.182	0.558	0.130
CALC	351.137	0.148	0.469	1.594	0.336

Grand Means (across all landmarks)

Standard Error = 0 .041 mm

Standard Deviation = 0.128 mm

Range = 0.420 mm

95 % Confidence Level = 0.092 mm

Reliability Statistics for the 10 Wooden Foot Trials: Z Values

(values in mm)	**Mean**	**Std Error**	**Std Dev**	**Range**	**95% C.L.**
TC1	233.245	0.039	0.124	0.428	0.088
TC2	220.775	0.044	0.139	0.424	0.100
TC3	209.420	0.031	0.097	0.350	0.070
MMAL	92.282	0.087	0.277	1.079	0.198
LMAL	94.527	0.083	0.262	0.764	0.187
1st METT	42.757	0.023	0.074	0.223	0.053
5th METT	42.492	0.024	0.076	0.289	0.054
TMT	42.873	0.015	0.047	0.134	0.034
TALMA	79.909	0.063	0.198	0.526	0.142
TALLA	75.668	0.042	0.133	0.358	0.095
TALMP	82.814	0.076	0.242	0.841	0.173
TALLP	86.853	0.039	0.123	0.372	0.088
TIBMA	106.780	0.065	0.204	0.690	0.146
TIBLA	106.727	0.035	0.112	0.423	0.080
TIBMP	111.360	0.032	0.100	0.290	0.071
TIBLP	116.569	0.075	0.237	0.739	0.170
1st METB	5.153	0.031	0.099	0.282	0.071
5th METB	4.546	0.045	0.143	0.443	0.102
CALC	4.866	0.037	0.118	0.385	0.085

Grand Means (across all landmarks)

Standard Error = 0 .047 mm

Standard Deviation = 0.148 mm

Range = 0.476 mm

95 % Confidence Level = 0.106 mm

APPENDIX D: Cylinder Optimization Objective Function

Objective.m – Matlab objective function code for cylinder lsqnonlin optimization input

```
function F=objective(x,surface)

% objective.m
% Represents the objective function for a cylindrical regression
% The goal is to minimize the error between the the radius and the
% perpendicular distance from a surface point to the center line of the
% cylinder.  E = f (P,u,r,pts)
% where E = error, P= point on cylinder axis, u = unit direction of axis,
% ans pts = surface points to be fit to.


[r,c] = size(surface);

x(1:3) = x(1:3)/norm(x(1:3));

for i=1:r

   qr = surface(i,:)-x(4:6);

   cp1 = cross(x(1:3),qr);

   dist = cross(x(1:3),cp1);

   mag = sqrt(dist(1)^2+dist(2)^2+dist(3)^2);

   F(i) = mag - x(7);

end
```

APPENDIX E: Correlation Tables

Talus: Pearson Correlations and Partial Correlations (Controlling for Sex)

	Pearson Correlation (N = 8)	Partial Correlation controlling for Sex (df = 5)
	Optimized Radius	Optimized Radius
Age	.266	-.243
Sex	.967 **	--
Whole Foot Measurements		
Foot Length heel to1st toe	.744 *	.915 **
Foot Length heel to 5th toe	.708 *	.048
Heel Width	.522	.381
Forefoot Width	-.039	-.413
Arch Height	.404	.600
Malleoli Height Medial	-.496	-.034
Malleoli Height Lateral	-.449	.337
Transmalleolar Width	.662	.542
Articular Surface Measurements		
Length Medial	.913 **	.880 **
Length Lateral	.917 **	.360
Length Center	.957 **	.810 *
Width Anterior	.866 **	.747
Width Posterior	.348	.120
Width Center	.899 **	.650
Lateral Radius Anterior	.480	.408
Lateral Radius Posterior	.536	.457
Lateral Radius Center	.572	.396
Medial Radius Anterior	.724 *	.936 **
Medial Radius Posterior	.713 *	.917 **
Medial Radius Center	.694	.666
Medial Height Anterior	.763 *	.752
Overall Width	.751 *	.075

* Correlation is significant at the 0.05 level (2-tailed).
** Correlation is significant at the 0.01 level (2-tailed).

Tibia: Pearson Correlations and Partial Correlations (Controlling for Sex)

	Pearson Correlation (N = 8)	Partial Correlation, Control for sex (df = 5)
	Optimized Radius	Optimized Radius
Age	-.065	-.496
Sex	.742 *	--
Whole Foot Measurements		
Foot Length heel to1st toe	.910 **	.883 **
Foot Length heel to 5th toe	.638	.219
Heel Width	.253	-.136
Forefoot Width	.150	.149
Arch Height	.394	.305
Malleoli Height Medial	-.322	.091
Malleoli Height Lateral	-.229	.302
Transmalleolar Width	.672	.454
Articular Surface Measurements		
Medial Depth	.532	-.258
Center Depth	.799 *	.444
Lateral Depth	.173	-.190
Anterior Width	.543	.107
Center Width	.869 **	.704
Posterior Width	.588	.756 *
Medial Malleolus Narrow Width	.441	.237
Medial Malleolus Wide Width	.452	.035
Medial Malleolus Height	.180	.033
Fibula Width	.751 *	.701
Fibula Height	.622	.415

* Correlation is significant at the 0.05 level (2-tailed).
** Correlation is significant at the 0.01 level (2-tailed).

About the Author

Andrew R. Fauth was born in Oregon in 1977. After growing up in Salem, OR, Andrew attended Linfield College where he graduated Magna Cum Laude in 1999 with a B.A. in Exercise Science and a minor in Physics. After college, Andrew was employed by adidas International in Portland, Oregon in the Human Performance/Research and Innovation laboratory. During his tenure at adidas Andrew was responsible for biomechanical testing of the footwear and apparel, as well as R & D work on a variety of products ranging from footwear to snowboard bindings.

In 2000 Andrew moved to State College, PA and began his graduate work in the Department of Kinesiology at The Pennsylvania State University. As a graduate student in the Center for Locomotion Studies (CELOS) working under the guidance of Dr. Neil Sharkey, Andrew worked on a variety of projects characterizing the structural and mechanical behavior of joints and tissues within the foot, and eventually received his M.S. in Kinesiology/Biomechanics in 2002. After completing his masters work, the CELOS lab was merged with the department of Kinesiology to become the Biomechanics Laboratory. It is here that Andrew completed the work outlined in this thesis to receive his Ph.D. in Kinesiology, with a graduate minor in Mechanical Engineering in August, 2005.